Faculteit Industriële Ingenieurswetenschappen

master in de industriële wetenschappen: nucleaire technologie

Masterthesis

The impact of molten salt waste loadings on the properties of geopolymers and Portland cement for radioactive waste immobilization

Jordy Wauters

Scriptie ingediend tot het behalen van de graad van master in de industriële wetenschappen: nucleaire technologie, afstudeerrichting milieu

PROMOTOR :
Prof. dr. Diederik JACQUES

PROMOTOR :
dr. ir. Quoc Tri PHUNG

Gezamenlijke opleiding UHasselt en KU Leuven

Universiteit Hasselt | Campus Diepenbeek | Faculteit Industriële Ingenieurswetenschappen | Agoralaan Gebouw H - Gebouw B | BE 3590 Diepenbeek

Universiteit Hasselt | Campus Diepenbeek | Agoralaan Gebouw D | BE 3590 Diepenbeek
Universiteit Hasselt | Campus Hasselt | Martelarenlaan 42 | BE 3500 Hasselt

2024
2025

Faculteit Industriële Ingenieurswetenschappen

master in de industriële wetenschappen: nucleaire technologie

Masterthesis

The impact of molten salt waste loadings on the properties of geopolymers and Portland cement for radioactive waste immobilization

Jordy Wauters

Scriptie ingediend tot het behalen van de graad van master in de industriële wetenschappen: nucleaire technologie, afstudeerrichting milieu

PROMOTOR :

Prof. dr. Diederik JACQUES

PROMOTOR :

dr. ir. Quoc Tri PHUNG

UHASSELT KU LEUVEN

Preface

This master's thesis marks the final step in my studies in nuclear technology at UHasselt and KU Leuven. From early on, I've had a strong interest in environmental issues and the long-term challenge of managing nuclear waste has always fascinated me. That personal motivation ultimately led me to focus my thesis on improving waste immobilization strategies, an area where I hope to contribute, even in a small way, to more sustainable and responsible nuclear practices.

I would like to thank my promotors, Prof. dr. ir. Diederik Jacques and dr. ir. Quoc Tri Phung, for the opportunity to work on this topic and for their formal guidance throughout the project.

A very special thank you goes to dr. Lander Frederickx, whose support in the lab was not only technically essential but also a source of steady guidance throughout the experimental phase. His help made a significant difference in both the progress and quality of this work.

I also wish to acknowledge the broader SCK CEN staff for providing the facilities, materials and occasional advice that enabled this research to be carried out.

Lastly, I want to sincerely thank my parents, Ann De Vocht and Alain Wauters, for their endless support and encouragement; my girlfriend Emma Vermeiren, for her patience and motivation throughout this journey; and my dog Lillipup, whose joyful presence helped me through long days of writing.

Jordy Wauters
Nijlen, June 2025

The impact of MS waste loadings on the properties of geopolymers and Portland cement for radioactive waste immobilization

Table of contents

List of figures

List of tables

Abbreviations

AAM	Alkali-Activated Material
BET	Brunauer–Emmett–Teller
BFS	Blast Furnace Slag
C-A-S-H	Calcium-Alumino-Silicate Hydrate
C-S-H	Calcium Silicate Hydrate
EDX	Energy-Dispersive X-ray Spectroscopy
GP	Geopolymer
LILW	Low- and Intermediate-Level Waste
MK	Metakaolin
MS	Molten Salt
MSR	Molten Salt Reactor
N-A-S-H	Sodium-Aluminosilicate Hydrate
NA	Nitrogen Adsorption
OPC	Ordinary Portland Cement
PC	Portland Cement
PWR	Pressurized Water Reactor
RH	Relative Humidity
SEM	Scanning Electron Microscopy
SF	Silica Fume
SMR	Small Modular Reactor
UT	Ultrasonic Testing

Abstract in het Nederlands

De overgang naar geavanceerde kernreactoren, zoals Molten Salt Reactors (MSR's), brengt nieuwe uitdagingen met zich mee voor de veilige immobilisatie van radioactief afval. Deze studie onderzoekt het potentieel van Portlandcement (PC) en geopolymeren (GP's) op basis van hoogovenslak (BFS) en metakaolien (MK) voor de immobilisatie van natriumcarbonaat-gebaseerd gesmolten zout (MS)-afval. Hoewel PC veel wordt toegepast voor de immobilisatie van radioactief afval, leidt de hoge CO_2-voetafdruk tot groeiende interesse in alternatieven zoals GP's.

De effecten van 10 en 15 gew.% MS-afval op de materiaaleigenschappen worden geëvalueerd en vergeleken met een referentie zonder MS. Pre-geconditioneerd MS-afval werd verwerkt in drie bindmiddelsystemen: PC, GP-BFS en GP-MK. Het testprogramma omvat metingen van mechanische sterkte, uithardingstijd, viscositeit, carbonatiebestendigheid, hydratatiewarmte, scanning-elektronenmicroscopie (SEM), stikstofadsorptie en ultrasoon onderzoek.

Zowel PC- als GP-matrices tonen potentieel, maar hun prestaties hangen sterk af van de combinatie van MS-afvalgehalte en het bindmiddelsysteem. Toevoeging van MS verbetert de sterkte en verlaagt de porositeit, maar vermindert de werkbaarheid van zowel PC als GP-BFS. MK-gebaseerde GP's voldoen niet aan de acceptatiecriteria en zijn ongeschikt voor immobilisatie. Deze bevindingen onderstrepen de complexiteit van afvalvormontwikkeling en het belang van bindmiddelen die zijn afgestemd op de specifieke afvalstroom, voor duurzame en veilige langetermijnopslag.

Abstract in English

The transition to advanced nuclear reactors, such as Molten Salt Reactors (MSRs), introduces new challenges for the safe immobilization of radioactive waste. This study investigates the potential of blended Portland cement (PC) and geopolymers (GPs) using blast furnace slag (BFS) and metakaolin (MK) as precursors to immobilize sodium carbonate-based molten salt (MS) waste. While PC is widely used for the immobilization of low- and intermediate-level waste, its high CO_2 footprint has driven increasing interest in alternative binders such as GPs.

The effects of 10 and 15 wt% MS waste loadings on the material properties are evaluated and compared to a reference without MS. Preconditioned MS waste was incorporated into three binder systems: PC, GP-BFS and GP-MK. A comprehensive testing program was conducted, including mechanical strength, setting time, viscosity, carbonation resistance, hydration heat, scanning electron microscopy (SEM), nitrogen adsorption and ultrasonic testing.

Results indicate that both PC and GP matrices show potential, but performance strongly depends on the combination of MS waste loading and binder system. MS additions improved strength and reduced porosity, but workability declined with higher loadings for both PC and GP-BFS. MK-based GPs did not meet acceptance criteria and are unsuitable for immobilization. These findings highlight the complexity of waste form development and the importance of using binder systems tailored to the specific waste stream to ensure long-term durability and safety.

Chapter 1
Introduction

As the world accelerates its transition to low-carbon energy systems, advanced nuclear technologies have gained renewed attention for their potential to provide clean, safe and reliable power. Among these technologies, Molten Salt Reactors (MSRs) stand out due to their unique operational characteristics and enhanced safety profile. Their promise lies primarily in their efficient use of nuclear fuel and inherent safety mechanisms. However, MSRs present their own waste management challenges due to the chemically reactive and radiologically complex nature of the salt-based waste streams they generate.

This chapter introduces the broader context of MSR development and their role within the evolving nuclear landscape, with particular attention to the distinct waste streams they generate. As MSRs approach commercialization, the nuclear industry must anticipate how best to condition and dispose of these waste products in compliance with safety regulations and environmental standards.

The chapter opens with a contextual overview of MSR technology, highlighting key differences from conventional nuclear reactor designs and exploring their development within the framework of Small Modular Reactor (SMR) concepts. It then discusses the waste management challenges specific to MSRs and the existing strategies for immobilizing low- and intermediate-level radioactive waste (LILW), with a focus on cementitious materials. The final sections of the chapter define the research problem, objectives and methodology of this study, centred on evaluating the effects of MSR-derived salt waste loadings on the performance of Portland cement (PC) and geopolymer (GP) matrices.

This foundational chapter aims to position the research within current scientific, technological and environmental developments, highlighting its relevance and potential contributions to the long-term safety and feasibility of next-generation nuclear waste management.

1.1 Contextualization

MSRs are clean and sustainable energy technologies that offer potential solutions to climate change, energy security and nuclear waste management challenges. As nations around the globe seek to transition towards cleaner and more sustainable energy sources, MSRs have emerged as frontrunners in the quest for next-generation nuclear power.

MSRs represent a shift in nuclear reactor design, utilizing molten fluoride or chloride salts as both coolant and fuel carrier. In contrast, pressurized water reactors (PWRs) rely on pressurized water as the primary coolant, circulating through the reactor core to transfer heat to a steam generator. The form of the fuel is another key difference between the two reactor types. In MSRs, nuclear fuel is dissolved in the molten salt (MS) coolant, allowing for continuous reprocessing and potentially higher fuel utilization. PWRs use solid fuel rods containing enriched uranium (UOX) or mixed uranium and plutonium oxide (MOX) fuel, which must be replaced periodically. In terms of inherent safety features, MSRs possess advantages such as passive cooling mechanisms and low-pressure operation, thereby reducing the risk of accidents and meltdown scenarios. PWRs rely on active safety systems and complex engineering controls to maintain safe operations, which may be susceptible to human error or equipment failure.

SMRs are a newer generation of nuclear reactors designed to generate electric power up to 300 MW. Their components and systems can be fabricated and transported as modules for on-site installation, allowing for flexible deployment based on demand. Many SMRs incorporate advanced or inherent safety features and can be deployed as single- or multi-module plants. The key driving forces behind SMR development include the need for flexible power generation, replacement of aging fossil-fired units, enhancing safety and improving economic affordability. SMRs are particularly suited for niche electricity and energy markets in which large-scale reactors are not viable, such as remote areas, small electricity grids and hybrid nuclear-renewable energy systems. The modular design of SMRs also targets improved economics through serial production and reduced construction time [1].

Among the various SMR designs, MSR technology has gained significant momentum, progressing from concept to production stages. This is largely driven by the increasing global demand for electricity due to population growth, estimated at an annual rate of 17%–19%. With the urgent need for decarbonization and transition to sustainable energy sources, nuclear power has become a crucial element in the future energy landscape. MSRs are being actively developed as reliable and sustainable energy sources that are capable of integrating conventional and renewable energy systems. Their role in addressing climate change and growing energy demands underscores their potential as a key player in the future of clean energy [1].

Although MSRs offer numerous advantages in terms of efficiency and safety, they are not exempt from the challenge of managing the waste generated throughout their lifecycle. Unlike PWRs, which primarily produce solid fuel rods and radioactive coolant, MSRs generate a unique array of waste streams, including off-gas streams, salt waste, metal waste, carbon waste, decommissioning and decontamination and operating waste. The management of each waste stream carries its own set of complexities and considerations [2].

Cementation is the preferred method for solidification treatment of LILW in most countries. This method ensures that the release of confined radionuclides underground is minimized during disposal, whether on a surface or in a deep geological repository [3]. The encapsulation of radioactive waste in ordinary Portland cement (OPC) began in the early years of the nuclear industry. This is primarily because of its low cost, availability and compatibility with aqueous waste [4]. OPC is the most common type of cement used for the solidification of liquid and solid wastes worldwide. Blended PC systems, which include supplementary cementitious materials such as blast furnace slag (BFS), offer cost reduction, energy saving and superior long-term performance [3].

In response to the environmental concerns associated with PC's high carbon footprint, there is growing interest in alternative cementitious systems such as GP. These materials are promising candidates for the immobilization of LILW radioactive wastes due to their cationic binding sites and better durability properties [5]. GPs are formed by the reaction between a concentrated alkaline solution (activator) and solid aluminosilicate precursors (e.g., fly ash (FA), BFS or metakaolin (MK)) [3]. GPs has some advantages over PC, such as more rapid strength development and lower heat output [4]. The long-term safety of these alternative cementitious systems is yet to be fully established.

Therefore, this study investigates key mechanical and microstructural properties to enhance the understanding of the suitability and reliability of these materials for long-term waste immobilization.

1.2 Problem definition

Despite the promise of both PC and GP matrices for immobilizing LILW radioactive waste, there is limited understanding of how these materials interact with MS waste, particularly from MSRs. Unlike more traditional aqueous or solid waste streams, MS waste presents distinct chemical challenges that may alter the performance and durability of the binding matrices.

Current research does not adequately address how varying loadings of MS waste influence key mechanical and microstructural properties of PC and GP systems. The presence of high alkali content, potential salt–matrix reactions and differing setting and hydration behaviours could critically impact the long-term stability of the immobilized waste form. This lack of systematic data prevents informed decisions about the most suitable materials for conditioning MS waste, especially in the context of regulatory disposal criteria.

A deeper understanding of these interactions is essential to evaluate the viability of these materials for long-term MSR salt waste immobilization. This thesis aims to bridge that knowledge gap through a detailed investigation of the effect of MS waste loadings on the mechanical behaviour and microstructure of PC and GP matrices.

1.3 Objective

The objective of this thesis is to evaluate the effect of sodium carbonate (Na_2CO_3)-based MS waste loadings on the mechanical and microstructural properties of PC and GP matrices for the immobilization of radioactive waste. The cementitious matrices examined in this study include CEM-, BFS-AAM- and MK-AAM based systems. These were selected due to their established or emerging roles in radioactive waste solidification, as well as their differing chemical compositions and binding mechanisms.

To assess the influence of MS waste incorporation, a series of tests will be conducted to evaluate the effects of 10 and 15 wt% MS waste loadings on the material properties, in comparison to a reference without MS. Mechanical properties such as compressive strength will be measured to evaluate the structural integrity of the waste forms. The setting time will be determined to understand the curing kinetics, while viscosity measurements will provide insight into the workability of the fresh pastes. In addition, isothermal calorimetry will be used to monitor the heat of hydration, providing information on the reaction rate and thermal behaviour during curing. Carbonation tests will be carried out to assess the material's resistance to environmental CO_2 exposure over time, which can impact long-term durability.

On a microstructural level, advanced characterization techniques such as scanning electron microscopy (SEM) will be employed to analyse the morphology, phase composition and interface between the matrix and the MS residues. These investigations aim to identify any salt-induced changes in structure, such as microcracking, porosity or the formation of secondary phases, which may compromise the waste form's long-term stability.

By systematically comparing the performance of PC and GP matrices under controlled MS waste loading conditions, this research seeks to determine which material systems offer the best balance of mechanical robustness, chemical resistance, workability and microstructural stability. The results will contribute to a better understanding of how these alternative cementitious systems behave in the presence of MSR-derived salt waste, thereby supporting the development of safe, effective and regulatory-compliant immobilization strategies for next-generation nuclear reactors.

To address these objectives, the remainder of the thesis is structured as follows: Chapter 2 provides a literature review on MSR waste and cementitious immobilisation methods. Chapter 3 outlines the experimental methodology. Chapter 4 presents the results and analysis and Chapter 5 concludes the thesis with a summary of findings.

Chapter 2
Literature review

Safe and effective management of radioactive waste is crucial for the sustainability of nuclear energy, ensuring environmental protection and long-term sustainability. Among the various waste management strategies, immobilization plays a fundamental role in the containment and isolation of radionuclides to prevent their release into the environment. This process typically involves encapsulating waste in stable matrices, such as PC and GPs, which enhance containment and durability.

A key factor in waste management is the classification of radioactive waste based on its radioactivity level, half-life and disposal requirements. Proper classification is essential for determining the appropriate handling, storage and disposal strategies.

MSRs represent a promising advancement in nuclear reactor technology, offering inherent safety features, improved fuel utilization and reduced high-level waste generation compared to conventional PWR reactors. However, MSR waste streams differ significantly from those of PWRs, necessitating specialized management approaches. A comparison of these reactor types highlights key differences in reactor operation, fuel cycle, waste production and safety mechanisms, providing a foundation for understanding the unique challenges associated with MSR waste.

MSR-derived radioactive waste comprises a complex mix of fission products, off-gases and salt-based residues, requiring tailored immobilization techniques. Cementation has long been an established method for radioactive waste immobilization, particularly for LILW. OPC matrices have been widely employed because of their cost-effectiveness and compatibility with aqueous waste streams. However, concerns over the carbon footprint of cement and the need for enhanced durability have driven growing interest in GP-based immobilization.

An emerging area of research involves investigating the effects of incorporating MS waste into GP and PC matrices. The interaction between MS waste and these cementitious materials influences their mechanical and microstructural properties, ultimately affecting the long-term stability of the immobilized waste forms. Understanding these effects is essential for optimizing waste immobilization strategies and ensuring safe disposal of MSR-derived radioactive waste.

This literature review aims to provide a comprehensive overview of these topics, evaluate the existing research and identify knowledge gaps to support the advancement of effective radioactive waste immobilization techniques.

2.1 Introduction to radioactive waste

We live in a naturally radioactive environment. The universe originated 13.8 billion years ago, the Big Bang [6]. As the gas cooled, solid dust particles formed, eventually aggregating into the first celestial bodies. Over time, radionuclides within these bodies have decayed, yet some isotopes with exceptionally long half-lives, such as ^{235}U, ^{238}U, ^{232}Th and ^{40}K, persist today as remnants of Earth's natural radioactive history [7].

The discovery of natural radioactivity in 1896 marked a significant breakthrough, leading to its application in medicine and scientific research. By the 1930s, scientists had successfully produced artificial radioactive materials, facilitating their widespread use in science, medicine, industry and agriculture. However, both natural and artificial sources of radioactivity generate waste that contains significant levels of radionuclides, necessitating safe management and disposal [7].

Radioactive waste is defined as any material that contains or is contaminated with radionuclides at concentrations or activity levels exceeding the clearance thresholds set by national regulatory authorities for which no further use is currently anticipated [8]. The potential hazard of radioactive waste increases with the radionuclide concentration, but the risk is also influenced by the specific radiological properties of individual isotopes [7].

The classification of radioactive waste is a regulatory measure. Waste with activity concentrations at or below clearance levels is considered non-radioactive, despite being radioactive from a physical standpoint. However, at such low levels, the associated radiological risks are considered negligible [7].

2.2 Radioactive waste classification

The International Atomic Energy Agency (IAEA) divides radioactive waste into six categories based on two key parameters: the half-life of radionuclides and their level of activity [9]. A visual representation is shown in Figure 1.

1. Exempt Waste (EW): This waste meets the criteria for clearance, exemption or exclusion from regulatory control for radiation protection purposes.

2. Very Short-Lived Waste (VSLW): This category includes waste containing radionuclides with very short half-lives, often used in research and medical applications. It can be stored for decay for a limited period (up to a few years) and subsequently cleared from regulatory control for uncontrolled disposal, use or discharge, following approval by the regulatory body.

3. Very Low-Level Waste (VLLW): Although VLLW does not meet the criteria for exempt waste, it requires only minimal containment and isolation. It is suitable for disposal in near-surface landfills, which may also accommodate other hazardous waste with limited regulatory control. Typical examples include soil and rubble, which have low activity concentrations. The presence of long-lived radionuclides in VLLW is generally minimal.

4. Low-Level Waste (LLW): This waste exceeds clearance levels but contains only limited amounts of long-lived radionuclides. It requires robust isolation and containment for up to a few hundred years and is suitable for disposal in engineered near-surface facilities. LLW may include short-lived radionuclides at higher activity concentrations and long-lived radionuclides at relatively low levels.

5. Intermediate-Level Waste (ILW): ILW requires greater containment and isolation than LLW because of its higher long-lived radionuclide contents. Unlike HLW, ILW do not generate significant heat and do not require active cooling. However, due to the presence of long-lived radionuclides, particularly alpha emitters, ILW is unsuitable for near-surface disposal and must be stored at depths ranging from tens of meters to a few hundred meters.

6. High-Level Waste (HLW): This category consists of waste with high activity concentrations that generates significant heat due to radioactive decay or contain large amounts of long-lived radionuclides. HLW disposal requires deep and stable geological formations, typically several hundred meters below the surface, to ensure long-term containment and isolation.

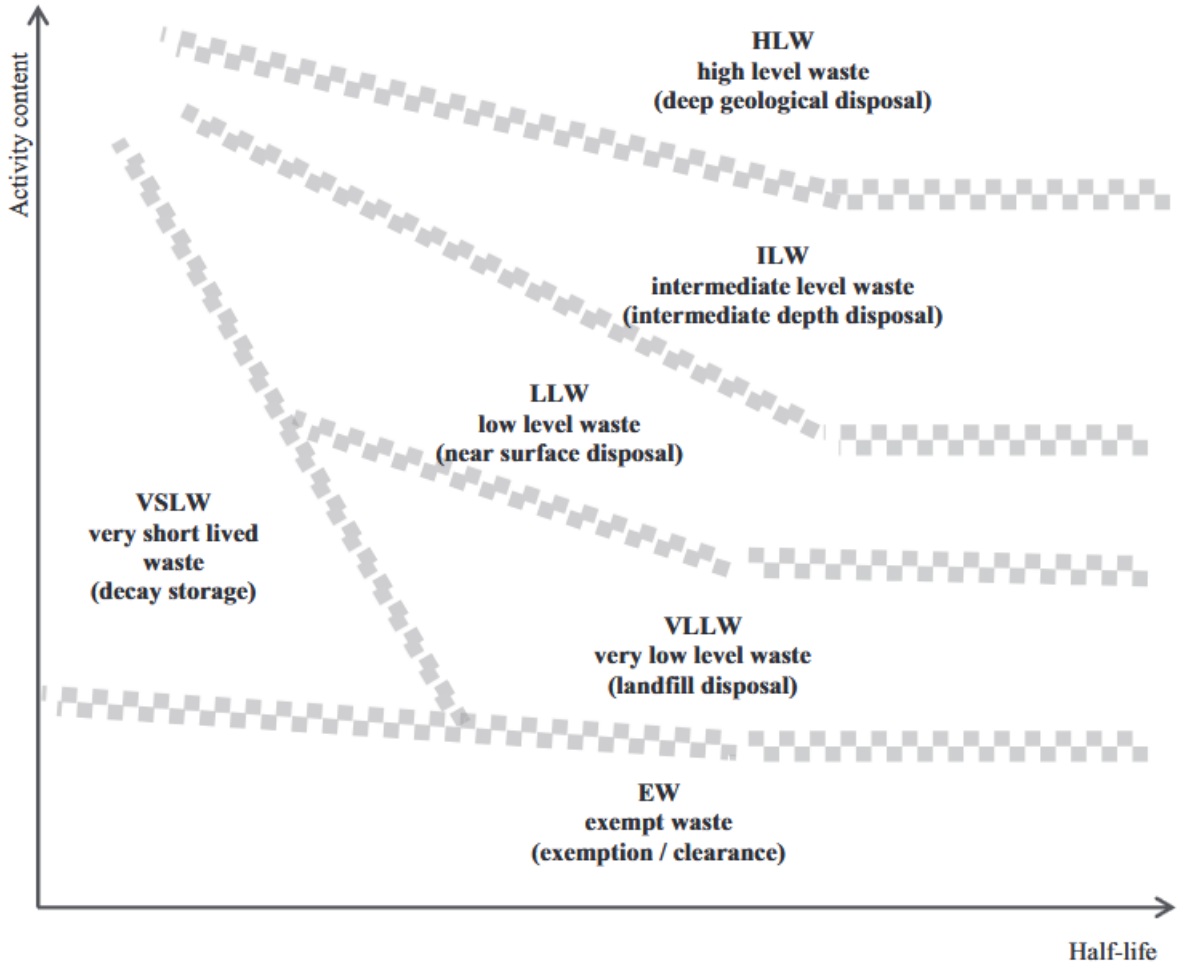

Figure 1: Radioactive waste classification [9]

The half-life of radionuclides in waste can range from seconds to millions of years. For waste management purposes, radionuclides with half-lives of less than 30 years are classified as short-lived. This distinction is crucial, as the radiological hazards associated with short-lived radionuclides diminish significantly over a few hundred years due to radioactive decay. Consequently, differentiating between short- and long-lived radionuclides is essential for optimizing waste disposal strategies and ensuring long-term safety [9].

2.3 MSR

An MSR is a nuclear reactor that uses MS as both fuel and coolant, distinguishing it from other reactor types that rely on liquid metal, gas or water. MS liquefies at elevated temperatures and can store massive amounts of thermal energy at atmospheric pressure**.** The MS in an MSR consists of a solution of uranium and thorium fluorides dissolved in a mixture of lithium and beryllium fluorides, that serves as the fuel medium [1] [10].

When used as fuel, fissile materials such as U-235, Pu-239 or U-233 are dissolved in the MS. These are sometimes mixed with fertile materials such as U-238 to sustain the fuel cycle [10].

The layout of a MSR is illustrated in Figure 2.

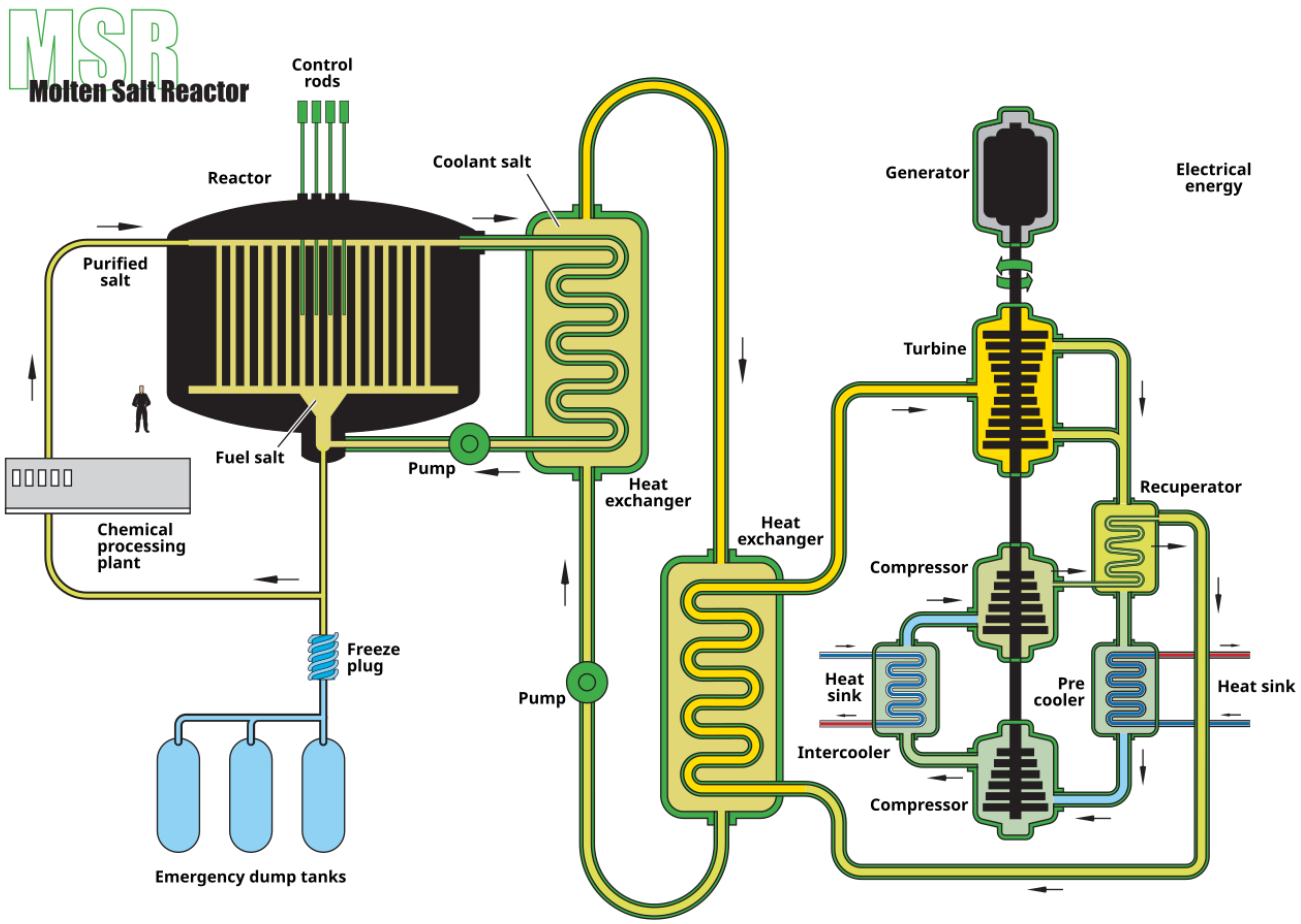

Figure 2: Layout of MSR [1]

The safety design of MSRs is evident when attempting to imagine any possible scenario for the release of radioactive materials. While a salt spill is possible, fission products remain within the MS, significantly reducing the risk of contamination [1].

MSRs employ a three-tier containment system, similar to solid-fuel reactors. The first containment barrier is the primary loop itself, which holds the MS. This loop is entirely enclosed within the second containment layer, a sealed zone with only the necessary penetrations for pump drive shafts, intermediate coolant lines and possibly a shutdown rod. This containment zone, which houses the primary heat exchangers, is designed to collect and redirect any salt spill into decay heat dump tanks [1].

The entire system is enclosed within a building containment, ensuring no external release pathways. In the event of an excessive core temperature, such as a complete pump failure, the system relies on passive freeze plugs, which melt when the salt overheats, allowing it to drain safely into the dump tanks. This prevents overheating and ensures passive safety. Once the salt cools, it can be pumped back into the core for reactor restart [1].

Unlike conventional reactors, MSRs operate at ambient pressure because the salts have an exceptionally high boiling point (~1400 °C). In addition, the primary salt loop is maintained at the lowest pressure in the system, ensuring that any leak results in an inward flow, further enhancing safety [1].

MSR technology has a long and technically rich history, which began in the 1940s. The concept of using MS as both fuel carriers and coolants was first proposed in 1944, when Nordheim of Oak Ridge National Laboratory described the Th-U breeding cycle in a homogeneous reactor system. Early experimental work focused on aqueous homogeneous reactors, but these were soon found to suffer from significant technical issues, including the radiolytic decomposition of water, corrosion, instability from hydrogen gas formation and a lack of suitable materials for high-pressure operation. These challenges led to a shift toward molten fluoride salts as a more viable medium, with experiments beginning in 1947 [11].

By the early 1950s, MSR development had been integrated into the United States' Aircraft Nuclear Propulsion program. This led to the construction and operation of the Aircraft Reactor Experiment in 1954, the first MSR. Following this success, the Molten Salt Reactor Experiment (MSRE) was designed and built in 1965 to achieve initial criticality. However, four key technical issues emerged in the late 1960s: neutron embrittlement of nickel alloys, radiation damage to graphite, the need for advanced chemical separation of Pa and U, and tritium permeation. Although these problems were actively addressed through design modifications and material R&D in the 1970s, the U.S. MSR program gradually lost political momentum and was effectively discontinued by 1977 [11].

Outside the U.S., the interest in MSRs has grown steadily. Switzerland, the Netherlands, France and the Soviet Union conducted extensive R&D from the 1960s to the 1980s, focusing on chloride and fluoride salt systems. France re-engaged with the MSR concept in the 1990s and 2000s, proposing advanced designs such as the Molten Salt Fast Reactor (MSFR), a non-moderated, iso-breeder (a state in which the reactor produces as much fissile material as it consumes) system using fluoride salts. Simultaneously, China initiated its own MS research program in the 1970s, culminating in the construction of a liquid-fuelled 2 MW test reactor (TMSR-LF1), which was commissioned in 2021 and licensed for operation in 2023 [11].

Today, MSRs are once again a focal point of international nuclear innovation. There have been active development efforts across Europe, Asia and North America, including projects focused on high-temperature process heat, nuclear waste transmutation and proliferation-resistant Th cycles. While no MSR is yet commercially deployed, operational experiments such as TMSR-LF1 and coordinated R&D efforts, particularly in France and China, signal a serious push toward demonstration reactors [11]. In 2023, an MS-based SMR concept in Canada became the first MSR to complete a crucial pre-licensing vendor design review. Other projects in China, Russia and the US continue to progress, with the hope that MSRs could begin to see deployment as soon as the mid-2030s [10].

MSRs can be classified into various types based on their characteristics such as neutron spectrum (thermal or fast), fuel configuration (homogeneous or heterogeneous), salt composition (typically fluoride or chloride) and the presence or absence of a moderator such as graphite. Each of these design families has distinct implications for waste production. For example, graphite-moderated thermal MSRs produce additional structural waste due to graphite degradation, whereas fast-spectrum, non-moderated MSRs, often using chloride salts, are designed for efficient actinide burning, which can reduce the volume of long-lived transuranic waste. Moreover, reactors with online fuel processing tend to minimize the accumulation of HLW by continuously removing fission products, whereas systems operating on an open fuel cycle may require more frequent salt replacement, thus generating more waste [11].

While most MSRs studied in the IAEA report are based on fluoride or chloride salts, this research focuses on the use of sodium carbonate (Na_2CO_3) as the MS. This introduces a novel perspective, as Na_2CO_3 is not commonly used in MSR designs and may influence waste generation differently. By investigating sodium carbonate in an MSR context, this study aims to broaden the understanding of how alternative salt chemistry affects waste characteristics, reactor performance and long-term waste management strategies [11].

Nonetheless, several challenges for MSRs remain. Standardized safety designs, fuel-salt transportation protocols and reliable supply chains for MSR-specific components are still under development. Potential accident scenarios and radionuclide behaviour under both normal and abnormal conditions must be further investigated. These knowledge gaps highlight the need for continued experimental research and safety testing before commercial deployment can proceed [10].

2.4 Comparison between PWR and MSR

In both water- and MS-cooled reactor designs, the primary coolant is heated at the reactor core and circulated upward through the reactor vessel. In the upper portion of the vessel, the coolant is redirected downward to flow over the heat exchangers, transferring heat to a secondary coolant that drives the power generation system [12].

One of the primary advantages of liquid-fuelled MSRs is their ability to process fuel during operation. Unlike traditional reactors, which must be shut down to refuel or redistribute fuel, MSRs can perform these functions while running at full power. Although periodic maintenance shutdowns may still be required, MSRs are expected to have a higher operational uptime than conventional reactors [1].

Furthermore, when fission occurs, the resulting products can be continuously extracted from the reactor. This process reduces neutron absorption by unwanted isotopes, improving neutron economy and sustaining the chain reaction more efficiently. Traditional PWRs experience neutron losses due to structural materials such as cladding, fuel ducts and grid spacers, none of which are present in an MSR. As a result, MSRs achieve a significantly higher fuel efficiency [1].

If MS is used as the primary coolant rather than water, it can absorb significant amounts of heat at atmospheric pressure and operate at high temperatures. This enables MSRs to produce high-grade heat, suitable for decarbonizing industrial processes, such as hydrogen production for green steel, without greenhouse gas emissions. MSRs are also designed with modular construction in mind, allowing systems to be assembled in factories and transported for on-site installation, potentially lowering costs and increasing scalability [10].

Additionally, liquid-fuelled MSRs eliminate the need for solid fuel fabrication and can achieve a higher fuel burnup, resulting in smaller quantities of HLW. MSRs can also support more sustainable fuel cycles by utilizing uranium, plutonium or thorium, all of which can be dissolved in MS. Thorium, which is more abundant and easier to mine than uranium, is particularly promising for long-term resource sustainability [10].

MSRs have several intrinsic safety advantages due to their design, as listed in Table 1.

Table 1: Safety features MSR [1]

Feature	Explanation
Fuel and coolant integration	Loss of coolant = loss of power ➔ cannot meltdown.
Atmospheric operating pressure	No risk of pressure explosions.
No explosive gas production	No risk of gas explosions.
Chemical stability in liquid	No dangerous radioactive gasses.
Very low excess reactivity	Continual refueling removes the need for extra fissile material, minimizing risks from events causing reactivity spikes.
Negative temperature coefficient of reactivity	Fuel expansion reduces reactivity as temperature rises, ensuring stability (not always true in graphite-moderated MSRs).
Low pressure	Operating at atmospheric pressure prevents leaks and enables passive decay heat removal.
No chemical reactivity with air or water	Fuel salt is not violently reactive with the environment, avoiding hydrogen explosions or sodium fires typical of other reactor types.
Drain tank failure mechanism	In an emergency, a freeze plug melts, draining the core into subcritical tanks connected to a heat sink, mitigating accidents.

Despite these benefits, MSRs also face significant challenges:

1. Mobility of fission products and corrosion risks

A major concern with MSRs is that radioactive fission products are not confined within solid fuel pins, but rather suspended within the liquid salt. Some of these fission products, particularly actinides, are highly radioactive, whereas others have corrosive chemical properties that can degrade reactor materials over time. Structural corrosion is a key issue that requires advanced materials to prevent long-term degradation of reactor components.

Additionally tritium (^{3}H) is produced if lithium is used in the salt. Tritium is a radioactive isotope that is extremely mobile due to its small atomic size, allowing it to permeate through metal surfaces, posing additional containment challenges [1].

2. Protactinium removal in Th-cycle MSRs

Many Th-cycle MSRs require continuous ^{233}Pa extraction to allow their decay into ^{233}U, which is needed to sustain the fuel cycle. If left in the reactor, protactinium absorbs too many neutrons, reducing the ability of the reactor to maintain a breeding cycle. This necessity for online chemical separation adds complexity to reactor operation [1].

3. Fuel salt enrichment requirements

To enable an efficient neutron economy in thermal-spectrum MSRs, the lithium and chloride salts used in the fuel must be isotopically enriched. ^{7}Li must be highly purified, as ^{6}Li acts as a strong neutron poison and converts into tritium. In chloride salt MSRs, enrichment to ^{37}Cl is necessary because ^{35}Cl absorbs neutrons and forms ^{36}Cl, a long-lived, beta emitter that complicates waste disposal [1].

4. Uncertainties in MSR waste composition

The nuclear waste generated by MSRs remains an area of limited research. Unlike traditional reactors, which produce well-characterized spent fuel, the exact composition, behaviour and long-term management of MSR waste are still uncertain. Addressing this knowledge gap is one of the key objectives of this study, which aim to provide a clearer understanding of the waste streams from MSRs and their potential immobilization strategies [1].

2.5 Radioactive waste from MSR

The primary coolant is in direct contact with the active core and becomes contaminated with radionuclides. In MS-cooled systems, the primary coolant is chemically reactive, operates at temperatures exceeding 500°C and is highly radioactive. These extreme conditions accelerate material degradation and reduce the lifetime of reactor components compared to standard PWRs, which typically last for 60 years. As a result, the volume of LILW is expected to increase compared to that of conventional reactor systems, primarily because of the presence of chemically reactive MS waste, a type of waste that is uncommon in traditional nuclear waste management. The MSR vessel lifespan is constrained by exposure to corrosive, high-temperature and radioactive environments. [12].

Most thermal-spectrum MSR designs employ graphite as both a neutron moderator and reflector, occupying 60–80% of the core volume. The remaining volume contains liquid fuel-coolant salt, which flows through hollow channels in the graphite matrix, carrying dissolved fuel isotopes and fission products. Over time, graphite in the reactor accumulates surface contamination from solid fission products, whereas gaseous fission products diffuse into its structure. Prolonged neutron irradiation causes graphite expansion and cracking, which limits its operational lifespan. Depending on neutron flux exposure, graphite lifetimes in MSRs range from 2.5 to 30 years, necessitating the periodic replacement and disposal of activated graphite waste [12].

When a PWR is decommissioned, most radionuclides in its cooling water are removed by filters and ion exchange resins. Storage, decontamination and disposal of radioactive MS–based coolants will need to account for their chemical complexity and tendency to generate explosive or corrosive by-products upon contact with air or moisture [12].

While MSRs and PWRs generate a similar array of radioisotopes, MSRs use fuels with fundamentally different chemistry. The lack of solid fuel cladding in MSRs allows for the direct release of gaseous fission products, including xenon isotopes, which decay into high-activity or long-lived caesium isotopes, contributing to the HLW stream. Additionally, noble metal fission products tend to precipitate onto reactor structures, increasing the risk of contamination. However, MS fuel offers some advantages: it effectively retains salt-soluble fission products and actinides, which eventually solidify, simplifying some aspects of waste management [12].

MSR fuel salt contains actinides, fission products, contaminants and activated corrosion products. Unlike solid fuel, MS does not suffer from mechanical radiation damage, giving it no defined mechanical lifetime. Reasons for discarding fuel salt include decreased fissile solubility, neutronic inefficiency or unfavourable thermophysical changes, such as increased viscosity or melting point due to accumulated by-products. These effects may take decades to develop. Many MSR concepts have proposed using recycled fuel salt, either from the same reactor or reprocessed from solid fuel. Throughout reactor operation, the salt composition evolves, with actinides added to compensate for burnup and chemical adjustments performed as needed. While some of this salt may be reused in future reactors, all fuel salts become waste upon reactor shutdown, unless recycled [13].

Solid fission and corrosion products form during operation and can be deposited as surface layers on components in contact with salt. These deposits may slowly diffuse into the structural alloy, forming intermetallic compounds, particularly at higher operating temperatures. Tellurium is known to cause cracking in nickel-based alloys, while materials with limited solubility tend to accumulate in the cooler parts of the loop, potentially forming blockages due to solid buildup. These deposits can limit component lifetimes if they are not removed [13].

Despite this potential for reuse, the management of fuel salt waste remains essential. Fuel salt contacting components will likely need to be replaced multiple times during the reactor's life. The draining and flushing of the system is a necessary first step in its maintenance. Radiation damage, particularly neutron embrittlement in nickel-based alloys, may limit the lifespan of major components such as reactor vessels, whereas heat exchangers face additional challenges from erosion and creep [13].

Some of this waste may be suitable for disposal in a near-surface, short-lived LILW repository (<30-m deep). However, neutron-activated, long-lived LILW are more complicated to manage because radiation exposures must be mitigated on both operational and geologic timescales. Because MSRs will generate more neutron-activated steel than energy-equivalent PWR and will introduce the need to chemically treat radioactive MS coolants, they may significantly increase the costs and exposure risks associated with nuclear decommissioning [12].

The packaging of spent nuclear fuel from MSRs differs from that of the conventional approaches. One proposed method involves allowing the spent liquid fuel salt to solidify within the reactor vessel. However, the potential formation and migration of volatile actinide-fluoride complexes raises concerns regarding their recriticality. To ensure long-term stability and safety, actinides must be chemically processed and converted into a stable waste form to minimize the risks of criticality and environmental contamination [12].

2.6 Immobilization of radioactive waste by cementation

Waste immobilization involves converting raw waste, which usually contains mobile contaminants, into a solid and stable form. The resulting waste form allows for safe handling, storage and disposal, significantly reducing the risk of radionuclide release into the environment. Choosing a suitable waste form for nuclear waste immobilization is difficult and durability is not the sole criterion. It must also be reliable, simple and resilient. The choice of immobilization technology depends on the physical and chemical characteristics of the waste and the acceptance criteria for the long-term storage and disposal facility to which the waste will be consigned [14].

Cementation is a widely used method for immobilizing LILW due to its simplicity, cost-effectiveness and stability. OPC is the most commonly used cement type, sometimes blended with materials such as BFS or silica fume (SF) to enhance the durability of the waste form. These industrial byproducts can improve the resistance to chemical degradation, reduce permeability and mitigate cracking, thereby enhancing the long-term containment of radionuclides. They also react with portlandite ($Ca(OH)_2$), a byproduct of cement hydration, to form an additional calcium silicate hydrate (C-S-H) gel, which strengthens and densifies the cement matrix. The advantages of OPC are listed in Table 2 [14].

Table 2: Advantages of immobilization by cementation [14]

Feature	Explanation
Cost and availability	Cement is inexpensive and readily available.
Simple processing	Processing at ambient temperature is simple and low-cost.
Diffusion barrier	The cement matrix acts as a diffusion barrier and provides sorption and reaction sites.
Suitability	Suitable for sludges, liquors, emulsified organic liquids and dry solids.
Stability	Waste forms have good thermal, chemical and physical stability.
Alkaline chemistry	Ensures low solubility for many key radionuclides.
Non-flammable	The waste form is non-flammable.
Radiation resistance	Not degraded by radiation and provides good self-shielding.
Mechanical strength	Good compressive and flexural strength facilitates handling.
Remote processing	Easily processed remotely.
Flexibility	Can be modified for a particular waste stream.

PC is a hydraulic cement that sets up and hardens in air and water. It is produced by pulverizing clinker, which consists of hydraulic calcium silicates and blending it with calcium sulfate (gypsum) as a setting regulator. Clinkers are produced by heating clay materials with lime at high temperatures (>1500°C). The low cost and wide availability of limestone and naturally occurring silica sources make PC one of the lowest cost materials used worldwide. The major phases present in PC are listed in Table 3 [14].

Table 3: Principal clinker minerals of cement [14]

Compound	Oxide composition	Abbreviation
Tricalcium silicate	$3CaO{\cdot}SiO_2$	C_3S
Dicalcium silicate	$2CaO{\cdot}SiO_2$	C_2S
Tricalcium aluminate	$3CaO{\cdot}Al_2O_3$	C_3A
Tetracalcium aluminoferrite	$4CaO{\cdot}Al_2O_3.Fe_2O_3$	C_4AF
Lime	CaO	C
Calcium sulphate	$CaO{\cdot}SO_3$	C$

The primary reactions involve C_3S and C_2S, which react with water to form C-S-H gel and calcium hydroxide. C-S-H gel forms the main binding phase responsible for the strength and low permeability of hardened cement, while calcium hydroxide contributes to the alkaline environment, which can aid in immobilizing certain radionuclides. Minor phases such as C_3A and C_4AF contribute to early setting and sulphate resistance. In waste immobilization contexts, these hydration products help encapsulate waste components, reducing their mobility and enhancing long-term performance.

There are five primary classes of PC, with Type I (OPC) being the most commonly used when no special properties are required. Other types provide enhanced resistance to sulphate attack, lower heat generation or higher early strength. The composition of each class is listed in Table 4 [14].

Table 4: Classes of PC, their mineral composition (wt.%) [14]

Type	C_3S	C_2S	C_3A	C_4AF	Others	Use
I	50	24	11	8	7	General purpose cement, when there are no extenuating conditions
II	42	33	5	13	7	Aids in providing moderate resistance to sulphate attack
III	60	13	9	8	10	When high-early strength is required
IV	26	50	5	12	7	When a low heat of hydration is desired (in massive structures)
V	40	40	4	7	7	When high sulphate resistance is required

The increasing demand for cementitious binders and the need for sustainable construction highlight the need for more durable and environmentally friendly alternatives to OPC. The carbon footprint of OPC production is substantial, contributing to approximately 5% of global CO_2 emissions. This high emission level is primarily due to limestone decarbonation during clinker production and high-temperature processing (>1400°C) required for clinker formation [15].

Consequently, alternative cementitious binders that reduce carbon emissions and energy consumption are gaining interest. One promising alternative is the group of alkali-activated materials (AAMs), which includes GPs. These materials offer a more sustainable approach by utilizing industrial by-products (SF and BFS) instead of clinker and reducing energy consumption by avoiding high-temperature processing. This makes them an environmentally friendly alternative to conventional cement-based binders [15].

2.7 Immobilization of radioactive waste by GPs

GPs are inorganic, AAMs that form a three-dimensional aluminosilicate network through the reaction of an aluminosilicate precursor (such as MK or BFS) with an alkali activator (such as sodium hydroxide and sodium silicate). Unlike traditional PC, which primarily forms C-S-H phases, GPs develop a rigid Si-O-Al network through a process known as geopolymerisation. The choice of precursor material significantly influences the chemical composition, reaction mechanism and final properties of GP [16].

AAMs are classified based on their calcium content, which influences their reaction mechanisms, microstructures and final properties. Low-calcium AAMs, commonly referred to as GPs, are materials that primarily rely on aluminosilicate-rich precursors (e.g., MK ($Al_2O_3 \cdot 2SiO_2$)) and form sodium-aluminosilicate hydrate (N-A-S-H) gels. High-calcium AAMs include BFS-based materials, which react differently because of their calcium-rich composition, forming calcium-alumino-silicate hydrate (C-A-S-H) gels, similar to conventional PC hydration [17].

Low-calcium undergoes alkali activation in a high-pH environment. The reaction involves the formation of N-A-S-H gels, which provide structural integrity and durability [17].

The formation of MK-based AAMs follows a three-step reaction mechanism [17]:

1. **Dissolution:**
   - Strong alkali (e.g., NaOH and KOH) breaks down the Si–O–Si and Al–O–Si bonds in MK.
   - This releases silicate (SiO_4^{4-}) and aluminate (AlO_4^{5-}) units into solution.

2. **Oligomer formation & reorganization:**
   - The dissolved species undergo polymerization, forming aluminosilicate oligomers.
   - These oligomers condense into a three-dimensional Si–O–Al network.

3. **Hardening & solidification:**
   - The gel was polycondensed into an amorphous sodium-aluminosilicate hydrate (N-A-S-H) gel, which is the primary binding phase.
   - The material hardens over time, forming a rigid structure.

The general reaction for MK-based AAM is:

$$Al_2O_3.2SiO_2\ (MK) + 2\ NaOH + x\ H_2O \rightarrow Na_2O \cdot Al_2O_3 \cdot SiO_2 \cdot x\ H_2O\ (NASH)$$

High-calcium AAMs undergo different reaction mechanism due to the presence of calcium. The reaction forms C-A-S-H gels, which provide a faster strength development and enhanced workability [17].

The formation of BFS-based AAMs follows a three-step reaction mechanism [17]:

1. **Dissolution:**
    - Alkali activators dissolve Si, Al and Ca species from BFS.
    - Calcium ions (Ca^{2+}) enter the reaction solution.

2. **Simultaneous formation of C-A-S-H and N-A-S-H gels:**
    - In high-calcium systems, a C-A-S-H gel forms, similar to OPC hydration.
    - Some N-A-S-H gels may still be present, particularly at low to moderate Si/Al ratios

3. **Hardening & solidification:**
    - A more compact microstructure is formed due to C-A-S-H gel development.
    - The material gains strength more quickly than MK-based AAM.

The general reaction for BFS-based AAM is:

$$CaO \cdot Al_2O_3 \cdot SiO_2(BFS) + NaOH + x\ H_2O \rightarrow CaO \cdot Al_2O_3 \cdot SiO_2 \cdot x\ H_2O\ (CASH) + minor\ NASH$$

Figure 3 provides a simplified overview of the geopolymerisation process in alkali activation.

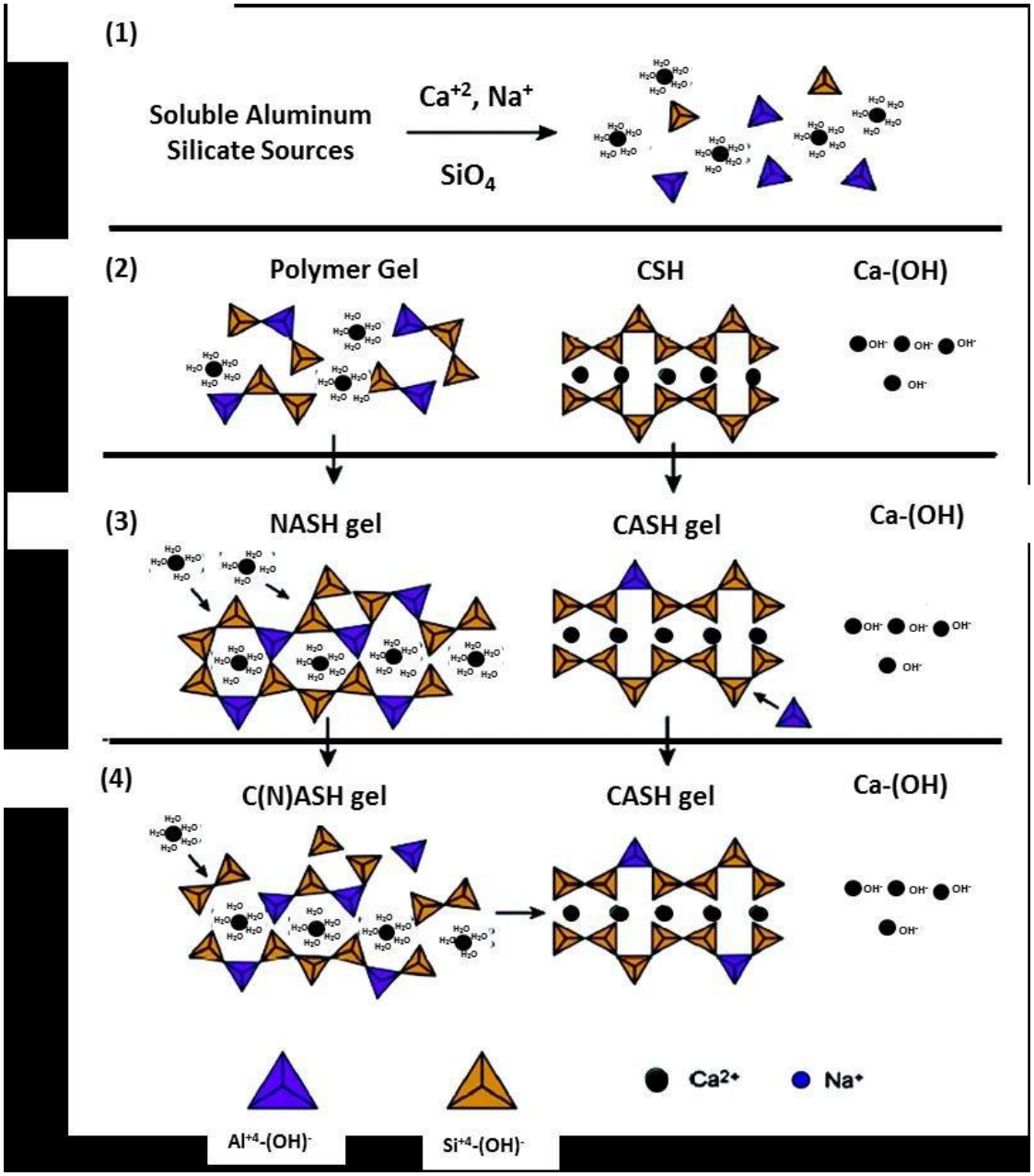

Figure 3: The GP reactions mechanism of an alkali activation process [18]

The choice of the precursor material significantly influences the chemical composition, reaction mechanism and final properties of the GP. Table 5 illustrates the key differences between MK- and BFS-based AAM in terms of reaction mechanisms, durability and applications [17].

Table 5: Comparison MK- and BFS-based AAM

Property	MK-based AAM	BFS-based AAM
Main reaction product	N-A-S-H gels	C-A-S-H gels
Setting and strength gain	Slower; requires heat curing	Faster; ambient curing possible
Chemical durability	Higher; resistant to acids and sulphates	Lower; prone to degradation in aggressive environments
Thermal resistance	High	Lower
Workability	Moderate; dependent on activator ratio	Generally better
Shrinkage	Higher due to rapid alumina dissolution	Lower due to calcium involvement in reaction
Industrial applications	Fire-resistant materials, coatings, waste encapsulation	Concrete, precast elements, road bases

2.8 Effect of MS incorporation in GP and PC matrices

Incorporating MS waste into GPs and PC matrices is critical for radioactive waste immobilization. Recent studies have focused on understanding the interactions between these materials and MS waste in order to enhance the safety and stability of waste encapsulation. GPs have demonstrated potential for immobilizing radioactive contaminants. Their unique composition provides a high-strength and adaptable gel network with a low environmental impact, aligning with radioactive waste disposal requirements. The IAEA has launched a Coordinated Research Project to further understand the performance of GPs in this area and facilitate their deployment [19].

In the context of the [1]PREDIS project, the immobilization of an MS waste stream was investigated. This study aims to determine the feasibility of incorporating MS waste into alkali-activated or blended cementitious matrices. The findings indicated that GPs could effectively encapsulate MS waste, ensuring structural integrity and reducing the leachability of hazardous components [20].

The incorporation of MS waste into PC is challenging. The high solubility of the MS components, particularly halide salts, can interfere with cement hydration, leading to the formation of expansive phases that weaken the matrix. A study on solidification and stabilization technology for radioactive wastes using PC highlighted that while cement can encapsulate various waste streams, it remains susceptible to salt-induced degradation and increased leaching rates over time [21].

[1] PREDIS Project, *Pre-Disposal Management of Radioactive Waste*, accessed May 2, 2025, available at: https://predis-h2020.eu/

Nevertheless, PC can be used for the immobilization of MS waste. However, its effectiveness is highly dependent on the composition of both the cementitious matrix and waste. MS waste primarily composed of sodium carbonate interacts differently with cement-based systems than other types of radioactive solid organic waste. Because of its alkaline nature, MS can act as an additional activator within the matrix, potentially enhancing or hindering hydration reactions depending on its concentration and specific binder formulation [22].

The experimental results showed that both CEM I and CEM III cementitious matrices are capable of incorporating up to 10 wt% MS while still achieving a waste acceptance criterion of at least 10 MPa compressive strength after 28 days. These outcomes demonstrate that PC can be a viable matrix for MS waste immobilization, provided the MS content is carefully limited and the matrix composition is appropriately adjusted [22].

GPs and PC matrices are viable options for incorporating MS waste. Ongoing research is essential to address the challenges related to waste-matrix interactions, optimize formulations for enhanced performance and assess large-scale disposal viability. Future work should focus on refining GP and PC formulations to enhance resistance against salt-induced crystallization, developing hybrid cement-GP composites and conducting extensive field studies to evaluate long-term stability in real-world disposal environments.

Chapter 3
Methodology

This chapter outlines the experimental procedures used to evaluate the influence of MS waste loadings on the performance of GP and PC matrices. The methodology encompasses four main areas: sample preparation, mechanical and workability testing, long-term stability testing, and non-destructive and microstructural analysis.

In the first section, the sample preparation process is described in detail, including the selection of binder compositions, preconditioning of MS waste and design of mix formulations. Various ratios of waste loadings are incorporated into GP and PC systems to systematically assess their effects on the material properties.

Subsequently, the mechanical properties and workability of the prepared samples are evaluated. These tests included measurements of flexural and compressive strength, setting time and viscosity to provide insights into the initial performance and handling behaviour of the mixes.

Long-term stability was assessed through tests designed to simulate extended environmental exposures. Hydration heat measurement is used to monitor the evolution of chemical reactions over time, while carbonation resistance is tested to determine the durability of the matrices under atmospheric CO_2 exposure.

Finally, non-destructive and microstructural characterization techniques are employed to further understand the internal structure and degradation mechanisms. SEM offered visual insights into the morphology and phase distribution of the materials, while ultrasonic testing (UT) provided a means of evaluating the internal defects and overall integrity of the hardened samples.

Together, these methods provide a comprehensive understanding of how MS waste affects the physical, chemical and structural properties of GP and PC systems.

3.1 Sample preparation

The preparation of the PC and GP samples is a critical step in ensuring consistent and reproducible experimental results. This process involves the formulation of different mix designs, mixing, moulding and curing of the samples under controlled conditions. Proper sample preparation is essential for accurately assessing the influence of waste loadings on the properties [23].

One of the key aspects of this study is the preconditioning of MS waste, which is necessary due to its chemical form and potential instability in the final immobilization matrix. Without preconditioning, the salts may remain water-soluble or react undesirably with the binder system, leading to material degradation, increased porosity or even complete disintegration over time. The preconditioning process is designed to chemically stabilize the salts, ensuring their long-term incorporation into the matrix. To evaluate the effects of preconditioning, two additional formulations are prepared without preconditioning. These control samples were used to assess the stability in comparison to preconditioned samples.

After preconditioning, the treated waste is incorporated into nine distinct mix designs, consisting of three PC-based recipes, three MK-based AAM recipes and three BFS-based AAM recipes, each with varying MS loadings.

Each mixture is prepared according to predefined weight ratios of binders, activators and waste to ensure controlled experimental conditions. The mixing procedure follows a standardized sequence to achieve homogeneity and once mixed, fresh pastes are poured into moulds.

This section outlines the specific methodologies used for salt preconditioning, mix-design preparation and sample curing.

3.1.1 Waste material and preconditioning

In this study sodium carbonate (Na_2CO_3) is used as a simplified simulant for MS waste. While Na_2CO_3 is not directly used in MSRs as a fuel carrier or coolant, its chemical behaviour makes it a suitable proxy in immobilization research. Actual MSR systems rely on fluoride- or chloride-based salts such as LiF-BeF_2 (FLiBe), LiF-NaF-KF (FLiNaK) or NaF-ZrF_4, often mixed with fissile or fertile materials like UF_4 or ThF_4. These salts are selected for their favourable thermal and neutron properties, as well as their chemical stability at elevated temperatures [24].

Na_2CO_3 may pose significant challenges when directly incorporated into cementitious or GP matrices. Preliminary experiments in this study indicated that samples containing untreated Na_2CO_3 showed signs of severe degradation after exposure to water or humid conditions. It is possible that a portion of the Na_2CO_3 reacted with the precursor material, leading to partial matrix formation, while the remaining unreacted salt persisted within the structure. Upon exposure to moisture, the residual Na_2CO_3 may have undergone hydration from the monohydrate form ($Na_2CO_3 \cdot H_2O$) to the more hydrated decahydrate ($Na_2CO_3 \cdot 10H_2O$), a transformation known to be associated with volumetric expansion [20].

This expansion can introduce internal stress within the matrix, potentially leading to cracking or structural failure over time. These observations suggest that, without preconditioning, the direct incorporation of Na_2CO_3 in larger amounts may compromise the long-term integrity of the waste form. The literature supports this concern, with successful immobilization of alkali salts often reported only at relatively low concentrations (typically ≤1 wt%) [25]. Although such low loadings may help avoid degradation, they are unlikely to be viable from a practical radioactive waste immobilization standpoint, where a higher percentage of waste incorporation is generally required.

To overcome these challenges, a preconditioning step is introduced to chemically stabilize the Na_2CO_3 before incorporation into the binder systems. The aim is to reduce the solubility of the salt, limit its ability to hydrate and prevent structural damage due to expansive reactions during curing or exposure to moisture. The preconditioning method involves a chemical reaction in an aqueous, alkaline environment.

The procedure begins with dissolving calcium hydroxide ($Ca(OH)_2$) in water to create a high alkaline solution. $Ca(OH)_2$ dissociates into Ca^{2+} and OH^- ions, significantly increasing the pH to about 12.5. The resulting solution provides a reactive environment for carbonate stabilization. Na_2CO_3 is gradually added to the solution under continuous stirring. In this alkaline medium, carbonate ions (CO_3^{2-}) can react with Ca^{2+} to form calcium carbonate ($CaCO_3$), which is a sparingly soluble and stable compound. This reaction removes excess free carbonate from the solution and limits the availability of the reactive, water-soluble species in the final waste form.

By promoting the in situ formation of a less soluble solid phase ($CaCO_3$) while leaving Na^+ ions in solution, this preconditioning step improves the compatibility between the salt and the host binder and reduces the risk of delayed hydration reactions and associated material expansion.

The preconditioned waste is incorporated into a series of nine distinct formulations to evaluate its impact on different binder systems. These include:

- Three PC based formulations;
- Three MK-based AAM formulations;
- Three BFS-based AAM formulations.

Each formulation series includes variations in waste loading, allowing for a systematic investigation of the influence of salt concentration and preconditioning on the chemical stability, mechanical properties and microstructural integrity of the resulting materials.

3.1.2 Mix design

Within each binder category, three variations were formulated with increasing waste level. Each mix design family includes a reference sample without waste (denoted "_00"), as well as two formulations containing increasing amounts of preconditioned salt waste (denoted "_10" and "_15" indicating a waste loading of respectively 10 and 15 %).

Despite differences in chemical composition, all mixes were prepared using a standardized procedure to ensure reproducibility. The mixing times, curing conditions and mould sizes were kept constant. The use of sand as a filler component provided dimensional stability and a better comparison with real-world mortars used in waste encapsulation scenarios.

This structured mix design matrix allows for targeted analysis of:

- The role of binder type in immobilization performance,
- The effect of increasing waste content on mechanical and chemical stability,
- The interaction between preconditioned salt and the different matrices.

3.1.2.1 Cement-based formulations (CEM_xx)

These systems use:

- CEM I as the primary reactive precursor, providing the necessary calcium silicate phases for hydration.
- $Ca(OH)_2$ acts as an activator, initiating the hydration reactions of the cement and forming C-S-H, which is the key binding phase.
- Limestone filler (LF) and SF as supplementary components. LF acts as an inert filler, while SF contributes additional pozzolanic reactivity, improving the strength and durability by reacting with $Ca(OH)_2$ to form additional C-S-H.
- BFS is included as a supplementary cementitious material (SCM), that reacts with water and contributes to the formation of additional C-S-H.

The composition of the different CEM mixes can be found in Table 6 and Table 7.

Table 6: CEM-based formulations in mass [g]

Mix	CEM I	LF	SF	BFS	Water	Sand	$Ca(OH)_2$	Waste
CEM_00	158	197	171	723	1052	634	66	0
CEM_10	133	167	145	612	842	574	228	300
CEM_15	121	152	132	557	738	542	309	450

Table 7: CEM-based formulations in weight %

Mix	CEM I	LF	SF	BFS	Water	Sand	$Ca(OH)_2$	Waste
CEM_00	5,26%	6,56%	5,70%	24,09%	35,05%	21,13%	2,20%	0,00%
CEM_10	4,43%	5,56%	4,83%	20,39%	28,06%	19,13%	7,60%	10,00%
CEM_15	4,03%	5,06%	4,40%	18,56%	24,59%	18,06%	10,30%	15,00%

3.1.2.2 BFS-based AAM formulations (BFS_xx)

These systems use:

- BFS as the sole reactive precursor, it contains calcium, alumina and silica. BFS is reactive in alkaline environments.
- A sodium silicate solution ($Na_2O{\cdot}2SiO_2$) is used as the chemical activator. This high-pH solution dissolves the slag structure, releasing Ca^{2+}, Al^{3+} and Si^{4+} species that re-polymerize to a C-A-S-H structure.
- Water is present as part of the activator solution and is also added to regulate the workability if the mix and promote ion transport during the activation and setting processes.

The compositions of different BFS-based AAM mixes are listed in Table 8 and Table 9.

Table 8: BFS-based AAM formulations in mass [g]

Mix	BFS	$Na_2O{\cdot}2SiO_2$	Water	Sand	$Ca(OH)_2$	Waste
BFS_00	1371 g	46 g	836 g	747 g	0 g	0 g
BFS_10	1157 g	39 g	705 g	630 g	170 g	299 g
BFS_15	1049 g	35 g	639 g	572 g	256 g	449 g

Table 9: BFS-based AAM formulations in weight %

Mix	BFS	$Na_2O{\cdot}2SiO_2$	Water	Sand	$Ca(OH)_2$	Waste
BFS_00	45,70%	1,53%	27,87%	24,90%	0,00%	0,00%
BFS_10	38,57%	1,30%	23,50%	21,00%	5,67%	9,97%
BFS_15	34,97%	1,17%	21,30%	19,07%	8,53%	14,97%

3.1.2.3 MK-based AAM formulations (MK_xx)

These systems use:

- MK is a reactive aluminosilicate precursor as it provides a high-purity source of reactive silica and alumina.
- $Na_2O{\cdot}2SiO_2$ as the alkaline activator. Under high-pH conditions, the activator dissolves the aluminosilicate framework of MK, releasing reactive species that undergo polycondensation to form a three-dimensional N-A-S-H gel.
- Water is present both as a component of the activator and added separately to adjust the rheology and facilitate the dissolution and gelation reactions.

The composition of the different MK-based AAM mixes are listed in Table 10 and Table 11.

Table 10: MK-based AAM formulations in mass [g]

Mix	MK	$Na_2O{\cdot}2SiO_2$	Water	Sand	$Ca(OH)_2$	Waste
MK_00	675 g	576 g	1005 g	744 g	0 g	0 g
MK_10	571 g	487 g	851 g	630 g	167 g	293 g
MK_15	520 g	443 g	774 g	573 g	251 g	440 g

Table 11: MK-based AAM formulations in weight %

Mix	MK	$Na_2O{\cdot}2SiO_2$	Water	Sand	$Ca(OH)_2$	Waste
MK_00	22,50%	19,20%	33,50%	24,80%	0,00%	0,00%
MK_10	19,04%	16,24%	28,38%	21,01%	5,57%	9,77%
MK_15	17,33%	14,76%	25,79%	19,09%	8,36%	14,66%

3.1.2.4 Comparison of binder systems

Table 12 presents an overview of the key differences between the three binder systems.

Table 12: Comparison of binder systems

Aspect	CEM-Based System	BFS-Based AAM	MK-Based AAM
Reactive precursor	CEM I, BFS, SF, LF	BFS	MK
Activator	Water	$Na_2O{\cdot}2SiO_2$, salt waste	$Na_2O{\cdot}2SiO_2$, salt waste
Binding phases	C-S-H	C-A-S-H	N-A-S-H

3.1.3 Mixing, casting and curing

A standardized mixing protocol was followed for both GP- and PC-based formulations to ensure homogeneity, repeatability and consistency across all samples. Although the general steps were similar, the sequence and handling were tailored to the specific behaviour of each material system.

A preconditioning step of the MS was performed one day prior to sample preparation, during which the salt waste was mixed with water and calcium hydroxide ($Ca(OH)_2$) to promote the in situ formation of calcium carbonate ($CaCO_3$). For samples prepared without salt waste, this preconditioning step was not required.

3.1.3.1 BFS- and MK-based AAM systems

The mixing procedure for GP pastes was as follows:

1. Both the mixing paddle and bowl were moistened prior to mixing to minimize material loss due to adhesion.

2. The dry materials expect sand are placed in the mixing bowl, followed by salt solution or water.
3. The mixture was stirred for 2 minutes at low speed.
4. The sides of the mixing bowl were scraped using a spatula to ensure that all materials were properly incorporated.
5. The sand is then added and the paste was mixed again for 2 min at low speed.
6. The bowl was once more scraped down to eliminate unmixed residue.
7. Finally, the mixture was blended for 1 min at high speed to achieve homogeneous and workable consistency.

After mixing, the fresh properties of the GP paste, such as the hydration heat, setting time, UT and viscosity were assessed immediately. The mixture is cast into moulds for curing to evaluate its mechanical strength and microstructural characteristics.

3.1.3.2 PC-based systems

For the PC-based formulations, the mixing sequence was slightly different:

1. Both the mixing paddle and bowl were moistened prior to mixing to minimize material loss due to adhesion.
2. All dry materials expect sand are mixed for 2 minutes at low speed.
3. The mixing bowl was scraped to ensure complete blending of powders.
4. The liquid phase (salt solution or water) is added, followed by 2 min of mixing at low speed.
5. After another scraping step, the mixture was stirred for an additional 2 min while sand was gradually incorporated.
6. The mixing process concluded with 1 minute at high speed.

As with the GP systems, the fresh properties of the cement paste were evaluated immediately after mixing and the material was cast into moulds.

3.1.3.3 Casting and curing

After mixing, the fresh pastes were poured into pre-cleaned and lightly oiled moulds with standardized dimensions (40 × 40 × 160 mm^3). The paste was poured into the mould and once the mould was completely filled, it was tapped to release the entrapped air and minimize void formation.

The samples were kept in the moulds for approximately one week under ambient laboratory conditions, at a constant temperature of 20 °C and a relative humidity (RH) of 60%. After this initial curing period, the specimens were demoulded and transferred to a curing bench, where they were stored at 20 °C and ≥95% RH for 28 days.

3.2 Mechanical and workability testing

The mechanical strength and workability of PC and GP are critical parameters for determining their suitability for radioactive waste immobilization. These properties influence not only the structural integrity and durability of the material but also the practicality of handling and application in real-world scenarios. Ensuring that these materials meet the required mechanical performance criteria is essential for long-term stability in storage and disposal environments.

The mechanical performance is assessed through flexural and compressive strength testing, which provides quantitative data on the ability of the material to withstand tensile and compressive forces. These strength parameters are key indicators of material durability and structural performance, particularly under mechanical stresses encountered during handling, transport and long-term use.

In addition to the strength, workability plays a crucial role in the mixing, casting and placement of these materials. The setting time determines the time frame available for processing and shaping the material before it hardens, which is particularly important when considering large-scale applications. Furthermore, viscosity testing provides insights into the flow behaviour of the fresh mix, ensuring that the material can be efficiently cast into moulds or forms without segregation or excessive stiffening.

3.2.1 Flexural and compressive strength

Flexural and compressive strength are key mechanical properties used to evaluate the performance and durability of PC and GP. These properties are typically determined using standardized methods to ensure the consistency and comparability of the results. One such standard is EN 196-1, which outlines procedures for testing the mechanical strength of cement-based materials.

According to EN 196-1, flexural and compressive strengths are measured using prismatic mortar specimens with dimensions of 40 mm x 40 mm x 160 mm. The test begins with flexural strength measurement (Figure 5), in which each specimen is subjected to a three-point bending test. This test determines the ability of the material to resist failure under a bending load and reflects its performance under tensile stresses that can occur in real-world applications.

After the flexural test, the two broken halves of each prism are used to measure the compressive strength (Figure 4). These halves are subjected to a uniaxial compressive load until failure, providing a measure of the capacity of the material to withstand compressive forces.

In practice, two prisms were tested per recipe for the flexural strength measurements. Each prism yields two broken halves after the three-point bending test, resulting in four individual samples for the compressive strength tests.

All samples will be tested after 28 d of curing, allowing sufficient time for the systems to develop their strength. The results will be compared to predefined acceptance criteria, which require a minimum of 1 MPa for the flexural strength and 8 MPa for the compressive strength, as specified by the internal NIRAS guidelines [26]. These benchmarks ensure that the materials meet the mechanical performance standards required for effective and safe immobilization applications.

Figure 5: Flexural strength testing

Figure 4: Compressive strength testing

3.2.2 Setting time measurement

The setting time of cement defines the transition of cement from a workable paste to a hardened material capable of bearing loads. It is typically divided into two stages: the initial setting time, which refers to the point at which the cement paste begins to lose its plasticity after mixing with water and the final setting time, which marks the moment when the paste completely loses plasticity and begins to develop a measurable degree of structural strength. According to standard specifications, the initial setting time of PC should not be earlier than 45 minutes, while the final setting time should not exceed 6.5 hours. The initial setting time should not be too fast to ensure sufficient working time for operations such as casting and the final setting time should not be excessively long, because the cement needs to complete its setting and hardening promptly after pouring and tamping to allow the next stage of work [27].

In this study, the setting time is determined using the Vicat apparatus, following the standardized procedure described in EN 196-3:1990 (Figure 6). This method involves preparing a cement paste of standard consistency and periodically measuring its resistance to penetration using a standardized needle. The initial setting time is defined as the moment when the needle no longer penetrates beyond a specified depth, whereas the final setting time is recorded when the needle fails to visibly indent the surface of the paste. The setting process must be conducted under controlled conditions, at a temperature of 20 °C ± 3 °C, to ensure reliable and repeatable results.

Figure 6: Vicat apparatus [28]

3.2.3 Viscosity measurement

Viscosity represents the resistance to flow and deformation under shear stress. In cementitious systems, viscosity directly influences the workability of the fresh mix, affecting the ease of mixing, pouring, casting and finishing before setting occurs.

Understanding the viscosity behaviour is essential for optimizing both processing and application, ensuring that the material can be efficiently handled while achieving proper filling of moulds, effective compaction and uniform encapsulation of waste materials. Furthermore, the evolution of viscosity can influence the setting kinetics, microstructure development, and ultimately the mechanical performance and durability of both PC and GP-based immobilization matrices.

For PC, the viscosity depends on factors such as the water-to-cement ratio, particle fineness and the presence of admixtures. Proper control of viscosity ensures that the paste is neither too fluid, which can cause segregation and bleeding, nor too stiff, which can hinder placement and compaction. In GPs, viscosity is influenced by the composition and concentration of alkaline activators, solid-to-liquid ratio, precursor particle size and temperature. Unlike PC, GP systems can be highly sensitive to these variables, resulting in significant changes in flow behaviour over time [29].

To quantify the viscosity of different immobilization mixes, a rotational viscometer (Figure 7) is used to measure the viscosity at varying shear rates, providing a detailed profile of the rheological behaviour of the paste. Measurements will be taken at three time points after mixing: 0, 30 and 60 min, allowing for the assessment of how viscosity evolves over time. This is particularly important in immobilization applications, where sufficient workability must be maintained during processing, however rapid stiffening may be desired for structural stability.

Figure 7: Viscosity Measurement

3.3 Long-term stability testing

The long-term stability of PC and GP materials used for radioactive waste immobilization depends not only on their mechanical properties but also on their thermal behaviour and chemical durability. Two critical factors that influence this stability are the hydration heat evolution and carbonation resistance. Understanding these processes is essential for predicting the material performance under different environmental conditions and ensuring the integrity of the immobilization matrix over time.

Hydration heat measurements provide insights into the exothermic reactions occurring during the setting and hardening of the PC and GP binders. Excessive heat release during hydration can lead to thermal cracking, increased porosity and microstructural defects, potentially compromising the long-term durability of the material.

Carbonation resistance testing assesses the susceptibility of the material to carbon dioxide (CO_2)-induced degradation, which can alter its chemical composition and mechanical properties over time. Carbonation of PC materials primarily leads to pH reduction, which may affect the stability of the immobilized waste. In GPs, it can influence the gel structure and long-term durability. Because carbonation can be accelerated under specific storage conditions, evaluating its resistance to this process is crucial for determining the suitability of each formulation for waste immobilization applications.

This section outlines the methodologies used to measure hydration heat evolution and carbonation resistance, ensuring a comprehensive assessment of the thermal and chemical stability of the prepared materials.

3.3.1 Hydration heat measurement

When water is added to the cement, a chemical process known as hydration begins. This reaction is exothermic, meaning that it releases heat as the cement components interact with water and begins to harden. This released energy is called the hydration heat and it plays a crucial role in understanding how cement sets and gains strength over time. Monitoring hydration heat helps assess the performance of cementitious materials, the impact of any additives and potential risks such as thermal cracking.

An isothermal calorimeter is used to measure the hydration heat accurately. As the name suggests, it maintains the sample at a constant temperature while continuously measuring the heat flow produced by the hydration reaction. The data from this process typically shows a heat flow versus time curve, providing insights into how quickly the material reacts and sets.

One such device, the Calmetrix i-Cal 8000 HPC (Figure 8), is a high-performance isothermal calorimeter designed specifically for cement, mortar and concrete testing. It allows up to eight samples to be tested simultaneously and is highly sensitive and capable of detecting even very small heat flows. This makes it especially useful for studying materials such as GPs or cement mixes. By maintaining strict isothermal conditions, the i-Cal 8000 HPC provides accurate, real-time data on the kinetics of hydration, helping to understand how different compositions and additives influence the setting behaviour and long-term material properties [30].

In the context of this research on MS waste loadings in GP and PC, the use of an isothermal calorimeter enables a comparative analysis of how varying waste concentrations influence hydration heat release. The resulting data can indicate whether the presence of MS waste accelerates or delays the hydration process, thereby providing insight into its effects on the overall performance of the material. This information is essential for identifying any necessary modifications to the formulation to ensure the safe, stable and effective immobilization of radioactive waste.

Figure 8: Calmetrix i-Cal 8000 HPC [30]

3.3.2 Carbonation resistance testing

Carbonation resistance testing is used to assess the durability of cementitious materials by evaluating their susceptibility to carbonation. This is a chemical reaction between atmospheric CO_2 and the components of the material. In PC and BFS-AAM, carbonation primarily involves the reaction of $Ca(OH)_2$ and C–S–H with CO_2, resulting in the formation of $CaCO_3$ [31]. This process leads to a reduction in alkalinity, which, in the case of reinforced concrete, can negatively impact durability due to the increased risk of steel corrosion. In unreinforced systems, however, carbonation may lead to densification and even an improvement in mechanical properties [32].

To assess carbonation resistance, samples are typically exposed to an accelerated carbonation environment with elevated CO_2 levels (1%) under controlled conditions (approximately 20°C and 60% RH). After a defined exposure period, the depth of carbonation is measured using phenolphthalein indicator, which turns purple-pink in non-carbonated areas (pH > 9) and remains colourless in carbonated zones (pH < 9). This allows for visual determination (Figure 9) of how far carbonation penetrated the material. The mechanical strength of the samples will also be evaluated.

While this method is effective for PC and BFS-based AAM, it is not suitable for MK-based AAM. The lack of free Ca limits the formation of solid carbonate phases during carbonation. Instead, any interaction with CO_2 typically involves alkali cations such as Na^+ or K^+, which can form alkali carbonates such as Na_2CO_3 or K_2CO_3. However, these reactions had a minimal impact on the overall pH of the system. Unlike PC, where carbonation leads to a clear reduction in pH due to the depletion of $Ca(OH)_2$, the pH in MK-AAMs remained uniformly high throughout the matrix, even after CO_2 exposure. This sustained high alkalinity renders traditional carbonation detection methods, such as phenolphthalein staining, ineffective. MK-based AAMs typically maintain a pH well above this threshold, even after partial carbonation, no visible colour change occurs. As a result, this method fails to indicate the carbonation depth or intensity [33].

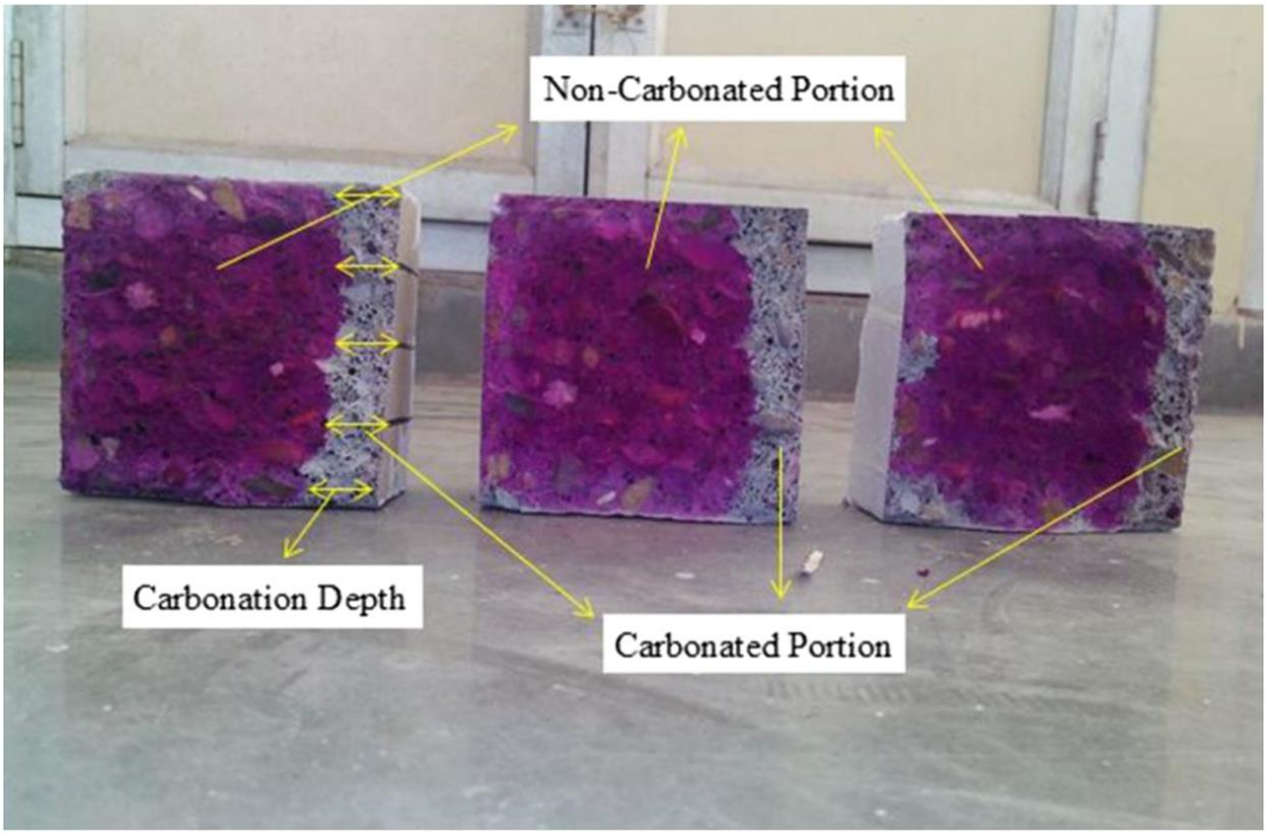

Figure 9: Carbonation depth [34]

After initial curing for 28 days under ambient conditions, the samples were divided into two groups: reference and carbonation. The reference samples were stored for an additional 28 days in a controlled environment chamber maintained at 20 °C and 60% RH, under atmospheric CO_2 levels (~0.04%). The carbonation samples were exposed for 28 days to an accelerated carbonation regime in a carbonation chamber set to the same temperature and humidity, but with an elevated CO_2 concentration of 1%. This accelerated exposure was used to simulate the long-term effects of atmospheric CO_2 on the materials within a shortened time frame, allowing for the assessment of carbonation-related changes in a practical and controlled manner.

In the laboratory, carbonation resistance was tested using three prism samples per binder system: two carbonation and one reference. Flexural strength was measured on the two carbonated samples, followed by compressive strength testing on three of the resulting broken halves. The remaining half from one of the broken prisms was used to determine the carbonation depth using the phenolphthalein method. The reference prism was tested similarly, with one half used for compressive strength and the other for carbonation depth. Carbonation depth was measured on all four cut sides of the prism fragment, with four measurements taken per side to improve accuracy. Additionally, the mass and length of both the carbonated and reference samples were monitored over time to evaluate dimensional and weight changes associated with carbonation.

3.4 Non-destructive and microstructural analysis

In addition to the mechanical strength and chemical durability, the microstructural characteristics of PC and GP materials play a crucial role in their long-term performance and stability. A well-developed microstructure contributes to low porosity, improved mechanical properties and enhanced resistance to degradation, all of which are essential for ensuring safe immobilization of radioactive waste. This section focuses on non-destructive UT and detailed microstructural analysis using SEM and nitrogen adsorption (NA).

UT is a non-destructive evaluation method used to assess the density, uniformity and internal defects of hardened materials. By measuring the velocity of the ultrasonic waves passing through the sample, insights into the structural integrity, porosity distribution and potential cracks can be obtained. This technique is particularly valuable for assessing how different waste loadings and preconditioning treatments influence the compactness and homogeneity of the final material.

SEM provides high-resolution imaging of the morphology and microstructural development of the material. This analysis helps to identify the formation of crystalline or amorphous phases, distribution of waste particles and presence of microcracks or pores. By comparing SEM images of different formulations, it is possible to assess how waste incorporation affects the final structure.

NA is used to quantify the specific surface areas and porosities of the samples. The porosity of the matrix influences the permeability, mechanical strength and long-term stability, making NA essential for understanding how different mix designs impact the overall durability.

This section details the experimental procedures for UT, SEM imaging and NA analysis, providing a comprehensive evaluation of the internal structure and physical characteristics of the prepared materials.

3.4.1 Ultrasonic testing

The method involves sending ultrasonic waves, typically pulse waves in the range of 20 kHz to several MHz, through a sample using transducers. One transducer acts as a transmitter, emitting the wave, whereas the other acts as a receiver, detecting the wave after it passes through the material. The key measurement is the time required for the ultrasonic pulse to travel through the sample, known as the pulse transit time (Figure 10) [35].

In the setup used were the transducers positioned with a fixed distance of 40 mm between them. The UT was monitored with a measurable upper limit of 8000 m/s to ensure accurate detection across a wide range of material stiffnesses. A dynamic elastic modulus threshold was set at 500 m/s; values below this were considered either artefacts or indications of severely compromised material integrity and were thus excluded from the dataset.

Higher velocities generally indicate denser, more compact materials with fewer internal defects, whereas lower velocities can signal porosity, cracks or weak bonding within the matrix. UT can be correlated with compressive strength and is especially useful for monitoring strength development over time, such as during curing.

UT in GPs helps assess how factors such as waste loading, activator concentration and curing conditions affect the internal structure without damaging the sample. It is also beneficial for comparing GP and PC materials, offering insights into their microstructural differences and durability potential.

Overall, UT provides a fast, reliable and non-destructive method for evaluating the quality and integrity of cementitious materials.

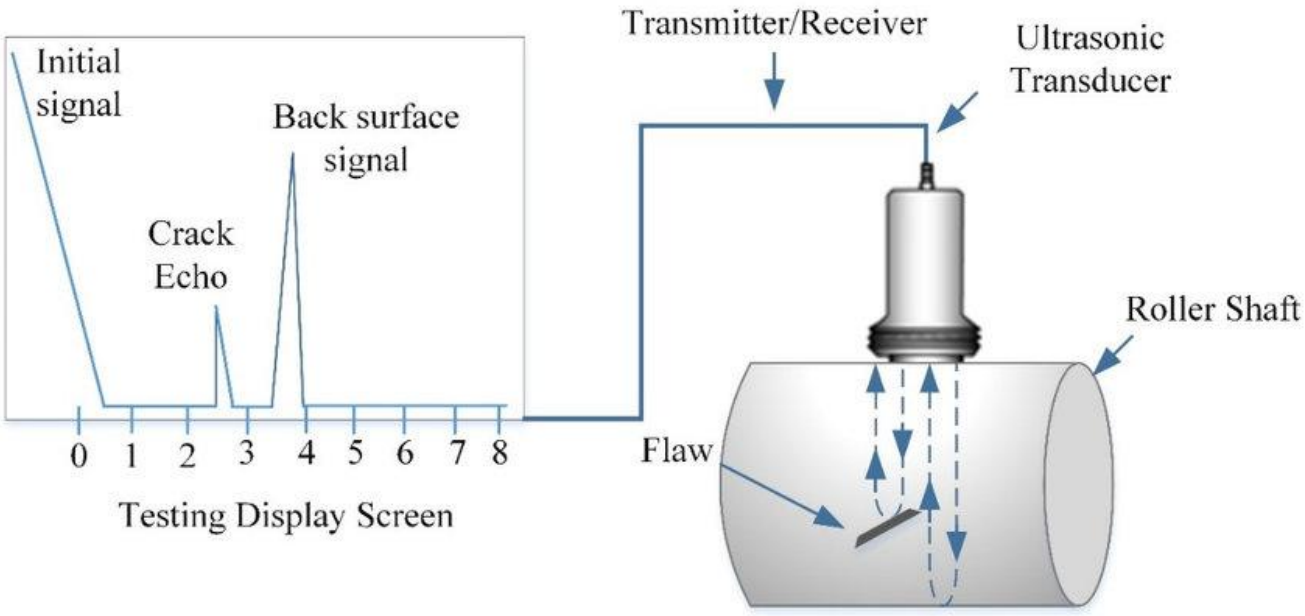

Figure 10: UT [35]

3.4.2 Microstructural analysis

Microstructural analysis plays a crucial role in understanding the internal structure of cementitious materials, as their microstructure directly influences key properties such as strength, durability and porosity. SEM and NA are two widely used techniques for investigating microstructure are SEM and NA.

SEM provides high-resolution images of the surface of materials by scanning a focused beam of electrons across the sample. This interaction generates detailed information about the morphology of the material, including the shape and size of the reaction products, presence of microcracks or voids and distribution of different phases [36]. In PC, SEM typically reveals a mixture of crystalline structures and gel phases, such as C–S–H, whereas GPs often exhibit a more amorphous, gel-like matrix formed by N-A-S-H. Thus, SEM allows for direct visual comparison of the influence of different formulations, curing conditions or waste additions influence the development and integrity of the binder matrix. A visual representation of SEM is shown in Figure 11.

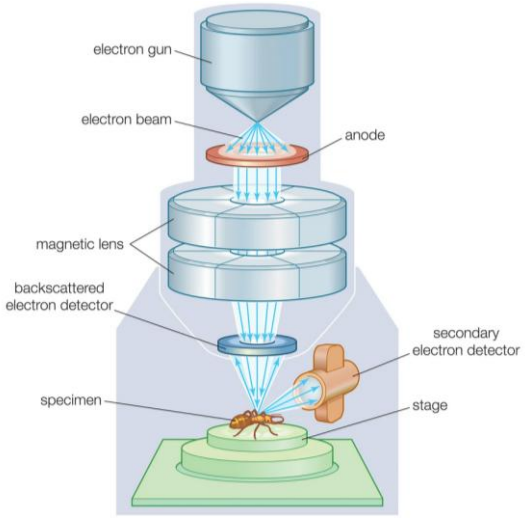

Figure 11: SEM [36]

In addition to SEM, NA analysis offers a quantitative assessment of the porous structure at the nanometre scale. The specific surface area, pore volume and pore size distribution are determined by measuring the amount of nitrogen gas adsorbed onto the surface of the material at varying pressures. In both PC and GP materials, NA helps track how changes in the mix composition or waste content influence the pore structure, which is especially important for assessing long-term durability and waste containment performance. A visual representation of NA is shown in Figure 12.

NA was used to determine the specific surface area and pore size distribution of the different binder systems. For each formulation, two measurements were performed. Approximately 1 to 2 grams of sieved material were used per test. Although the analysis was conducted externally, the results provide valuable insight into how formulation changes influence porosity, which is relevant for long-term durability and waste immobilisation performance.

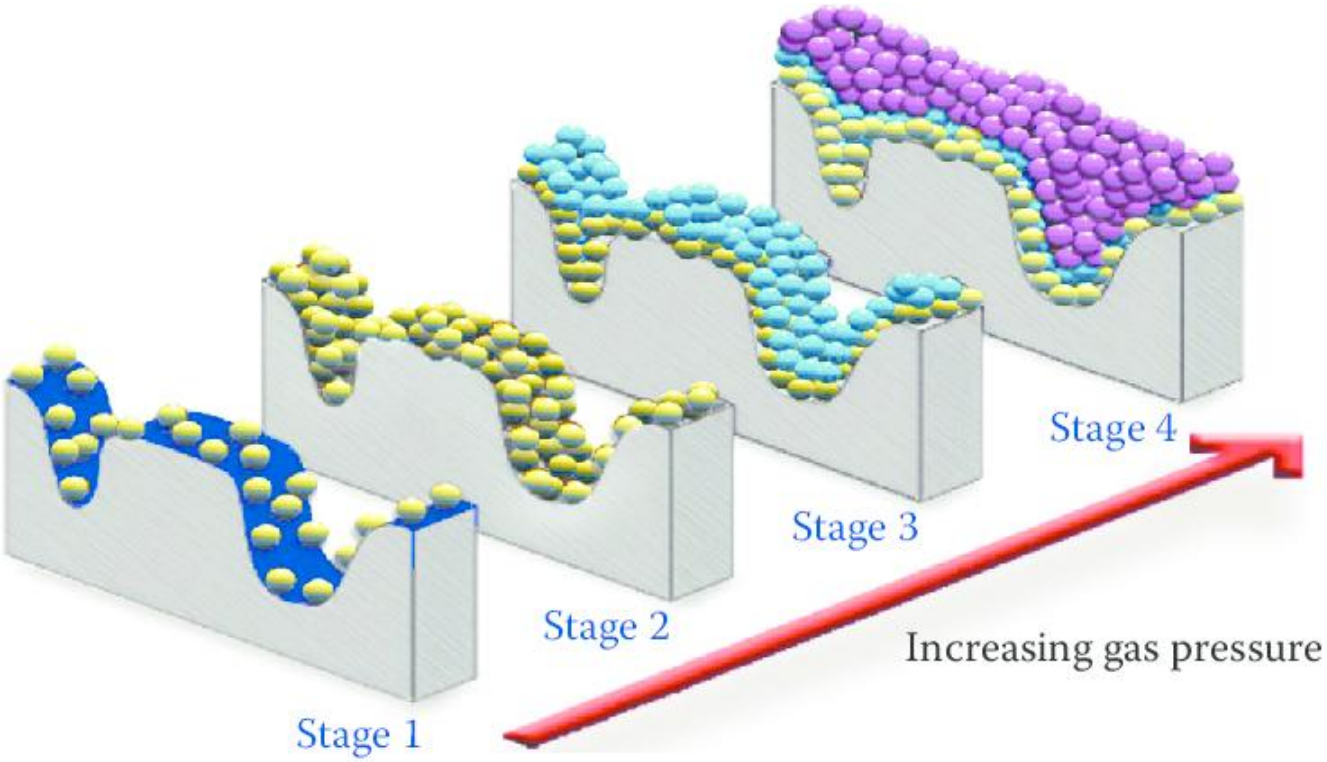

Figure 12: NA: Stage 1—the start of adsorption at low pressure stage; Stage 2—with increasing nitrogen pressure, adsorption molecules increase to form a monolayer ; Stage 3—further increasing nitrogen pressure forms multilayer coverage; BET (Brunauer–Emmett–Teller) theory can be used to determine the surface area; Stage 4—a further increase in nitrogen pressure causes the saturation of all pores [37].

SEM and NA provide a comprehensive understanding of the microstructure of cementitious systems. While SEM reveals visual details of the morphology and phase development, NA delivers quantitative data on the surface area and porosity, both of which are essential for correlating microstructural features with mechanical properties and durability. This combined analysis is particularly valuable for optimizing PC and GP formulations for safe and effective waste immobilization, ensuring material stability over extended periods.

Chapter 4
Results

This chapter presents the experimental results obtained to evaluate the effects of MS waste loadings on the mechanical, workability, stability and microstructural properties of GP and PC matrices. Nine mix designs were investigated, representing three binder systems, PC (CEM), BFS-based AAM (BFS) and MK-based AAM (MK), each recipe is tested with 10 wt% and 15 wt% preconditioned MS waste loadings and compared to a 0 wt% reference to evaluate the influence of MS on material performance. The tests were conducted in accordance with standardized protocols as detailed in Chapter 3.

The first sections of this chapter focus on mechanical performance, including compressive and flexural strength, followed by the assessment of workability characteristics such as setting time and viscosity. Subsequently, long-term stability indicators, hydration heat and carbonation resistance, are discussed, providing insight into the durability of the different binder systems. Finally, non-destructive and microstructural analyses are used to investigate internal matrix structure and porosity, further informing the material's suitability for radioactive waste immobilization. All findings are discussed comparatively across binder systems to identify trends and assess the influence of MS waste incorporation.

It is important to note that the CEM_00, BFS_00 and MK_00 systems, which did not contain MS, were not designed for immobilisation but rather served as reference formulations to evaluate the influence of MS on the properties of the waste form. Under the tested conditions, both BFS_00 and MK_00 failed to harden, likely due to the absence of MS as an activator. Without sufficient activation, the precursor materials did not develop a hardened structure and these systems were therefore excluded from the subsequent test programme. The CEM_00 system did achieve hardening and was retained in the programme to serve as a reference for assessing the impact of MS on the cementitious waste form properties.

4.1 Mechanical and workability results

This section presents the mechanical performance and workability characteristics of the prepared GP and PC matrices with varying MS waste loadings. The aim is to assess how the incorporation of preconditioned MS influences early-age strength development, processing behaviour and fresh-state rheology of the different binder systems.

4.1.1 Flexural strength

Flexural strength was determined using the three-point bending test, as specified in EN 196-1. Standard mortar prisms (40 × 40 × 160 mm³) were tested after 28 days of curing. The load was applied at the midpoint of each prism until failure. The detailed results of the flexural strength tests can be found in the appendix (Figure 34 – Figure 40).

A global overview of the different CEM-, BFS- and MK-based systems is illustrated in Figure 13, with error bars representing the standard deviation (n = 2). The acceptance criteria of 1 MPa to ensure the mechanical performance standards necessary for effective and safe immobilization applications is given by the horizontal line.

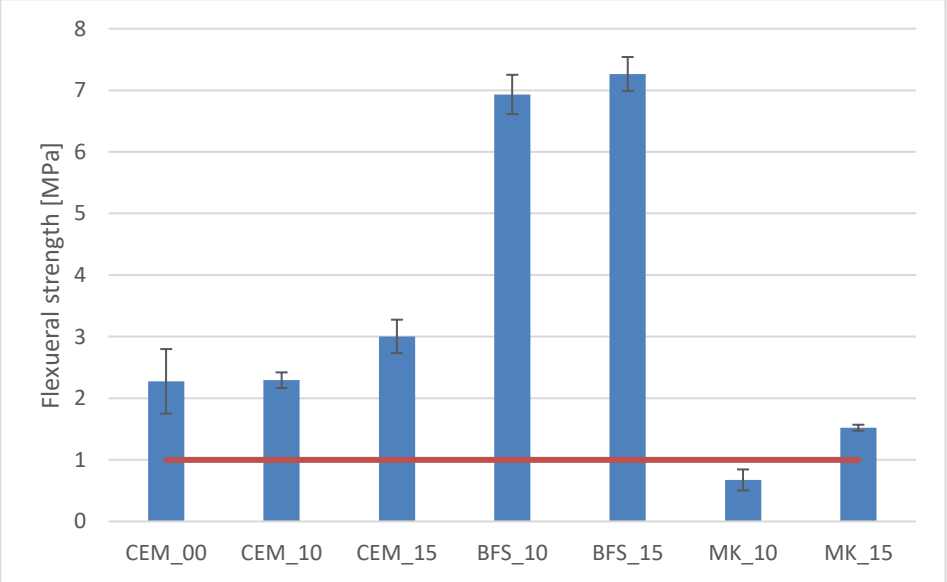

Figure 13: Global overview flexural strength

MK_10 does not meet the acceptance criteria of 1 MPa and thus this recipe is not suitable for the immobilization of radioactive waste, the other recipes are.

4.1.2 Compressive strength

Following the flexural strength tests, the fractured halves of the prisms were used to determine compressive strength, in accordance with EN 196-1. The halves were subjected to a uniaxial load until failure. The detailed results of the compressive strength tests can be found in the appendix (Figure 41 – Figure 47Figure 54).

A global overview of the different CEM-, BFS- and MK-based systems is illustrated in Figure 14, with error bars representing the standard deviation (n = 4). The acceptance criteria of 8 MPa to ensure the mechanical performance standards necessary for effective and safe immobilization applications is given by the horizontal line.

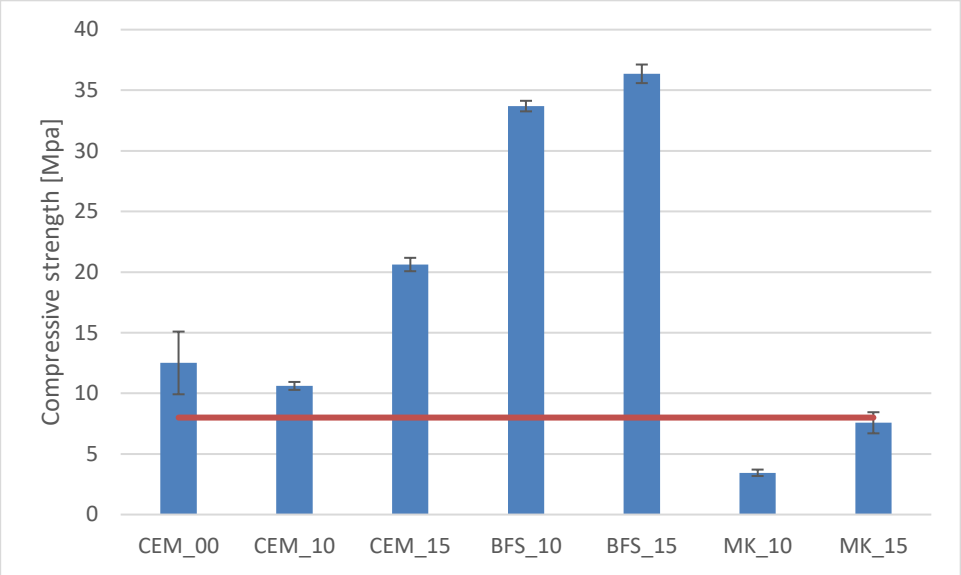

Figure 14: Global overview compressive strength

The recipes MK_10 and MK_15 do not meet the acceptance criteria of 8 MPa and thus these recipes are not suitable for the immobilization of radioactive waste, the other recipes are.

The BFS-based systems exhibited the highest flexural and compressive strength, attributed to the formation of a dense C–A–S–H gel. This reaction is further enhanced by the presence of MS, which increases alkali availability. In contrast, the MK systems developed the lowest strength. MK forms a N–A–S–H gel, which possess inherently lower mechanical performance due to their more open gel structure. The CEM systems displayed intermediate flexural strength. While PC primarily hydrates through its own intrinsic mechanisms, MS appears to act as a secondary activator.

4.1.3 Setting time

The initial and final setting times were measured using the Vicat apparatus, following EN 196-3, where 90 penetrations are made in a certain timeframe. All measurements were performed under controlled conditions at 20 °C ± 3 °C and consistent humidity. The detailed results can be found in the appendix (Figure 48 – Figure 54).

The initial and final setting times of the different systems are depicted in Table 13.

Table 13: Global overview of the setting time

Recipe	Initial setting time [hours]	Final setting time [hours]
CEM_00	> 30,67	> 30,67
CEM_10	6,39	8,45
CEM_15	1,39	2,58
BFS_10	< 3,00	4,47
BFS_15	< 3,00	< 3,00
MK_10	5,40	18,98
MK_15	3,78	16,58

The setting time measurements for the CEM-, BFS- and MK-based systems reveal significant differences in the early-age behaviour of the materials.

The CEM_00 system exhibited a setting time exceeding 30 hours, indicating extremely slow hydration under the given conditions. This slow reaction was expected, as the MS, which acts as an activator in the other systems, was absent in this formulation. The initial and final setting times could not be determined within the test duration, as the maximum of 90 penetrations occurred before the setting. The final measurement was taken after 30,67 hours, indicating that the initial setting time is likely beyond this point.

Incorporation of MS had a strong accelerating effect on the CEM-based systems. With a 10 wt% MS addition (CEM_10), the initial and final setting times drastically decreased to 6.39 hours and 8.45 hours, respectively. Further increasing the MS loading to 15 wt% (CEM_15) led to even more pronounced acceleration, with initial setting occurring at just 1.39 hours and final setting completed by 2.58 hours. This demonstrates that MS indeed acts as a powerful accelerator in CEM systems.

The BFS-AAM-based systems (BFS_10 and BFS_15) also exhibited very rapid setting behaviour. Both systems initiated setting within three hours, with BFS_15 reaching final setting within the same timeframe (<3 hours). The exact setting time could not be determined due to an incorrect prediction and adjustment in the laboratory setup. BFS systems are already known for their high reactivity and the addition of MS further intensified the early reaction rates, leading to extremely fast setting.

The MK-AAM-based systems (MK_10 and MK_15) behaved differently. Although the addition of MS accelerated the setting, the systems still maintained longer setting times compared to BFS-based counterparts. MK_10 had an initial setting time of 5.40 hours and a final setting time of 18.98 hours. Increasing the MS content to 15 wt% (MK_15) reduced the initial setting time to 3.78 hours and the final setting time to 16.58 hours.

Overall, the results indicate that the effect of MS addition on setting behaviour is strongly dependent on binder chemistry. While MS enables setting in all three types of systems, the speed and extent of setting vary considerably. In the BFS-AAM systems, setting occurred rapidly upon MS addition, with both formulations hardening within a very short time after mixing. The CEM-based systems also set relatively quickly, though with a somewhat longer workable window. In contrast, the MK-AAM systems remained workable for a significantly longer period, even with MS present. These differences have important implications for practical handling: very fast-setting mixes such as BFS_15 may require immediate mixing and casting to avoid premature hardening, whereas MK-based systems offer greater flexibility during processing due to their extended workability.

4.1.4 Viscosity

Viscosity measurements were performed on the fresh pastes using a rotational viscometer to assess rheological properties and temporal evolution of flowability. Each formulation was tested at three time intervals, 0 minutes, 30 minutes and 60 minutes after mixing, to capture changes in workability over time. The detailed results of the viscosity can be found in the appendix (Figure 55 – Figure 57 and Table 23 - Table 25).

Contrary to expectations, the viscosity of the samples decreases over time. A probable explanation for this behaviour is that the systems begin to harden around the spindle of the viscometer, which was observed in the lab. This lead to the formation of a cavity or 'hole' around the measuring element, which reduces resistance during measurement and thus artificially lowers the recorded viscosity.

Due to this measurement artifact, only the viscosity at 0 minutes, before significant structural changes occur, will be used for comparison between the different systems. The global overview of the viscosity can be found in Figure 15.

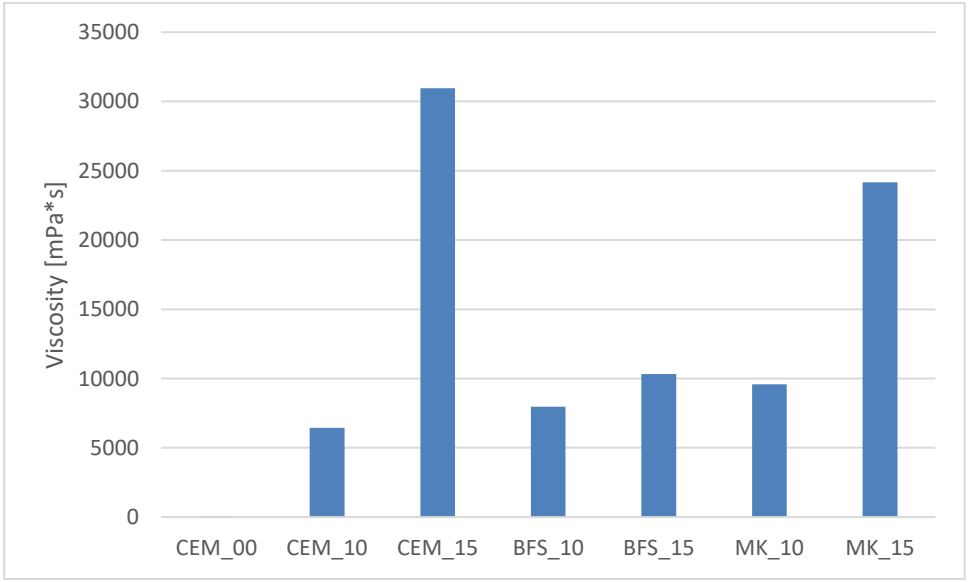

Figure 15: Global overview of the viscosity

A significant range of viscosities was observed between the different systems, highlighting the influence of binder composition and MS addition on workability. The CEM_00 formulation, which did not contain MS and served as a reference for evaluating the influence of salt addition, exhibited a very low viscosity of approximately 60 mPa·s, resulting in an extremely fluid mix. This fluidity was found to be undesirable, as it posed a clear risk of phase separation, bleeding and inadequate encapsulation of MS if it were present. Such low viscosities can compromise the homogeneity and long-term stability of immobilised waste forms.

In contrast, MS-containing systems showed much higher viscosities, ranging from over 6,000 mPa·s to around 30,000 mPa·s. Systems such as CEM_10, BFS_10, BFS_15 and MK_10, with the viscosities between 6,000 mPa·s and 10,000 mPa·s, exhibited excellent workability. They were sufficiently flowable to allow for effective mixing and mould filling. These formulations achieved a favourable balance between processability and immobilisation performance.

The third range, with viscosities exceeding 20,000 mPa·s, includes CEM_15 and MK_15. These systems were considerably stiffer, resulting in poor flow, difficulty in handling and an increased risk of air entrapment and incomplete mould filling. Such conditions could compromise the mechanical integrity and long-term durability of the final waste form, which is undesirable for long-term radioactive waste immobilization.

Based on practical observations during sample preparation and casting, it can be concluded that an initial viscosity window between approximately 5,000 mPa·s and 10,000 mPa·s is ideal for the systems studied. This range was found to offer the best compromise between sufficient workability and effective immobilisation of the MS within the binder matrix.

4.2 Long-term stability testing results

This section presents the results of the long-term stability tests conducted on the PC- and GP-based formulations. The tests include hydration heat evolution and carbonation resistance, both of which provide insight into the thermal reactivity and chemical durability of the waste-containing matrices. These properties are essential for evaluating the long-term performance of materials intended for radioactive waste immobilization.

4.2.1 Hydration heat

Hydration heat was monitored using isothermal calorimetry following mixing. This test was performed on representative samples from each binder system with and without MS waste to observe how salt incorporation affects the exothermic reactions during the early curing phase. The calorimetric data are presented as heat flow (W/g binder) versus time (h), providing information about the rate and intensity of hydration or geopolymerisation reactions. Cumulative heat release curves (J/g binder) are also included to compare total reaction heat across binder types and MS loadings.

For each formulation, the heat flow and the total heat released within the test window are reported. These parameters reflect the kinetics of the binder reactions and any potential retardation or acceleration effects caused by MS addition. The detailed results of the hydration heat can be found in the appendix (Figure 58 – Figure 71).

The global overview of the heat evolution is shown in Figure 16.

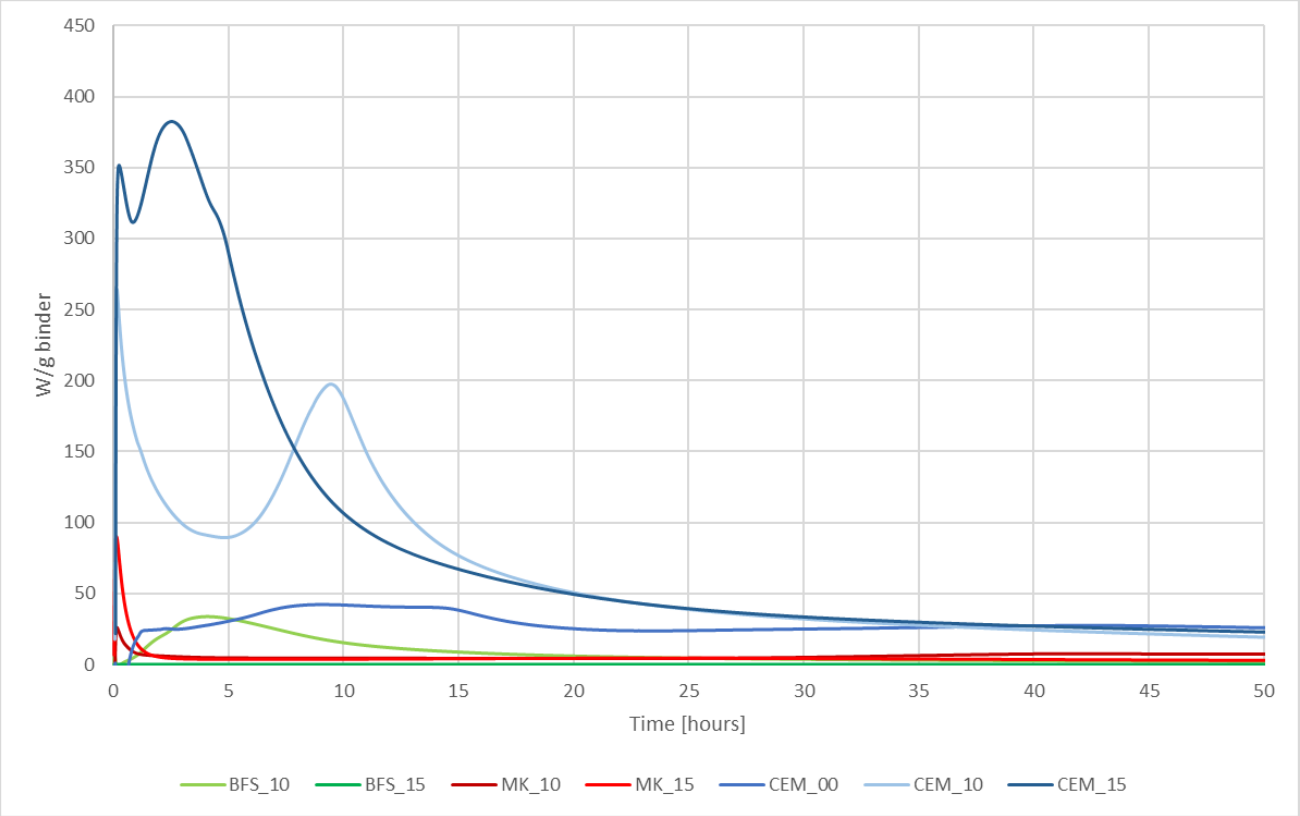

Figure 16: Global overview heat flow

The CEM-based systems (CEM_00, CEM_10 and CEM_15) exhibited the highest and sharpest heat flow peaks immediately after mixing. CEM_15 showed the most pronounced peak, reaching values around 400 W/g binder, followed by CEM_10 and CEM_00. This again confirms that MS addition strongly accelerates the hydration reactions in CEM systems, with higher MS content leading to a more intense and rapid exothermic response. After the sharp initial peak, the heat flow in these systems gradually declined over time, reflecting the continuation of slower hydration processes.

The MK-based systems (MK_10 and MK_15) showed a much lower and broader heat flow curve. Both MK systems exhibited small peaks early on, with MK_15 displaying slightly higher values than MK_10, indicating that MS addition moderately enhanced the reaction rate. However, the overall heat flow remained significantly lower than that of the CEM systems. This gradual and sustained heat evolution is typical for geopolymerisation reactions, where dissolution and reorganisation processes dominate rather than rapid hydration.

In contrast, the BFS-based systems (BFS_10 and BFS_15) displayed only minimal heat flow throughout the measured period. BFS_10 exhibited a small, delayed peak, whereas BFS_15 showed virtually no measurable heat flow. This suggests that under the given conditions, the BFS systems were not effectively activated by the MS addition alone, resulting in very limited reaction kinetics. However, the BFS_15 sample did harden and exhibited high mechanical strength, indicating that significant reaction must have taken place. This suggests that the lack of heat flow in the measurement may have been due to a setup issue or measurement error.

Overall, the heat flow data highlighting the strong dependency of reactivity on binder chemistry. The CEM systems responded rapidly and intensely to MS addition, the MK systems showed moderate acceleration with a broader reaction profile and the BFS systems remained largely inactive. These findings are particularly important for process design, as higher heat release increases the risk of thermal cracking. Controlling the heat evolution is therefore essential to ensure the structural integrity and long-term durability of waste immobilization systems.

The global overview of the total heat release is shown in Figure 17.

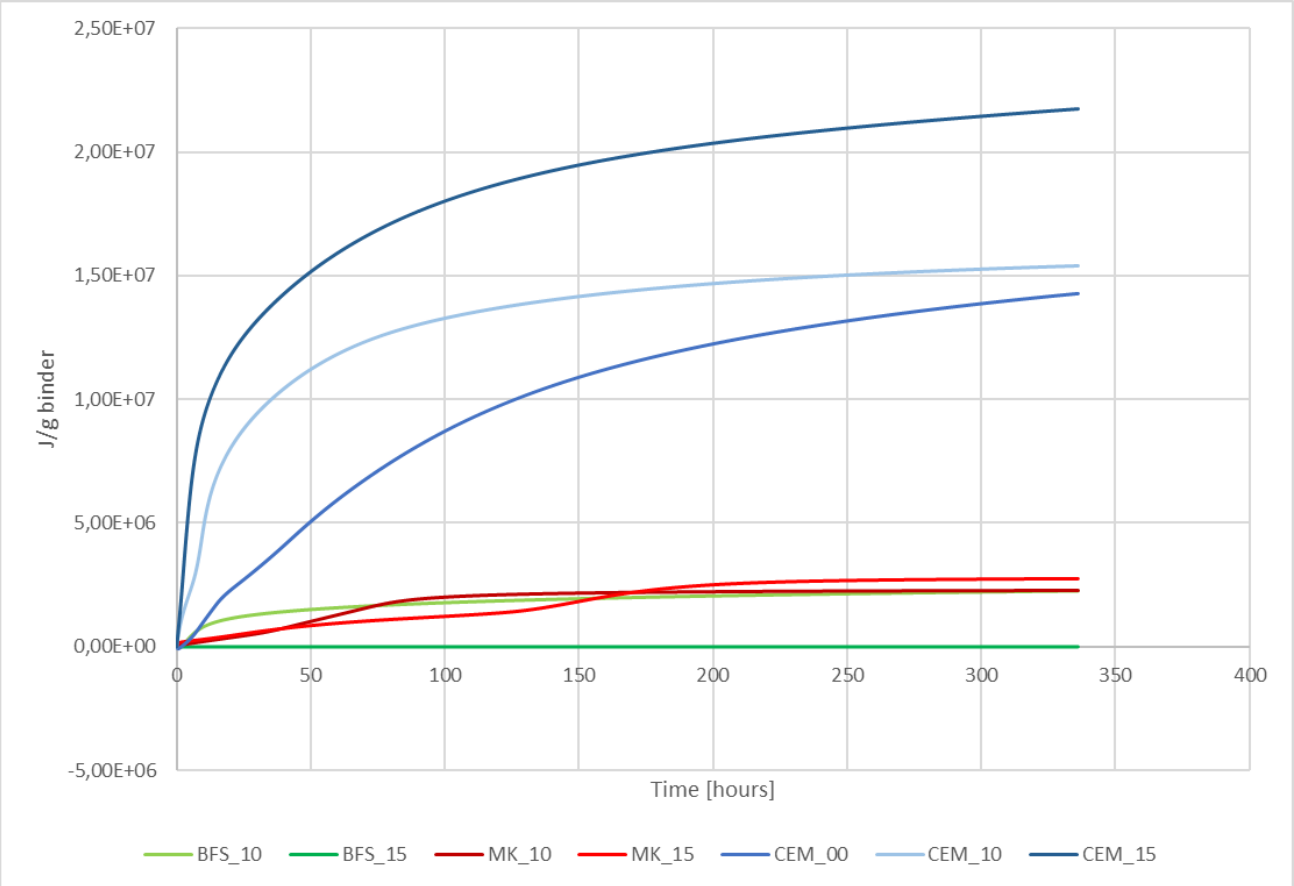

Figure 17: Global overview cumulative heat

The cumulative heat release measurements reveal clear differences between the CEM-, MK- and BFS-based systems. The CEM-based systems (CEM_00, CEM_10 and CEM_15) exhibited the highest overall cumulative heat release. CEM_00, without MS addition, still generated a substantial amount of heat over time. However, the systems containing MS, showed significantly higher heat evolution. This confirms again that MS acts as an effective activator in CEM systems.

In contrast, the MK-AAM-based systems (MK_10 and MK_15) displayed much lower cumulative heat release compared to the CEM systems. The MK systems released heat more gradually, reflecting the slower and less exothermic geopolymerisation reactions typical for MK-based AAMs. Although the addition of MS slightly increased the cumulative heat, as seen by the higher values for MK_15 compared to MK_10, the overall difference remained modest. This suggests that while MS does contribute to accelerating the reaction, it does not induce a dramatic increase in reaction kinetics in MK-based systems.

The BFS-AAM-based systems (BFS_10 and BFS_15) showed limited cumulative heat release throughout the testing period. BFS_10 exhibited a cumulative heat release similar to that of the MK-AAM- based systems, indicating a low but measurable degree of reaction.

In summary, the hydration behaviour is highly dependent on the binder chemistry. The CEM systems responded strongly to MS addition with intense heat evolution, the MK systems showed moderate acceleration and the BFS systems displayed almost no activation. Notably, while the BFS_15 sample did harden and exhibited high mechanical strength, indicating that significant reaction must have occurred, the corresponding hydration heat measurement showed no activity, likely due to a setup issue or measurement error. Therefore, the BFS_15 hydration heat data is excluded from further analysis. These findings are critical when designing formulations for MS waste immobilization, as they highlight the need to carefully tailor the activation strategy to the binder system employed.

4.2.2 Carbonation resistance

Carbonation resistance was evaluated using a combination of mechanical and visual methods. The recipes were exposed to an accelerated carbonation environment with elevated CO_2 levels. After exposure, flexural and compressive strength tests were performed to assess the mechanical impact of carbonation. In addition, carbonation depth was determined using the phenolphthalein indicator method, which visually distinguishes between carbonated (low pH) and non-carbonated (high pH) zones. Cross-sections of the samples were sprayed with the indicator and the carbonation front was measured at multiple points to calculate an average penetration depth. Mass and length were also monitored throughout the exposure period to identify any changes attributable to carbonation-induced volumetric or mass alterations.

All systems were analysed using this visual method. While the MK samples were included in the measurement process, they are predicted to exhibit limited resistance to carbonation and no quantifiable carbonation depths were recorded for these systems, due to the absence of calcium hydroxide and persistent high alkalinity

The results are presented as average carbonation depths (in mm) for each tested formulation, accompanied by representative photographs of the carbonation fronts, where visible. These findings offer a comparative overview of how MS content influences the carbonation resistance and overall durability of the different binder matrices under CO_2 exposure.

4.2.2.1 Flexural strength carbonation

A global overview of the different CEM-, BFS- and MK-based systems is illustrated in Figure 18Figure 18, with error bars representing the standard deviation (n = 2) for the carbonation samples. The reference samples are only tested with one sample and do not have error bars. The acceptance criteria of 1 MPa to ensure the mechanical performance standards necessary for effective and safe immobilization applications is given by the horizontal line. The detailed results of the flexural strength of the carbonation can be found in the appendix (Figure 72 – Figure 78).

For the CEM_00 system, the flexural strength measurements of samples A and B both triggered an 'ALARM' during testing, meaning that no clear point of failure could be determined. Visually, the maximum force applied was approximately 0.203 kN, which corresponds to an estimated flexural strength of around 0.48 MPa. However, as this value is only an approximation and not based on a properly recorded failure event, the flexural strength results for CEM_00 will not be considered further in the analysis.

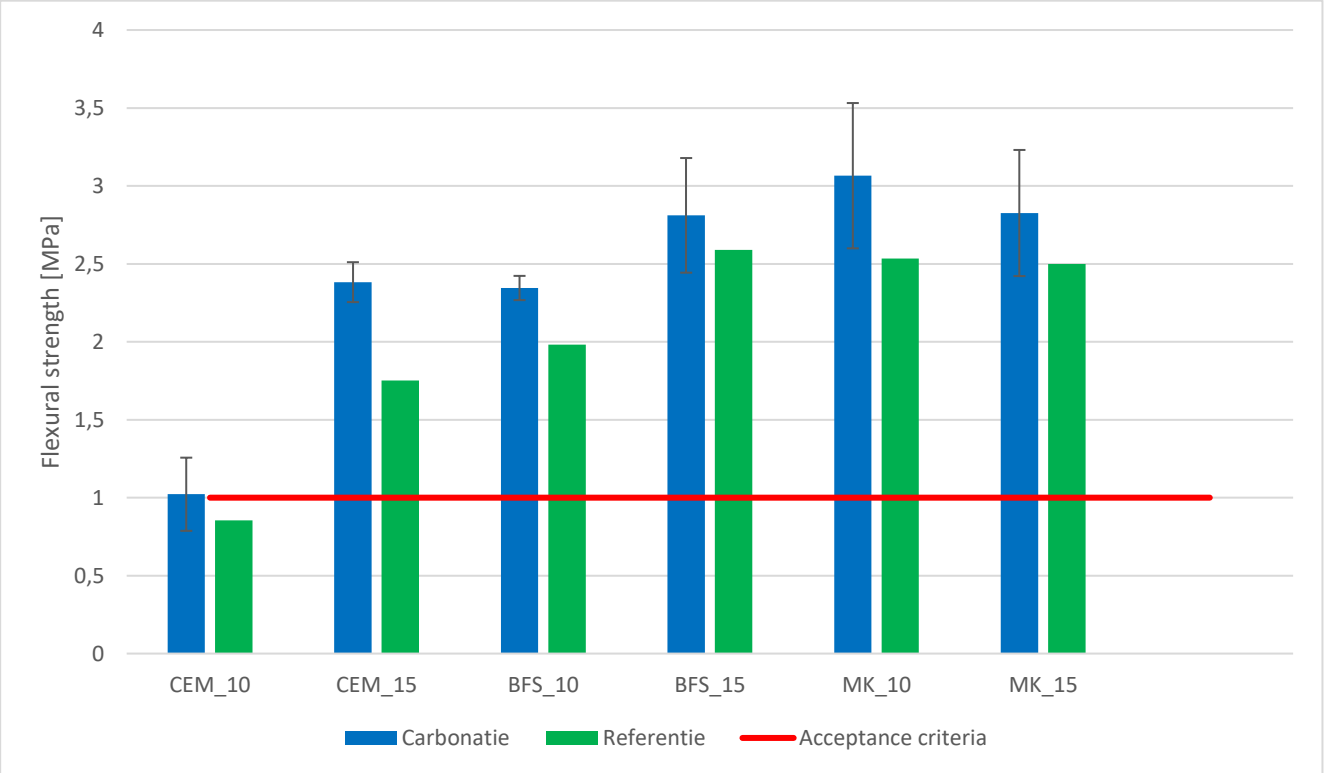

Figure 18: Carbonation global overview flexural strength

CEM_10 does not meet the acceptance criteria of 1 MPa and thus this recipe is not suitable for the immobilization of radioactive waste, the other recipes are.

4.2.2.2 Compressive strength carbonation

A global overview of the different CEM-, BFS- and MK-based systems is illustrated in Figure 19, with error bars representing the standard deviation (n = 3) for the carbonation samples. The reference samples do not have error bars, because only one sample was tested. The acceptance criteria of 8 MPa to ensure the mechanical performance standards necessary for effective and safe immobilization applications is given by the horizontal line. The detailed results of the compressive strength of the carbonation samples can be found in the appendix (Figure 79 – Figure 85).

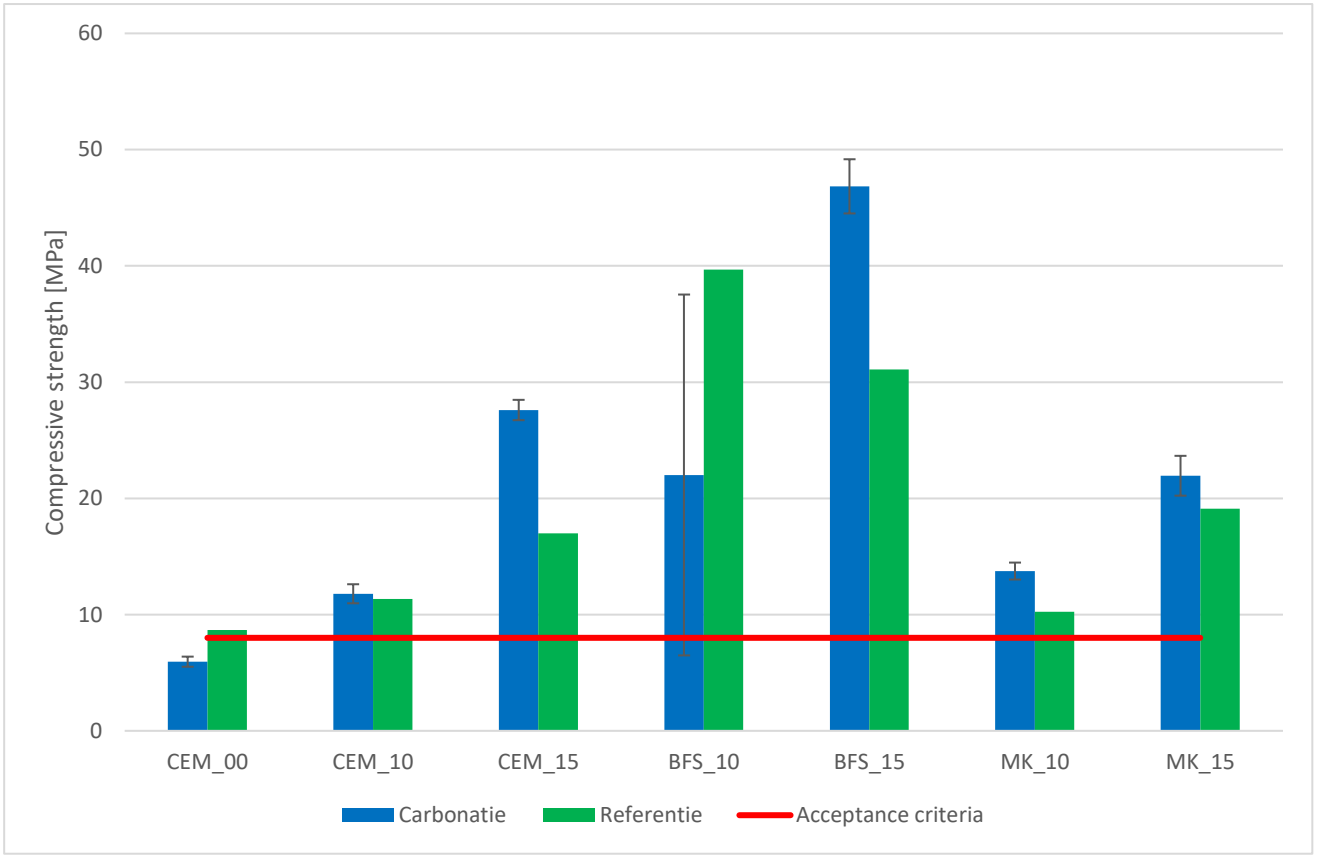

Figure 19: Carbonation global overview compressive strength

BFS_10 does not meet the acceptance criteria of 8 MPa and thus this recipes are not suitable for the immobilization of radioactive waste, the other recipes are. BFS_10 exhibited a high standard deviation in the strength measurements. This variability is likely due to the presence of a faulty sample, which significantly influenced the average strength result. Further testing is recommended to accurately assess the suitability of BFS_10 for radioactive waste immobilization.

Carbonation was found to have a generally positive effect on the flexural and compressive strength of the recipes studied. In some cases, such as BFS_10, the variability was higher and the apparent increase may not be statistically significant due to overlapping error bars. Nonetheless, the overall trend suggests that carbonation enhances the mechanical performance of these materials.

Carbonation promotes the formation of calcium carbonate ($CaCO_3$) through the reaction of CO_2 with calcium-bearing phases such as portlandite ($Ca(OH)_2$) or C–S–H/C–A–S–H gels. The resulting carbonate phases can fill pores and refine the microstructure, leading to reduced porosity, increased matrix densification and enhanced strength. These effects are most evident in calcium-rich systems (BFS and CEM), where reactive Ca is readily available. In MK-based systems, the improvement is less pronounced due to lower Ca content, but some strength gain may still occur via secondary reactions involving alkali-bearing phases or residual lime.

4.2.2.3 Carbonation depth

The carbonation depth of the different samples was determined through phenolphthalein spraying. A solution of 1 g phenolphthalein dissolved in 50 ml ethanol and 50 ml water was used as an indicator. Upon spraying freshly broken surfaces of the samples, areas with a pH above approximately 9–10 retained a pink to purple colour, while carbonated regions, where the pH was lower due to CO_2 ingress and its reaction with the binder, hydration products and/or other reaction products, remained colourless. This clear colour contrast allowed accurate measurement of the carbonation front. Each recipe has a reference sample (REF) and a carbonation sample (CAR).

4.2.2.3.1 CEM-based systems

The tested samples can be found in Figure 20 and Figure 21, the average carbonation depth of the different CEM samples can be found in Table 14 .

Figure 20: Carbonation depth CEM_15_CAR; CEM_15_REF; CEM_10_CAR; CEM_10_REF

Figure 21: Carbonation depth CEM_00_CAR; CEM_00_REF

Table 14: Carbonation depth CEM

Sample	Average carbonation depth [mm]
CEM_00_CAR	20.00
CEM_00_REF	12.26
CEM_10_CAR	17.63
CEM_10_REF	10.35
CEM_15_CAR	10.80
CEM_15_REF	7.82

Relatively high carbonation depths were observed for the CEM samples, indicating notable susceptibility to carbonation. The CEM_00_CAR sample, exposed to accelerated carbonation conditions, exhibited the highest average carbonation depth of 20.00 mm, which means the whole sample was carbonated. Its corresponding reference sample, CEM_00_REF, showed a lower carbonation depth of 12.26 mm.

When 10% MS samples were introduced, carbonation depths slightly decreased. CEM_10_CAR showed a carbonation depth of 17.63 mm and CEM_10_REF recorded 10.35 mm. This indicates that partial substitution contributed to some improvement in carbonation resistance.

Further improvement was observed at 15% MS samples. CEM_15_CAR showed a reduced carbonation depth of 10.80 mm, while CEM_15_REF displayed a value of 7.82 mm. This trend suggests that increasing the MS percentage leads to enhanced resistance against carbonation, with less CO_2 penetration overall.

The increase in carbonation resistance with higher MS percentages can be explained by changes in the microstructure. MS not only acts as an additive but also serves as the chemical activator of the binder system. These MS-activated matrices generally exhibit a denser microstructure and reduced capillary porosity. This densification results in a less connected pore network, which significantly hinders the diffusion of CO_2 into the material. As a result, increasing MS content leads to improved carbonation resistance, reflected by lower carbonation depths.

4.2.2.3.2 BFS-based systems

The tested samples can be found in Figure 22, the average carbonation depth of the different BFS samples can be found in Table 15.

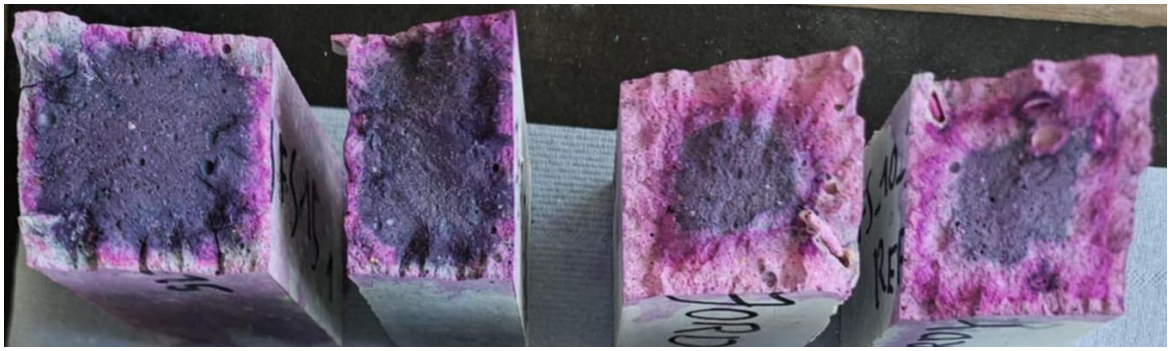

Figure 22: Carbonation depth BFS_15_CAR; BFS_15_REF; BFS_10_CAR; BFS_10_REF

Table 15: Carbonation depth BFS

Sample	Average carbonation depth [mm]
BFS_10_CAR	10.53
BFS_10_REF	10.87
BFS_15_CAR	3.47
BFS_15_REF	2.83

For the BFS binder series, significantly lower carbonation depths were observed compared to the CEM series, indicating improved resistance to CO_2 ingress. However, it is important to note that during the carbonation depth measurements, an unusual behaviour was observed: even before the application of phenolphthalein, the BFS samples already exhibited internal colour variations. After spraying with the indicator solution, little to no additional colour change was detected, the majority of the surfaces remained purple. As a result, the determination of carbonation depth relied largely on the natural colour differences visible within the BFS samples, rather than the typical sharp colour contrast expected from phenolphthalein. This suggests that the interpretation of carbonation fronts in BFS samples may carry some uncertainty.

Looking at the results, the BFS_10_CAR and BFS_10_REF samples showed very similar carbonation depths of 10.53 mm and 10.87 mm, respectively. This indicates that accelerated carbonation exposure did not substantially increase the carbonation penetration compared to natural conditions for these samples. In the 15% MS samples, carbonation depths were notably reduced: BFS_15_CAR showed a depth of 3.47 mm and BFS_15_REF only 2.83 mm. This significant decrease in carbonation depth with increasing MS content suggests that the combined effect of BFS and MS activation results in a denser and less permeable matrix.

4.2.2.3.3 MK-based systems

The tested samples can be found in Figure 23 and Figure 24, the average carbonation depth of the different MK samples can be found in Table 16.

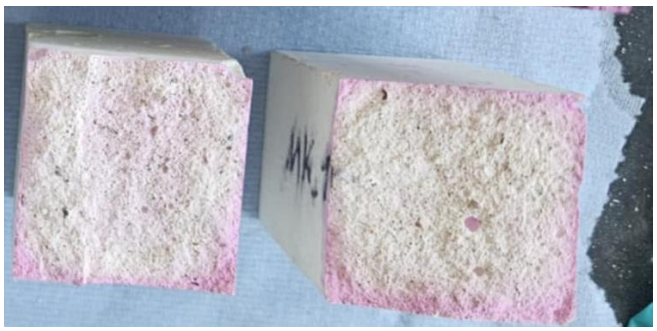

Figure 23: MK_10_CAR; MK_10_REF

Figure 24: MK_15_CAR; MK_15_REF

Table 16: Carbonation depth MK

Sample	Average carbonation depth [mm]
MK_10_CAR	7.24
MK_10_REF	10.53
MK_15_CAR	8.69
MK_15_REF	0.91

The carbonation behaviour of the MK binder series appeared more complex compared to the CEM and BFS binders. During the measurements, it was observed that MK_10 samples exhibited an atypical colour distribution after the application of phenolphthalein. Specifically, the outer regions of the samples remained purple, indicating a high pH and limited carbonation, while the inner core appeared clear, suggesting carbonation had occurred internally.

The unusual behaviour can be explained by the specific chemical characteristics of MK. MK-containing binders have a lower initial portlandite content due to the reaction of MK with calcium hydroxide, leading to a lower starting pH (around 10–11) compared to PC systems (pH 12–13). Because phenolphthalein only indicates a colour change between pH 8,5 and 9,5, small pH drops in the MK matrix, even without extensive carbonation, may already cause the indicator to turn colourless. This makes MK systems more sensitive to minor carbonation and complicates the interpretation of the carbonation front based on phenolphthalein.

The MK_15 samples showed a more expected carbonation profile: the centre remained dark purple, indicating high pH, while the outer zones were pink, suggesting partial carbonation from the surface inward. This indicates that with higher MS content, the MK system develops an even denser and more durable microstructure that better resists carbonation ingress.

Due to the unreliable colour response of phenolphthalein in MK samples and the atypical carbonation behaviour, the measured carbonation depths for the MK series cannot be considered fully accurate or trustworthy.

4.2.2.3.4 Global overview

The carbonation resistance of the tested samples varied significantly depending on the binder type and the MS content.

The CEM samples showed the highest carbonation depths overall, confirming the known vulnerability of PC matrices to carbonation. However, increasing MS content improved resistance, likely due to densification of the pore structure promoted by MS activation.

BFS samples exhibited much lower carbonation depths, particularly at higher MS contents. Nevertheless, the carbonation depth measurements in BFS were complicated by existing internal colour variations and limited phenolphthalein response, which may have affected the precision of the results.

The MK samples showed the most complex behaviour. Irregular carbonation patterns, linked to the inherently lower pH of MK-activated systems, made interpretation of the phenolphthalein results unreliable.

Overall, increasing the MS content generally enhanced carbonation resistance across all binders, but measurement reliability varied depending on the binder chemistry and the interaction with the phenolphthalein indicator.

4.2.2.4 Mass and weight evolution

The detailed results of the mass and weight evolution of the carbonation samples can be found in the appendix (Figure 86 – Figure 100)

The carbonation behaviour of samples based on CEM, BFS and MK binders was evaluated over a 28-day period by monitoring both mass and length changes. Overall, the trends observed across the different binder systems were largely similar. However, a more detailed inspection of the graphs indicates that the CEM-based samples were somewhat more affected by carbonation compared to BFS- and MK-based samples.

For all binder types, samples placed in the carbonation chamber exhibited either a stable or slightly increasing mass trend over time. The reference samples, which were not exposed to elevated CO_2 concentrations, showed a gradual mass decrease. This mass loss in the references is attributed to ongoing drying: although the samples were considered dry at the start of the experiment, some residual moisture remained. The fact that the carbonation chamber samples maintained or even increased their mass, while drying processes were still ongoing, indicates that the uptake of CO_2 through carbonation reactions outweighed the potential mass loss due to drying. Therefore, even in cases where the mass trend of the carbonation chamber samples appeared relatively constant, CO_2 absorption was occurring. The length evolution further supports this interpretation. Samples exposed to CO_2 generally showed slight expansions over time, consistent with the formation of carbonation products such as calcium carbonate, which can induce small volumetric changes. Meanwhile, reference samples tended to remain stable or show minor shrinkage, likely as a result of drying effects alone.

CEM-based systems showed a relatively pronounced increase in mass and a more noticeable expansion in length in the carbonation-exposed samples compared to the references. This suggests a stronger carbonation effect in these samples. The difference between carbonation and reference samples is clearer for CEM than for BFS or MK.

BFS-based systems showed mass stabilization and slight expansion, but the trends were more modest compared to CEM. The mass gain was less pronounced, indicating a somewhat lower carbonation reactivity under the given conditions. MK-based systems exhibited similar behaviour to BFS, with relatively stable mass and minimal expansion over the exposure period. This suggests that MK systems also undergo carbonation but to a slightly lesser extent compared to CEM.

Thus, while carbonation was observed in all systems, CEM-based samples were more sensitive to carbonation, as evidenced by clearer mass gains and greater expansions relative to the BFS- and MK-based samples. This observation is consistent with the chemical composition of CEM, which contains more free calcium hydroxide ($Ca(OH)_2$) that readily reacts with CO_2 to form calcium carbonate, promoting more mass and volume changes.

4.2.2.5 Global trends of carbonation

Carbonation resistance was evaluated through mechanical testing, phenolphthalein depth measurements, and mass and length monitoring. Overall, carbonation improved both flexural and compressive strength in most systems, due to matrix densification from $CaCO_3$ formation.

CEM-based systems showed the highest carbonation depths, confirming their vulnerability to CO_2, though resistance improved with higher MS content. BFS systems had lower depths and better performance overall, but phenolphthalein results were difficult to interpret due to internal colouration. MK systems displayed inconsistent carbonation fronts due to their lower pH, which made phenolphthalein results unreliable.

CEM samples gained the most mass and expanded more, reflecting greater carbonation reactivity, while BFS and MK samples were more stable. Despite some measurement limitations, the results clearly show that MS addition improves both carbonation resistance and mechanical performance across all binder types.

4.3 Non-destructive and microstructural analysis results

To further assess the internal structure and physical integrity of the binder matrices, non-destructive and microstructural characterization techniques were performed. These methods provide insights beyond mechanical and chemical performance, allowing for the evaluation of compactness, porosity, phase distribution and morphological development in the hardened materials. The analyses included UT, SEM and NA measurements.

4.3.1 Ultrasonic testing results

UT was used to assess the internal homogeneity and structural density of the hardened samples. Measurements were performed on specimens using a direct transmission method, where the time taken for ultrasonic pulses to travel through the material was recorded and used to calculate pulse velocity. Higher velocities typically indicate denser and more uniform internal structures, while lower velocities may reflect porosity, internal cracking or weaker bonding. The detailed results of UT can be found in the appendix (Figure 101 – Figure 106).

Typically, an acceleration peak in the ultrasonic signal is expected to correlate with significant changes in the microstructure, such as the transition from a plastic to a solid state and this peak usually aligns with the initial and final setting time determined by mechanical tests. However, in this study, the ultrasonic results showed inconsistent behaviour across the different samples. Only BFS_15 exhibited a clear acceleration peak, indicating a distinct microstructural transition. The other samples displayed scattered and irregular signals, without a clear peak that could be reliably linked to setting or hardening processes. Furthermore, there was no consistent correlation between the ultrasonic measurements and the independently measured setting times.

It should be noted that this was the first time this ultrasonic setup was used in the laboratory and the samples themselves served as a test case for evaluating the method. As such, some uncertainty regarding the sensitivity and calibration of the equipment remains. Factors such as imperfect coupling between the sensor and the samples, initial setup calibration or varying conditions (e.g., noise from laboratory ventilators) may have influenced the measurement quality. Therefore, while the ultrasonic data for BFS_15 suggest that the technique has potential to detect setting phenomena under favourable conditions, further method development and systematic calibration are needed before reliable conclusions can be drawn across all sample types.

The data from UT will not be taken into account in the remainder of this study.

4.3.2 SEM analysis

SEM imaging was conducted on the surface of the samples to visualize the microstructure of the hardened matrices. The images provide qualitative information about phase morphology, particle distribution, crack formation and the presence of unreacted precursors or crystalline inclusions. For each binder formulation, four SEM images were taken: two at the outer edge of the fractured surface and two towards the centre of the sample. This allowed for the observation of any spatial variation in microstructural features from the surface inward. Each SEM image was further analysed using Energy-Dispersive X-ray Spectroscopy (EDX), with 10 distinct spots measured per image to obtain localized elemental composition data. In total, 40 EDX spot analyses were performed per sample. Two samples were analysed per binder formulation, resulting in 80 EDX data points per recipe. The average elemental composition across these 80 spots was calculated to provide a representative chemical profile of the binder matrix, supporting interpretation of phase formation, homogeneity and the influence of salt waste incorporation. A representative SEM image taken from the middle of the sample is displayed for each sample.

4.3.2.1 CEM-based systems

The microstructural and compositional evolution of the CEM-based binders with increasing MS content reveals changes that reflect both chemical and physical transformations within the matrix. The composition of the CEM-based systems can be found in Table 17 and Table 18.

Table 17: SEM-EDX of CEM elements

Recipe	C [wt%]	O [wt%]	Ca [wt%]	Si wt[%]	Al [wt%]	Mg [wt%]	N [wt%]	Na [wt%]
CEM_00	35.53	34.42	15.29	8.07	1.92	1.05	3.27	0.44
CEM_10	28.21	36.70	16.63	7.43	1.62	1.19	2.57	5.35
CEM_15	13.68	50.07	16.76	12.09	2.14	0.20	0.00	0.00

Table 18: SEM-EDX of CEM oxides

Recipe	CaO [wt%]	SiO_2 [wt%]	Al_2O_3 [wt%]	MgO [wt%]	Na_2O [wt%]
CEM_00	25.50	20.13	4.27	2.02	0.78
CEM_10	27.97	18.26	3.57	2.31	9.01
CEM_15	29.68	32.64	5.13	0.41	9.19

CEM_00 presents a visibly heterogeneous microstructure (Figure 25), characterized by distinct phase boundaries, unreacted particles and a relatively irregular texture. The presence of bright and dark contrast regions suggests compositional variation and incomplete homogenization of hydration products. SEM-EDX analysis shows elevated levels of carbon (35.53 wt%) and calcium (15.29 wt%). The corresponding oxide composition includes CaO (25.50 wt%) and SiO_2 (20.13 wt%), which are typical constituents of PC. The heterogeneity may be due to early-age carbonation, uneven hydration or limited activation.

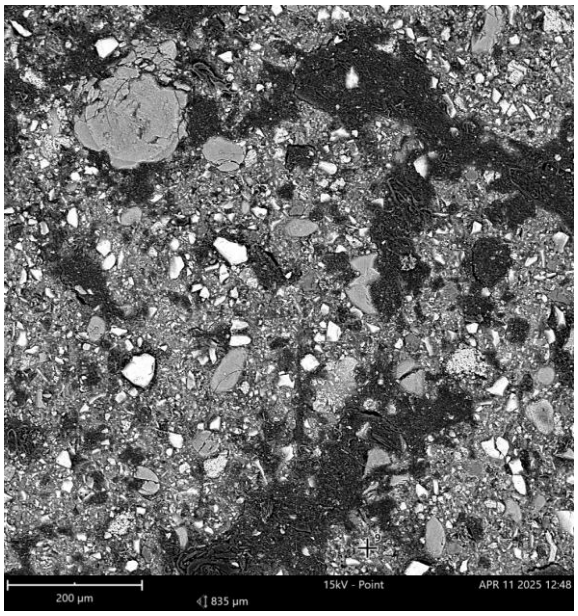

Figure 25: SEM of CEM with 0% MS (CEM_00) after 28 days of hardening

When 10% MS is introduced (CEM_10), the microstructure appears somewhat more refined, though still featuring a mix of matrix regions and localized inclusions (Figure 26). There is no major increase in porosity, but the visual differences suggest a subtle restructuring of the matrix, potentially due to the presence of sodium, which rises to 5.35 wt%, with Na_2O content increasing to 9.01 wt%. Carbon content drops to 28.21 wt% and oxygen increases to 36.70 wt%, likely due to the incorporation of oxygen-rich salt compounds such as Na_2CO_3. The lower carbon content in the MS containing sample likely reflects reduced carbonation compared to CEM_00, where more $CaCO_3$ has formed. Minor reductions in SiO_2 and Al_2O_3 may suggest altered gel chemistry or partial disruption of silicate and aluminate structures.

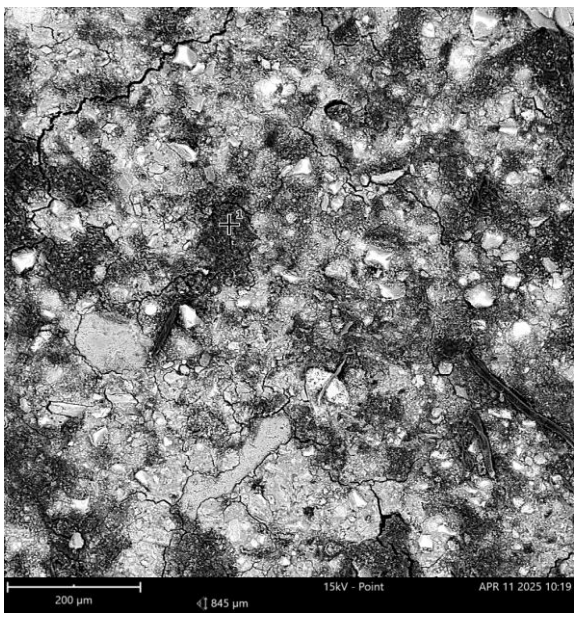

Figure 26: SEM of CEM with 10% MS (CEM_10) after 28 days of hardening

CEM_15 exhibits the most uniform microstructure (Figure 27). The matrix appears denser and more homogeneous, with only a few visible aggregates or unreacted particles and little evidence of significant porosity. Despite the absence of elemental sodium in the EDX spot data, Na_2O remains high at 9.19 wt%, suggesting that sodium may be incorporated into amorphous gel phases or redistributed uniformly beyond the detection limit of point analysis. Carbon content drops substantially to 13.68 wt%, while oxygen (50.07 wt%) and silicon (12.09 wt%) rise, reflected in a strong increase in SiO_2 to 32.64 wt%. This suggests a shift toward a silicate-rich, possibly glassy matrix with less phase contrast. CaO and Al_2O_3 also increase, further pointing to densification and enhanced formation of aluminosilicate reaction products.

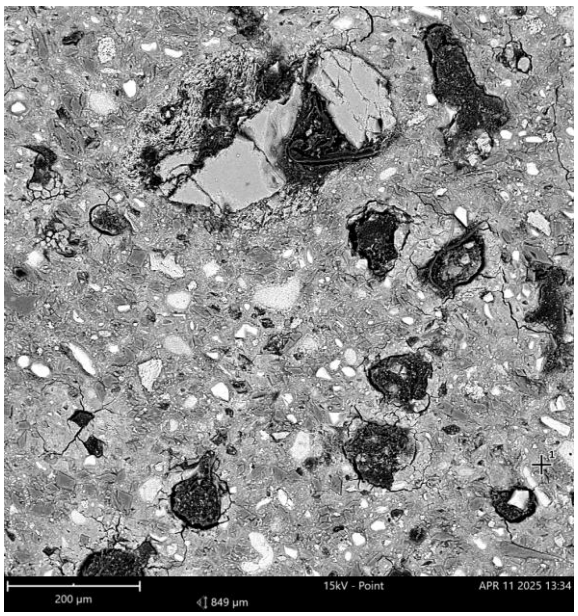

Figure 27: SEM of CEM with 15% MS (CEM_15) after 28 days of hardening

Overall, the data indicates that MS addition modifies both the chemistry and the morphology of the CEM matrix. While CEM_00 shows the most heterogeneity and CEM_10 begins to incorporate salt visibly and chemically, CEM_15 forms a more homogeneous, denser structure with altered elemental distributions. These observations imply that higher MS loadings may enhance matrix uniformity and reduce porosity, possibly through the formation of amorphous or glassy silicate-rich binding phases that immobilize salt constituents more effectively. This is somewhat expected, as the MS used also acted as an activator in the recipe. Its chemical reactivity contributed to a higher degree of reaction and a denser, more consolidated matrix.

4.3.2.2 BFS-based systems

The comparative analysis of recipes BFS_10 and BFS_15 reveals differences in both chemical composition and resulting microstructure. The composition of the BFS-based systems can be found in Table 19 and Table 20.

Table 19: SEM-EDX of BFS elements

Recipe	O [wt%]	Ca [wt%]	Si [wt%]	Al [wt%]	Mg [wt%]	Na [wt%]	C [wt%]	N [wt%]
BFS_10	43.80	16.17	10.16	3.83	3.21	7.35	13.69	1.73
BFS_15	45.99	13.77	9.76	3.91	3.58	10.27	11.45	0.00

Table 20: SEM-EDX of BFS oxides

Recipe	CaO [wt%]	SiO_2 [wt%]	Al_2O_3 [wt%]	MgO [wt%]	Na_2O [wt%]
BFS_10	27.35	25.00	8.13	6.20	12.74
BFS_15	24.74	25.30	9.11	7.33	18.40

In the BFS_10 sample (Figure 28), the microstructure shows a partially developed matrix with discernible heterogeneities. The chemical data indicate substantial Na (7.35 wt%) and Na_2O (12.74 wt%) incorporation, suggesting that Na_2CO_3 is actively participating in the alkali activation. The oxide profile confirms early-stage geopolymerisation or C-A-S-H-type gel formation, with CaO (27.35 wt%) and SiO_2 (25.00 wt%) suggesting ongoing hydration reactions.

Figure 28: SEM of BFS with 10% MS (BFS_10) after 28 days of hardening

BFS_15 (Figure 29) displays a denser and more homogeneous matrix, which aligns with expectations given the higher activator dosage. The increased Na (10.27 wt%) and Na_2O (18.40 wt%) levels support the idea that the higher Na_2CO_3 content enhances slag dissolution and reaction kinetics, leading to more complete formation of binding gels. The increase in Al_2O_3 (9.11 wt%) points to the formation of more complex aluminosilicate-silicate-hydrate phases (C-A-S-H gel). The slightly lower CaO (24.74 wt%) likely reflects more complete incorporation into the gel structure.

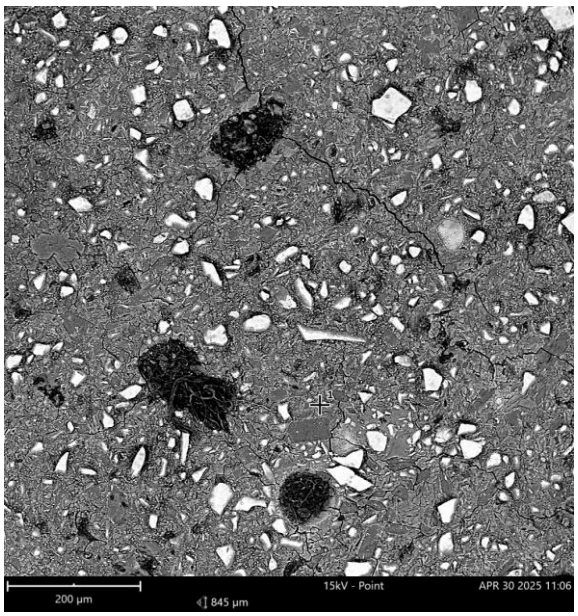

Figure 29: SEM of BFS with 15% MS (BFS_15) after 28 days of hardening

Together, these results indicate that increasing MS content in BFS-based binders leads to a denser, more chemically integrated matrix. BFS_10 begins to incorporate salt components visibly and chemically, while BFS_15 shows a more complete transformation, with a homogeneous structure and enhanced sodium retention. The EDX and SEM data point to a gradual evolution toward a chemically rich, potentially amorphous matrix with improved immobilization characteristics.

4.3.2.3 MK-based systems

The comparative analysis of recipes MK_10 and MK_15 reveals differences in both chemical composition and resulting microstructure. The composition of the MK-based systems can be found in Table 21 and Table 22.

Table 21: SEM-EDX of MK elements

Recipe	C [wt%]	O [wt%]	Si [wt%]	Na [wt%]	Al [wt%]	Ca [wt%]
MK_10	30.70	39.36	13.63	6.71	7.01	2.54
MK_15	17.98	44.20	15.93	8.23	7.10	6.44

Table 22: SEM-EDX of MK oxides

Recipe	SiO_2 [wt%]	Na_2O [wt%]	Al_2O_3 [wt%]	CaO [wt%]
MK_10	33.68	10.73	15.29	4.00
MK_15	38.56	13.18	15.36	10.97

In the MK_10 sample (Figure 30), the microstructure reveals a somewhat porous and heterogeneous matrix, suggesting incomplete reaction or limited gel formation. The chemical data show moderate Na (6.71 wt%) and Na_2O (10.73 wt%) concentrations, indicative of Na_2CO_3 participation in the alkali activation process. The presence of SiO_2 (33.68 wt%) and Al_2O_3 (15.29 wt%) supports the initiation of N-A-S-H gel formation, while the relatively low CaO (4.00 wt%) points to a limited C-A-S-H contribution.

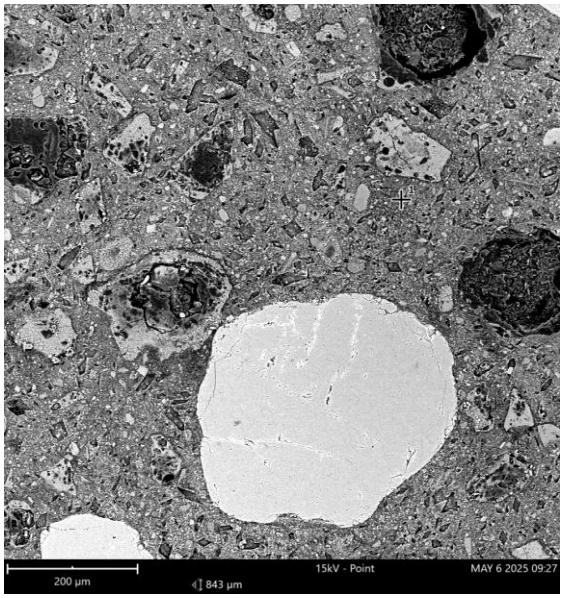

Figure 30: SEM of MK with 10% MS (MK_10) after 28 days of hardening

MK_15 (Figure 31) presents a denser and more homogeneous matrix. This observation correlates with the higher Na (8.23 wt%) and Na_2O (13.18 wt%) content, consistent with increased MS (Na_2CO_3) dosage acting as an effective activator. The elevated SiO_2 (38.56 wt%) further supports enhanced geopolymerisation, while the rise in CaO (10.97 wt%) suggests a stronger contribution of calcium-based phases, possibly forming C-N-A-S-H gels. The minor increase in Al_2O_3 (15.36 wt%) complements the formation of a chemically integrated, cross-linked matrix.

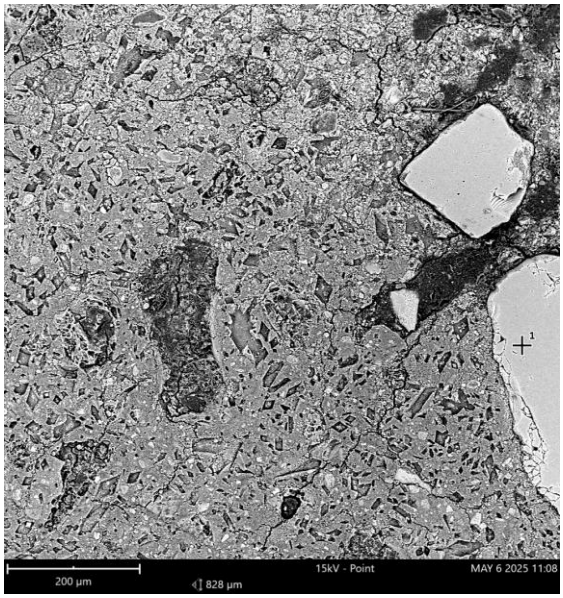

Figure 31: SEM of MK with 15% MS (MK_15) after 28 days of hardening

The microstructural differences suggest that increasing the MS content in MK-based binders leads to a more consolidated and chemically mature matrix. MK_10 begins to show chemical integration with visible porosity, while MK_15 advances to a significantly denser phase, reflecting a higher extent of reaction and immobilization potential. The SEM and EDX data indicate a transition toward a stable, sodium-rich and structurally cohesive binder with increasing MS content.

4.3.2.4 Global overview

Across all systems, higher MS loading leads to a denser and more homogeneous microstructure. This transformation is driven by chemical shifts that directly impact gel formation and matrix development.

Among the three systems, BFS responds most effectively to MS activation. The BFS_15 sample shows a balanced composition with high CaO (24.74 wt%), increased Al_2O_3 (9.11 wt%) and a substantial rise in Na_2O (18.40 wt%). These values indicate robust formation of C-A-S-H or even C-N-A-S-H gels. The dense and uniform matrix observed in SEM supports this, suggesting that the slag is efficiently activated and converted into a chemically rich binder. Compared to MK and CEM, BFS demonstrates the most efficient incorporation of calcium and aluminium into cohesive gel phases.

The MK system shows a strong geopolymeric character, particularly in MK_15, where the SiO_2 content reaches 38.56 wt%, the highest among all binders. This is paired with an increase in Na_2O (to 13.18 wt%) and a notable jump in CaO (from 4.00 to 10.97 wt%), suggesting a transition from pure N-A-S-H to hybrid C-N-A-S-H gel formation. The MK_15 matrix appears significantly more consolidated than MK_10, reflecting a higher degree of reaction and enhanced sodium retention.

The CEM system displays the most pronounced evolution in composition and texture. From CEM_00 to CEM_15, carbon content drops while SiO_2 and CaO increases. CEM_15 reaches the highest CaO content overall (29.68 wt%), pointing to strong cement hydration. However, unlike BFS and MK, the role of sodium is less prominent in terms of integration into identifiable gel phases. The structural improvements observed in CEM_15 are thus attributed more to enhanced hydration and phase consolidation than to gel evolution.

In summary, all three binder systems benefit from MS addition, but in distinct ways. BFS forms the most balanced and chemically integrated C-A-S-H gels, MK produces a sodium- and silicate-rich geopolymeric matrix and CEM develops a denser, hydration-driven structure with moderate sodium involvement. These findings highlight how the interplay between precursor type and activator chemistry defines the final microstructure and performance potential of each system.

4.3.3 Nitrogen adsorption

To quantify surface area and pore characteristics, NA analysis is performed on powdered samples taken from the hardened matrices. The specific surface area (m^2/g), total pore volume and pore size distribution were determined using the BET and t-Plot external surface area method. These parameters are key indicators of matrix porosity, which directly affect mechanical strength, permeability and long-term durability.

The NA measurements (Figure 32 and Figure 33) reveal clear and consistent trends in how MS addition alters the porous structure of the different binder systems. As MS content increases, the evolution of porosity and surface area strongly reflects the underlying changes in matrix formation, with direct implications for the performance of the material in radioactive waste immobilization.

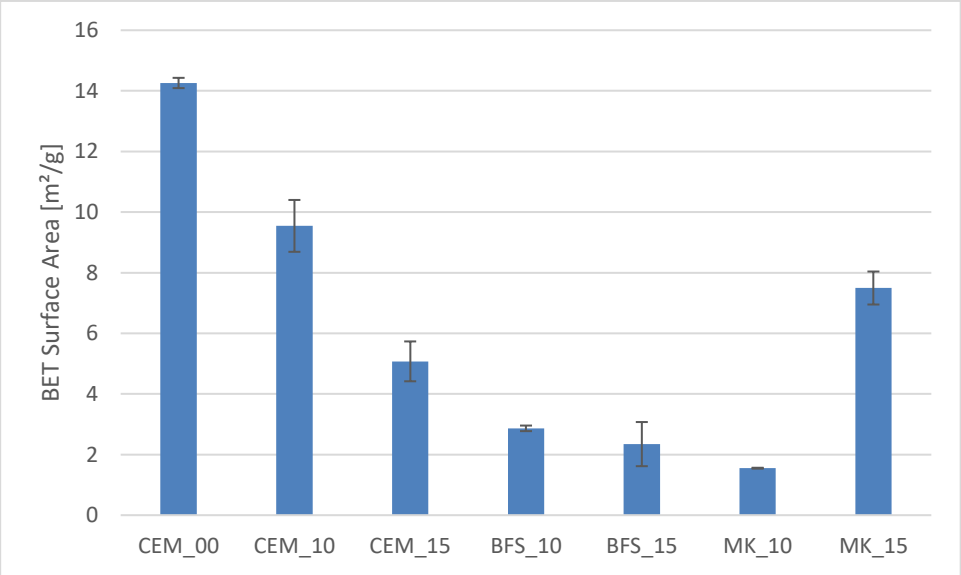

Figure 32: BET surface area

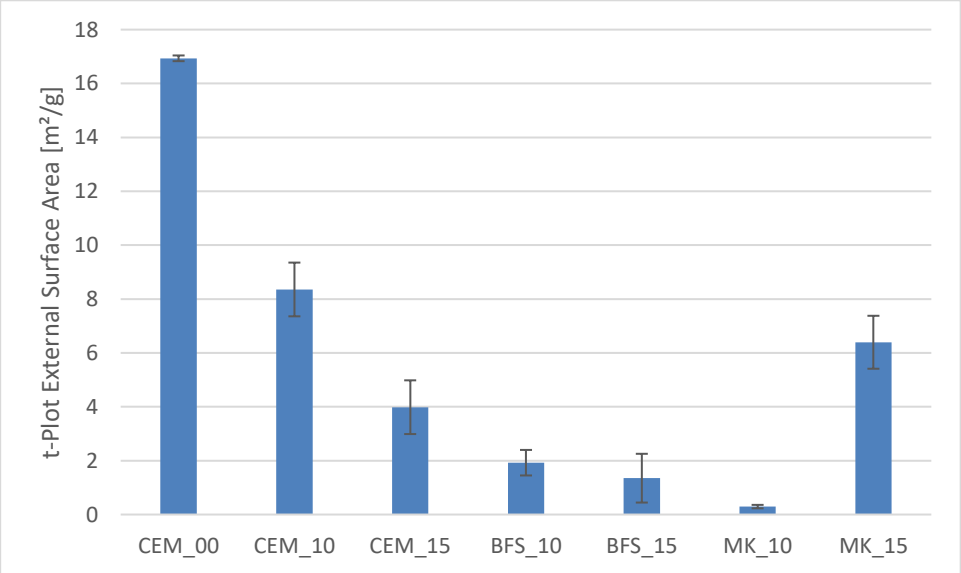

Figure 33: t-Plot external surface area

The NA results, including surface area, nitrogen uptake and pore size distribution (appendix Figure 107 – Figure 133), provide a coherent picture of how MS alters the porous structure of the different binder systems. These parameters together illustrate how MS content affects matrix densification and by extension the suitability of the material for radioactive waste immobilization.

In the CEM-based system a clear and progressive reduction in porosity is observed from CEM_00 to CEM_15. CEM_00 displays high surface area and nitrogen uptake, with isotherms indicating strong adsorption at both low and high relative pressures, typical of materials containing mesoporosity (2 – 50 nm pores). The corresponding pore size distributions show broad peaks around 20–30 nm. As MS is added, the uptake decreases and pore volume diminishes. By CEM_15, both the isotherms and pore distribution curves indicate a nearly non-porous structure, suggesting that MS-induced reactions lead to pore filling.

The BFS-based system starts off with much lower NA, even at lower MS content, indicating that BFS inherently forms compact, low-porosity matrices. Both BFS_10 and BFS_15 exhibit limited nitrogen uptake and narrow or indistinct pore size distributions, with no significant change as MS content increases.

The MK-based system behaves in the opposite manner. MK_10 is compact and nearly non-porous, with very low nitrogen uptake and flat isotherms. When the MS content increases in MK_15, NA rises significantly. The isotherms indicate increased mesoporosity and the pore size distribution broadens. This suggests more advanced geopolymerisation and gel formation.

In summary, the NA results clearly demonstrate that CEM and BFS systems become progressively denser with increasing MS, supporting their use in waste containment. MK, by contrast, becomes more porous, reflecting increased reactivity but insufficient structural integrity. These findings confirm that an effective immobilization matrix is not simply defined by reactivity or porosity alone, but by the right balance between mechanical strength, densification, chemical integration and practical workability.

4.4 Summary of key findings

This study explored the performance of three binder systems, PC (CEM), BFS-based GP (BFS) and MK-based GP (MK), in terms of their mechanical, viscosity, chemical and microstructural behaviour under varying levels of preconditioned MS waste. The goal was to determine their viability for immobilizing radioactive waste, where strength, durability and stability are paramount.

The incorporation of MS has a significant and beneficial impact across all three investigated binder systems. As an activator, MS not only initiates chemical reactions necessary for solidification but also enhances mechanical performance and structural integrity, all of which are critical for the safe immobilization of radioactive waste.

To understand the true influence of MS, the reference recipe CEM_00 serves as a baseline. This sample exhibited poor performance across the board: it remained largely unset after more than 30 hours, had low mechanical strength and showed a highly porous and heterogeneous microstructure. These observations underscore that without MS (the activator), the cementitious system remains largely inactive. It was included in the study only to observe the contrast and not as a viable candidate, because no MS is incorporated into this recipe.

When MS is introduced, a clear trend emerges across all systems: the mechanical properties, microstructural density and chemical integration improve significantly. In terms of mechanical strength, both compressive and flexural performance increase with higher MS content. This was expected, as MS activates the binder systems, thereby accelerating hydration or geopolymerisation reactions. The addition of MS also improves carbonation resistance and leads to the formation of denser, more uniform matrices.

The response to MS varies distinctly between binder types. The CEM-based systems show a strong initial reactivity to MS, with high hydration heat and rapid setting. CEM_15, which contains the highest MS content among the CEM group, develops a dense, consolidated matrix and exhibits improved carbonation resistance. However, it also shows the highest thermal output and the fastest setting time (initial set at just 1.39 hours), which may pose processing challenges and a higher risk of thermal cracking if not properly managed.

The BFS-based systems emerge as the strongest candidates. Both BFS_10 and BFS_15 achieve excellent mechanical strength and form chemically rich, homogeneous matrices characterized by robust C-A-S-H or C-N-A-S-H gel formation. BFS_15 in particular stands out due to its superior microstructural consolidation and strength performance. However, the rapid setting of BFS_15 requires swift and well-controlled mixing and casting procedures.

In contrast, the MK-based systems, while showing promising geopolymeric development, do not meet the mechanical strength criteria required for safe immobilization. Both MK_10 and MK_15 fall short in terms of compressive and flexural strength, despite MK_15 displaying a more consolidated structure and indications of C-N-A-S-H gel formation. On the positive side, MK systems offer greater workability with longer setting times, which can be advantageous in field applications, but their current formulations are not robust enough for practical deployment.

Across the different recipes, several trends emerge based on the conducted tests. Recipes that developed denser and more homogeneous microstructures, such as BFS_15, generally exhibited higher strength, lower porosity and improved resistance to carbonation. In contrast, more porous or heterogeneous systems, like CEM_10, tended to show weaker mechanical performance and greater carbonation depth. While not every result aligns perfectly across all binder systems, the findings suggest that the incorporation of MS enhances mechanical strength, promotes matrix densification and supports the formation of chemically stable structures, key factors contributing to the overall performance and durability required for radioactive waste immobilization.

BFS-based GP demonstrate the best overall performance, combining strength, chemical stability and microstructural homogeneity. CEM systems, though viable, are more prone to thermal cracking and exhibit more variability in performance depending on MS content. MK-based GP, while easier to process, are currently unsuitable due to inadequate mechanical properties.

In conclusion, BFS_15 emerges as the most promising formulation for the immobilization of radioactive MS waste. It offers superior mechanical strength and a chemically stable, dense microstructure. The only notable drawback is its limited workability due to rapid setting, which requires precise handling during application. CEM_15 represents a viable alternative, provided that challenges related to quick setting and elevated heat release are carefully controlled during processing. While MK-based formulations offer better workability, they fall short in terms of strength and overall performance, making them unsuitable in their current form. These results highlight the critical importance of optimizing binder chemistry in relation to MS content to ensure both the safety and long-term durability of nuclear waste immobilization systems.

Chapter 5
Conclusion

The objective of this study was to evaluate the impact of sodium carbonate (Na_2CO_3)-based MS waste loadings on the mechanical and microstructural properties of PC and GP matrices for the purpose of radioactive waste immobilisation. Three binder systems, CEM-based, BFS-based AAM and MK-based AAM, were systematically assessed at MS loadings of 0, 10 and 15 wt%.

A consistent and beneficial influence of MS incorporation was observed across all systems. Acting as an activator, MS initiated the necessary hydration or geopolymerisation reactions and significantly enhanced mechanical strength, matrix density and chemical integration, which are key factors in ensuring long-term stability.

Within the CEM series, increasing MS content led to improvements in mechanical strength, carbonation resistance and microstructural uniformity. CEM_15 formed a dense, consolidated matrix. However, its rapid setting, high viscosity and elevated hydration heat may lead to challenges for workability and an increased risk of thermal cracking, necessitating careful thermal and process management.

The BFS-based formulations, particularly BFS_15, demonstrated the most favourable overall performance. These mixes exhibited high mechanical strength, a dense and homogeneous microstructure and strong gel development (C-A-S-H and C-N-A-S-H). However, both BFS_10 and BFS_15 displayed a very rapid setting time, which can complicate mixing and casting operations, requiring precise handling during processing.

MK-based systems, while characterised by longer setting times, did not meet the required mechanical strength thresholds. Although MK_15 showed some evidence of gel formation and improved microstructural development, both MK_10 and MK_15 lacked sufficient robustness for practical use in immobilisation in their current form.

In conclusion, BFS_15 stands out as the most promising candidate for the immobilisation of MS waste, offering excellent mechanical performance, a chemically stable matrix and superior carbonation resistance. Its primary limitation lies in its extremely rapid setting time, which demands precise and efficient mixing and casting procedures. CEM_15 also shows strong potential, forming a dense matrix with good mechanical properties. However, it suffers from high viscosity, which can hinder workability and exhibits lower carbonation resistance compared to BFS_15. BFS_10 and CEM_10 are viable alternatives, providing sufficient mechanical strength and carbonation resistance while offering improved handling characteristics and longer processing windows, making them suitable for applications where ease of placement and flexibility are essential.

REFERENCES

[1] B. Zohuri, "Molten Salt Reactor History, From Past to Present," *Molten Salt Reactors and Integrated Molten Salt Reactors*, pp. 1–58, 2021, doi: 10.1016/b978-0-323-90638-8.00001-1.

[2] B. J. Riley, J. McFarlane, G. D. DelCul, J. D. Vienna, C. I. Contescu, and C. W. Forsberg, "Molten salt reactor waste and effluent management strategies: A review," *Nuclear Engineering and Design*, vol. 345, pp. 94–109, Apr. 2019, doi: 10.1016/j.nucengdes.2019.02.002.

[3] P. Perez-Cortes, I. Garcia-Lodeiro, F. Puertas, and M. Alonso, "Effect of incorporating a MS waste from nuclear power plants on the properties of geopolymers and Portland cement wasteforms," *Cement and Concrete Composites*, vol. 142, art. no. 105210, Sep. 2023, doi: 10.1016/j.cemconcomp.2023.105210.

[4] M. I. Ojovan, W. E. Lee, and S. N. Kalmykov, "Immobilization of Radioactive Waste in Cement," in *An Introduction to Nuclear Waste Immobilization,* 3rd ed. Amsterdam, The Netherlands: Elsevier, 2019, ch. 17, pp. 271–303. doi: /10.1016/b978-0-08-102702-8.00017-0.

[5] E. R. Vance and D. S. Perera, "Geopolymers for nuclear waste immobilization," in *Geopolymers: Structure, Processing, Properties and Industrial Applications*, J. L. Provis and J. S. J. van Deventer, Eds., Cambridge, UK: Woodhead Publishing, 2009, pp. 401–420.

[6] NASA, "Cosmic History," *science.nasa.gov*, 2024. Accessed: Apr. 5, 2025. [Online]. Available: https://science.nasa.gov/universe/overview/

[7] M. I. Ojovan, W. E. Lee, and S. N. Kalmykov, "Introduction to Immobilization," in *An Introduction to Nuclear Waste Immobilization*, 3rd ed., Amsterdam, The Netherlands: Elsevier, 2019, pp. 1–7, doi: 10.1016/b978-0-08-102702-8.00001-7.

[8] International Atomic Energy Agency, *Clearance of Materials Resulting from the Use of Radionuclides in Medicine, Industry and Research*, IAEA-TECDOC-1000, Vienna, Austria: IAEA, 1998.

[9] IAEA, *IAEA Safety Standards Classification of Radioactive Waste for protecting people and the environment,* No. GSG-1, General Safety Guide, 2009. Accessed: Apr. 5, 2025. [Online]. Available: https://www-pub.iaea.org/MTCD/Publications/PDF/Pub1419_web.pdf

[10] E. Midgley, "What are Molten Salt Reactors?," *Iaea.org*, Accessed: Mar. 11, 2025. [Online]. Available: https://www.iaea.org/newscenter/news/what-are-molten-salt-reactors

[11] IAEA, *Status of Molten Salt Reactor Technology*, Technical Reports Series No. 489, Vienna, Austria: IAEA 2023.

[12] L. M. Krall, A. M. Macfarlane, and R. C. Ewing, "Nuclear waste from small modular reactors," *Proceedings of the National Academy of Sciences*, vol. 119, no. 23, May 2022, doi: 10.1073/pnas.2111833119.

[13] S. Arm, D. Holcomb, R. Howard, and B. Riley, "Status of Fast Spectrum Molten Salt Reactor Waste Management Practice," *OSTI OAI (U.S. Department of Energy Office of Scientific and Technical Information)*, Dec. 2020, doi: 10.2172/1761520.

[14] M. I. Ojovan, W. E. Lee, and S. N. Kalmykov, "Immobilization of Radioactive Waste in Cement," in *An Introduction to Nuclear Waste Immobilization*, 3rd ed., Amsterdam, The Netherlands: Elsevier, Jan. 2019, pp. 271–303, doi: 10.1016/b978-0-08-102702-8.00017-0.

[15] V. Thapa and D. Waldmann, "A short review on alkali-activated binders and geopolymer binders." Accessed: Mar. 08, 2025. [Online]. Available: https://orbilu.uni.lu/bitstream/10993/35284/1/A%20short%20review.pdf

[16] J. L. Provis and J. S. J. van Deventer, Eds., Alkali Activated Materials. Dordrecht, The Netherlands: Springer Netherlands, 2014. doi: 10.1007/978-94-007-7672-2.

[17] M. T. Marvila, A. R. G. de Azevedo, and C. M. F. Vieira, "Reaction mechanisms of alkali-activated materials," *Revista IBRACON de Estruturas e Materiais*, vol. 14, no. 3, 2021, doi: 10.1590/s1983-41952021000300009.

[18] M. Sagnak, "Soil Stabilization of Bentonite and Kaolinite Clays Using Recycled Gypsum and Liquid Sodium Silicate," *ResearchGate*, Feb. 07, 2018. Accessed Mar. 03, 2025. [Online]. Available: https://www.researchgate.net/publication/324601488_Soil_Stabilization_of_Bentonite_and_Kaolinite_Clays_Using_Recycled_Gypsum_and_Liquid_Sodium_Silicate

[19] IAEA, *Geopolymers as an Immobilization Matrix for Radioactive Waste (T21029)*. Accessed Mar. 12, 2025. [Online]. Available: https://www.iaea.org/projects/crp/t21029

[20] Q. T. Phung, L. Frederickx, and E. Ferreira, "Immobilization of molten salt residue using alkali-activated and cement-based materials," presented at the *PREDIS Workshop*, May 2023. Accessed Mar. 8, 2025. [Online]. Available: https://researchportal.sckcen.be/en/publications/immobilization-of-molten-salt-residue-using-alkali-activated-and-

[21] N. Rakhimova and R. Rakhimov, "Recent advances in alternative cementitious materials for nuclear waste immobilization: A review," *Sustainability*, vol. 15, no. 1, p. 689, 2023. Accessed Mar. 8, 2025. [Online]. Available: https://www.mdpi.com/2071-1050/15/1/689

[22] PREDIS Project, *Conditioning of ashes from radioactive solid organic waste by geopolymer or cement-based encapsulation*, Deliverable 6.2, 2023. Accessed Apr. 4, 2025. [Online]. Available: https://predis-h2020.eu/wp-content/uploads/2023/09/PREDIS_D6.2_Conditioning-of-ashes_vFinal-31.8.2023.pdf

[23] Z. H. Abbas and H. S. Majdi, "Study of heat of hydration of Portland cement used in Iraq," *Case Studies in Construction Materials*, vol. 7, pp. 154–162, Dec. 2017, doi: 10.1016/j.cscm.2017.07.003.

[24] O. Beneš and R. J. M. Konings, "Thermodynamic Calculations of Molten-Salt Reactor Fuel Systems," in *Molten Salts Chemistry*, pp. 49–78, 2013, doi: 10.1016/b978-0-12-398538-5.00004-4.

[25] B. Yuan, Q. L. Yu, and H. J. H. Brouwers, "Time-dependent characterization of Na_2CO_3 activated slag," *Cement and Concrete Composites*, vol. 84, pp. 188–197, Nov. 2017, doi: 10.1016/j.cemconcomp.2017.09.005.

[26] NIRAS, *Acceptance criteria for surface disposal of category A waste (NIROND-TR-2001-17)*, Internal document, Belgium, 2001.

[27] "Cement," *Building Materials in Civil Engineering*, Oxford, UK: Woodhead Publishing, 2011, pp. 46–423, doi: 10.1533/9781845699567.46.

[28] "Computer Controlled Vicat Needle Apparatus 6 places," *Testing.de*, 2025. Accessed Mar. 19, 2025. [Online]. Available: https://testing.de/en/1.0366-1

[29] A. Yahia and A. Perrot, "Measuring Procedures," *RILEM State-of-the-Art Reports*, pp. 73–95, Oct. 2023, doi: 10.1007/978-3-031-36743-4_4

[30] "I-Cal 8000 HPC," *calmetrix*, 2024. Accessed Mar. 19, 2025. [Online]. Available: https://www.calmetrix.com/i-cal-8000-hpc

[31] K. L. Scrivener, V. M. John, and E. M. Gartner, "Eco-efficient cements: Potential economically viable solutions for a low-CO_2 cement-based materials industry," *Cement and Concrete Research*, vol. 114, pp. 2–26, Dec. 2018, doi: 10.1016/j.cemconres.2018.03.015.

[32] D. Jacques, L. Yu, M. Ferreira, and T. Oey, *Overview of state-of-the-art knowledge for the quantitative assessment of the ageing/deterioration of concrete in nuclear power plant systems, structures, and components*, Deliverable D1.1, ACES project, 2021. Accessed Apr. 4, 2025. [Online]. Available: https://aces-h2020.eu/deliverables/

[33] S. A. Bernal, J. L. Provis, R. Mejía de Gutiérrez, and J. S. J. van Deventer, "Accelerated carbonation testing of alkali-activated slag/metakaolin blended concretes: effect of exposure conditions," *Materials and Structures*, vol. 48, no. 3, pp. 653–669, Mar. 2014, doi: 10.1617/s11527-014-0289-4.

[34] R. Sharma and R. A. Khan, "Carbonation Resistance of Self-Compacting Concrete Incorporating Copper Slag as Fine Aggregates," *Journal of Materials in Civil Engineering*, vol. 32, no. 6, Mar. 2020, doi: 10.1061/(ASCE)MT.1943-5533.0003200

[35] M. Jamil *et al.*, "Internal Cracks and Non-Metallic Inclusions as Root Causes of Casting Failure in Sugar Mill Roller Shafts," *Materials*, vol. 12, no. 15, p. 2474, Aug. 2019, doi: doi.org/10.3390/ma12152474.

[36] B. J. Ford and S. Bradbury, "Scanning electron microscope | instrument," *Encyclopaedia Britannica*. Jan. 22, 2019. Accessed Mar. 12, 2025. [Online]. Available: https://www.britannica.com/technology/scanning-electron-microscope

[37] "*Nature and Chemistry of Coal and Its Products,*" Coal Production and Processing Technology, pp. 17–44, Nov. 2015, doi: 10.1201/b19352-6.

APPENDIX

Appendix A: Flexural strength

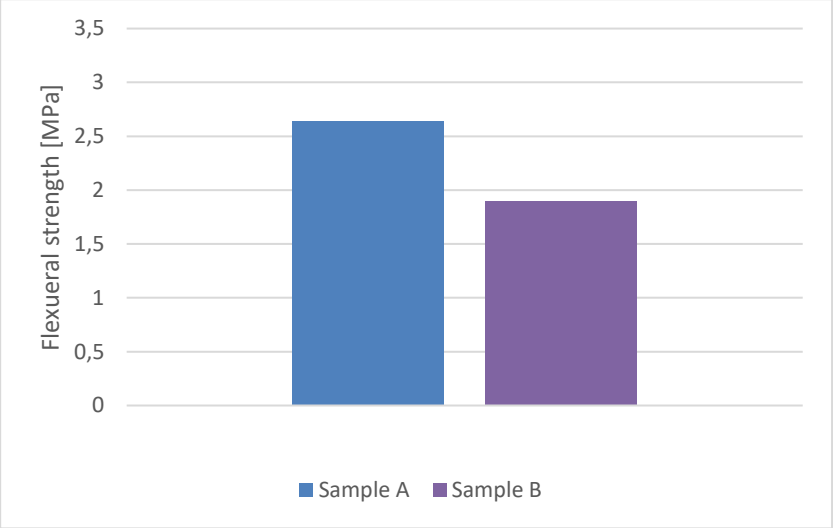

Figure 34: Flexural strength CEM_00

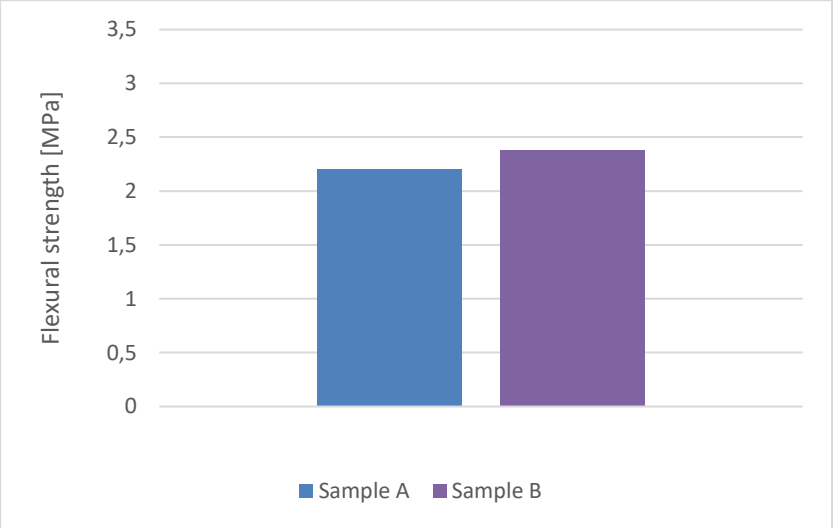

Figure 35: Flexural strength CEM_10

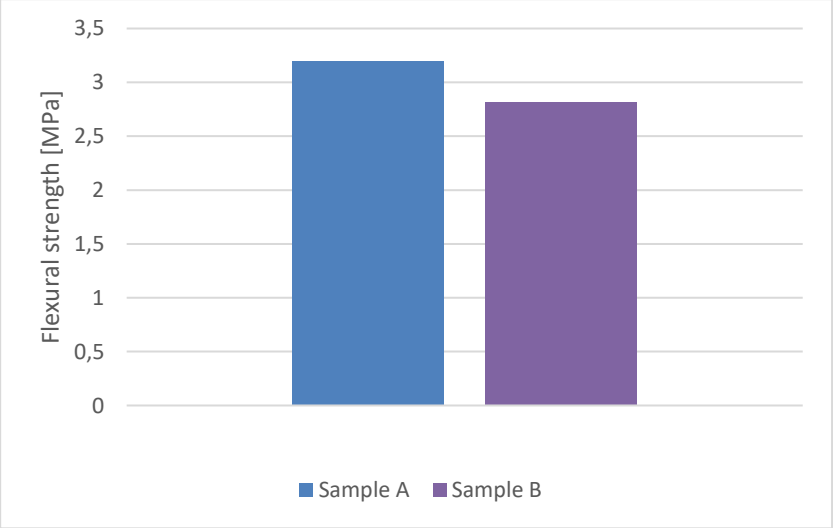

Figure 36: Flexural strength CEM_15

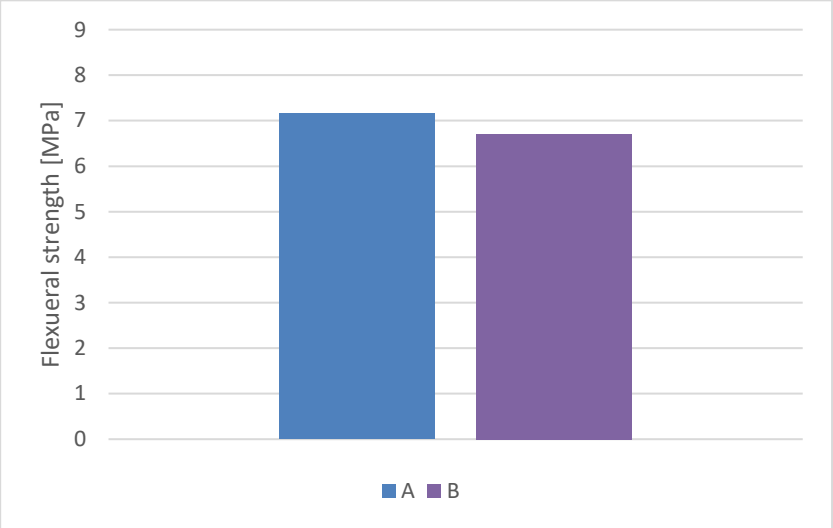

Figure 37: Flexural strength BFS_10

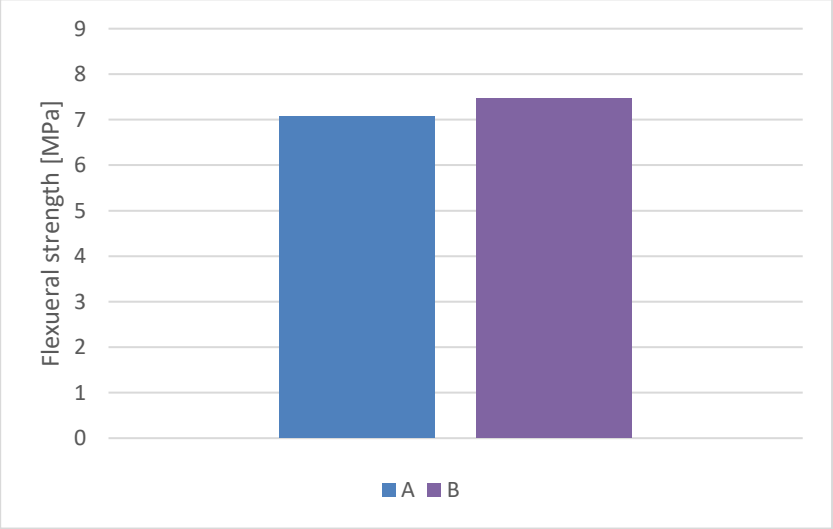

Figure 38: Flexural strength BFS_15

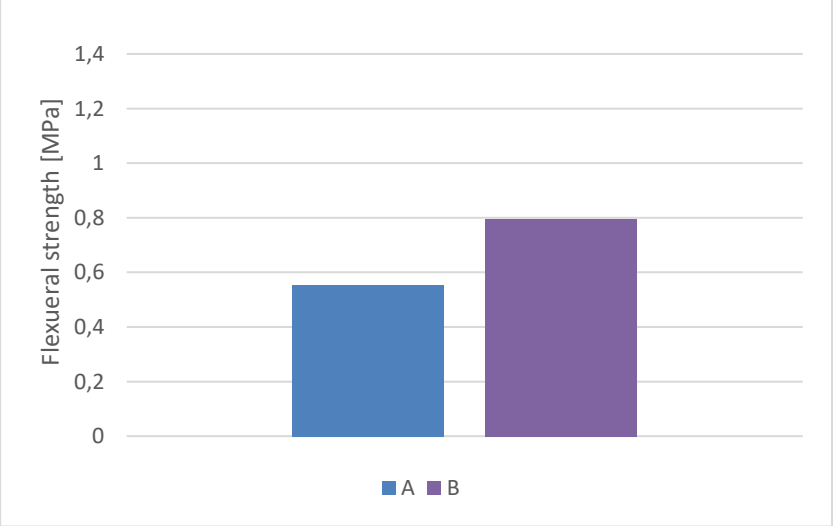

Figure 39: Flexural strength MK_10

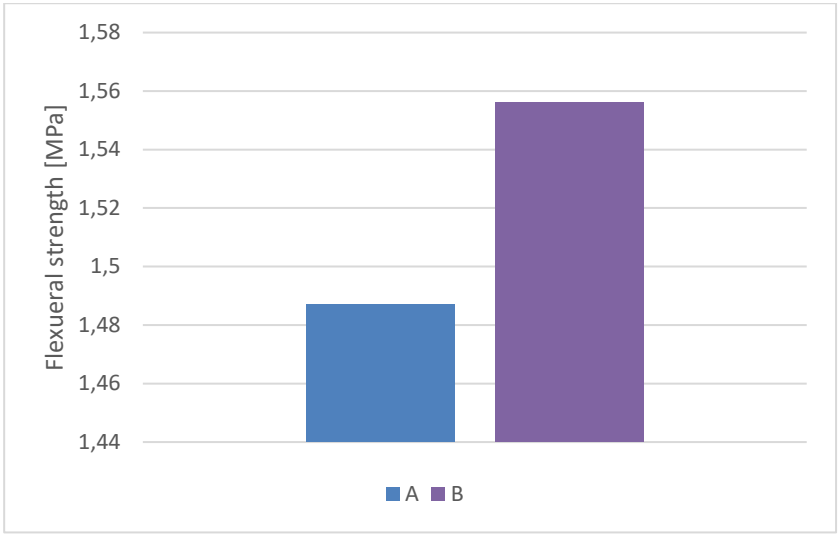

Figure 40: Flexural strength MK_15

Appendix B: Compressive strength

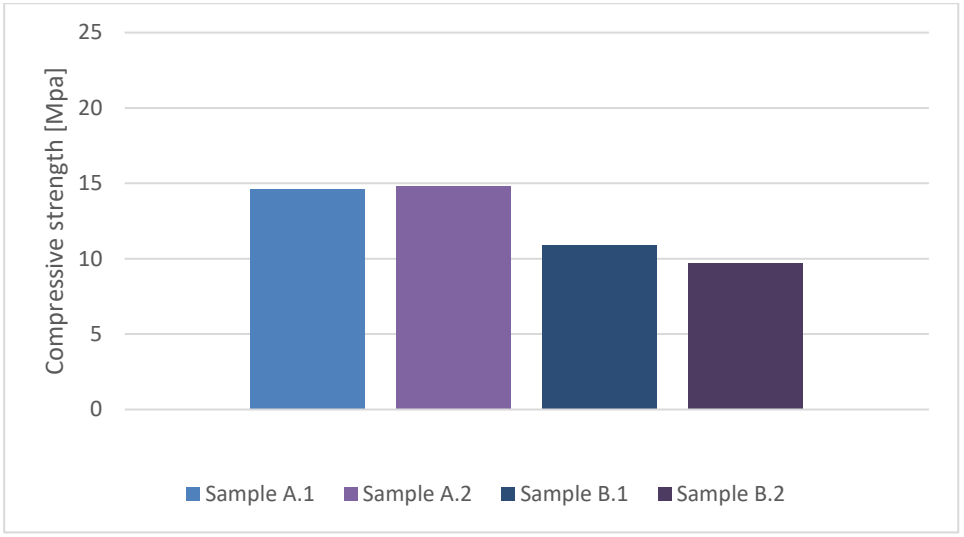

Figure 41: Compressive strength CEM_00

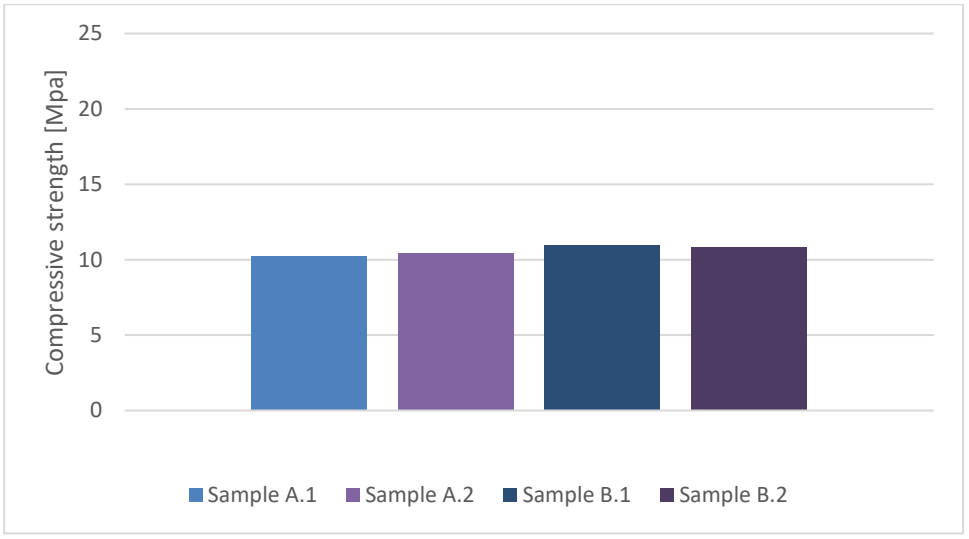

Figure 42: Compressive strength CEM_10

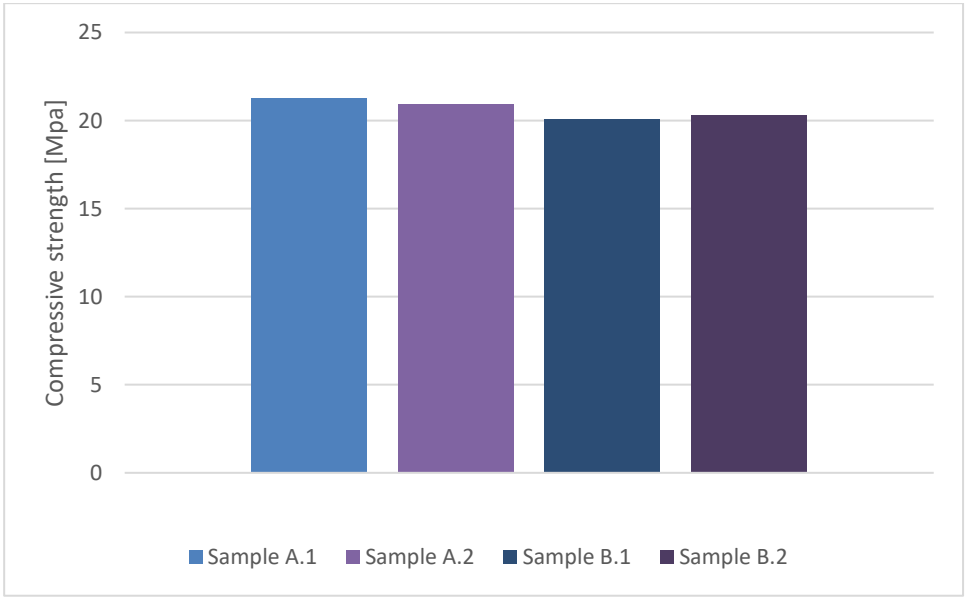

Figure 43: Compressive strength CEM_15

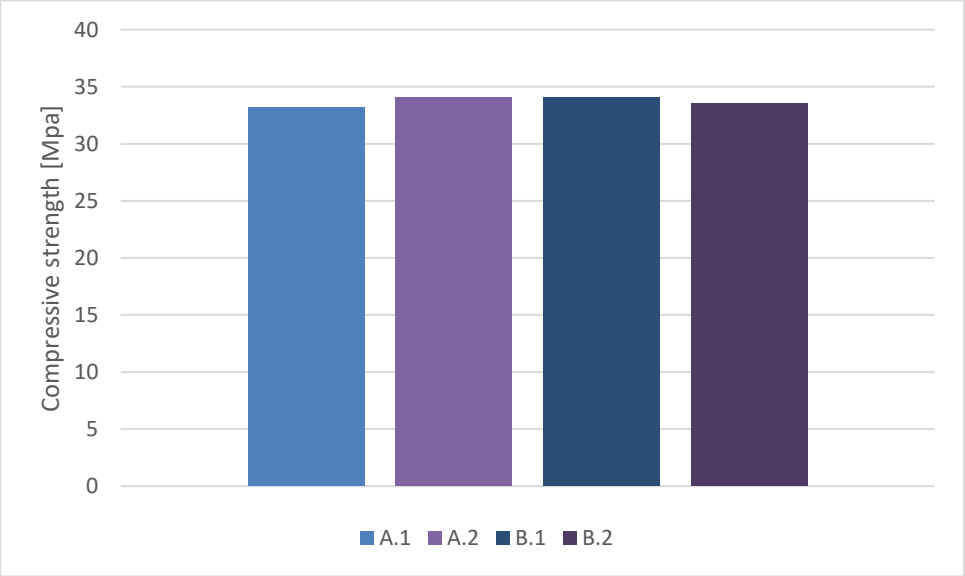

Figure 44: Compressive strength BFS_10

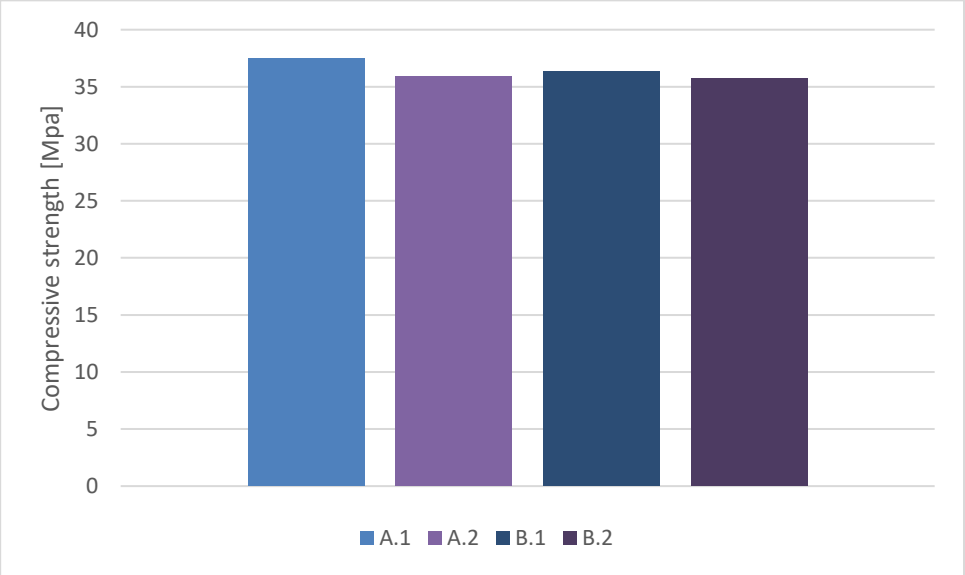

Figure 45: Compressive strength BFS_15

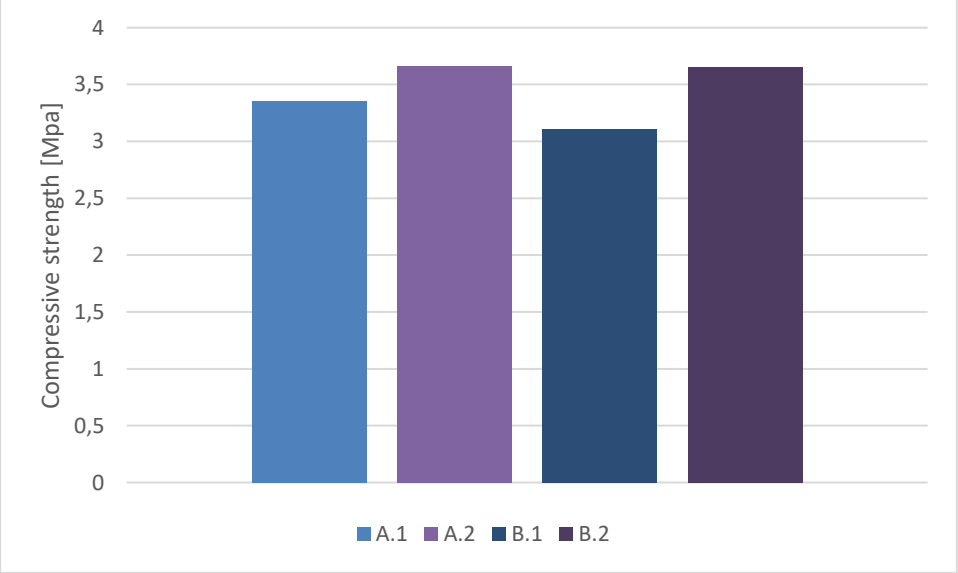

Figure 46: Compressive strength MK_10

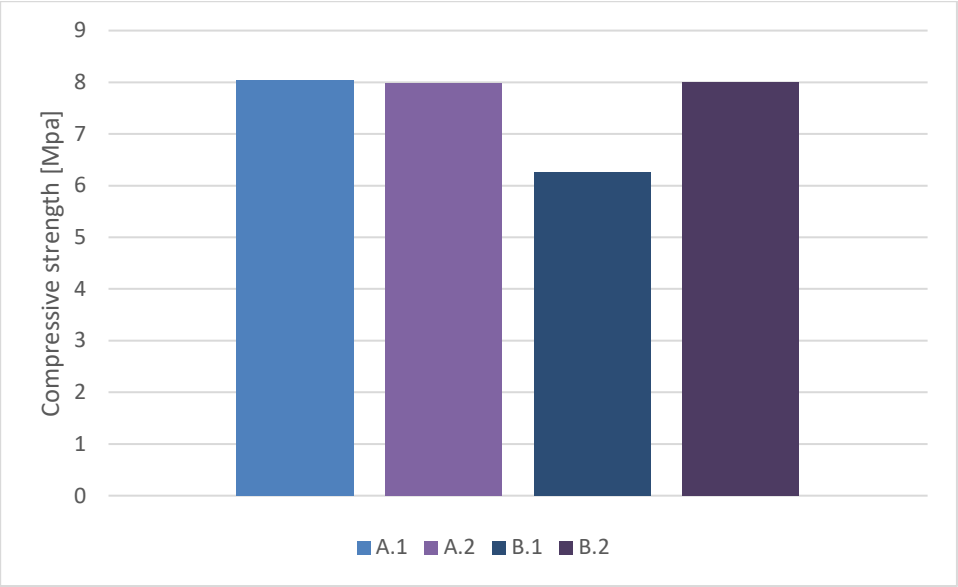

Figure 47: Compressive strength MK_15

Appendix C: Setting time

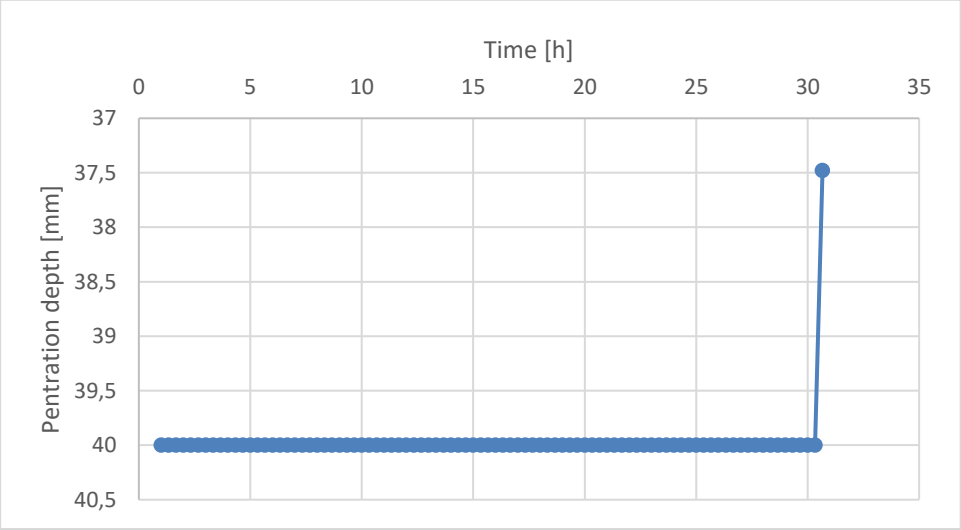

Figure 48: Setting time CEM_00

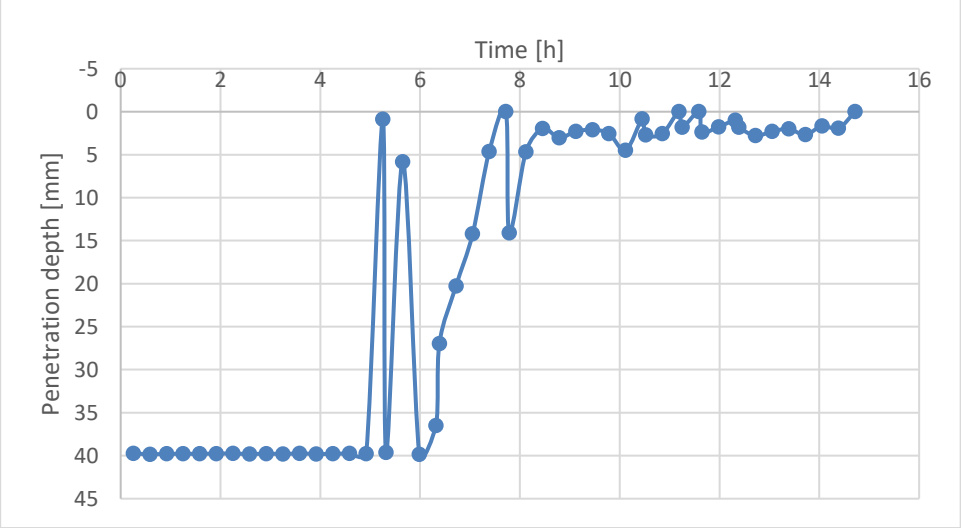

Figure 49: Setting time CEM_10

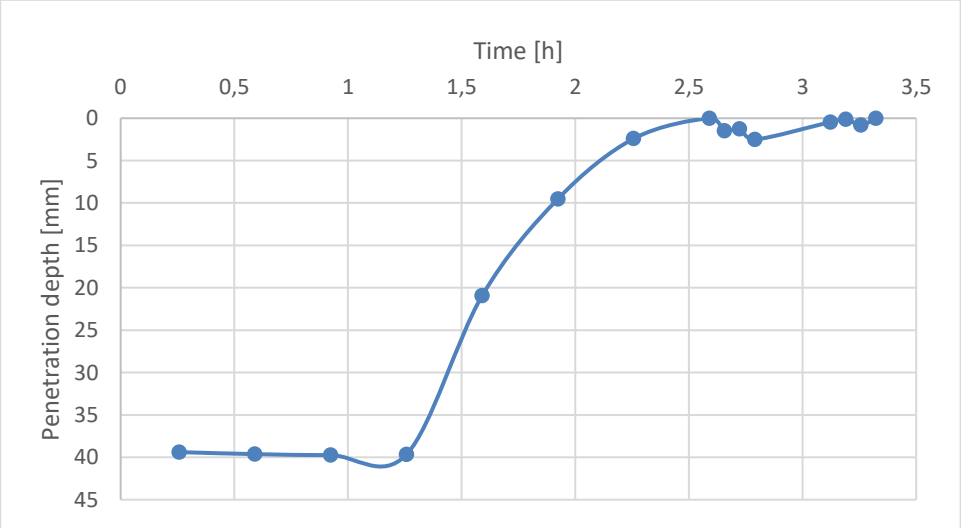

Figure 50: Setting time CEM_15

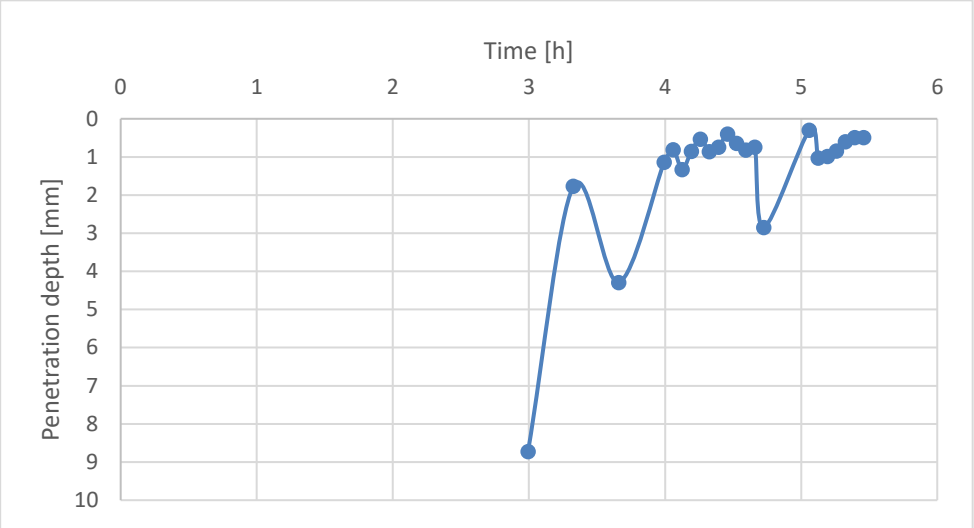

Figure 51: Setting time BFS_10

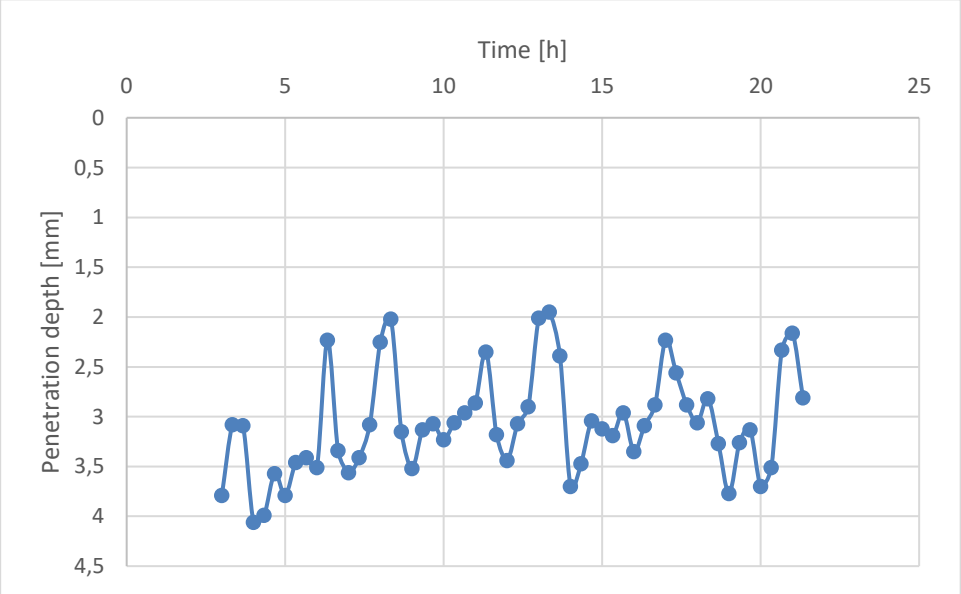

Figure 52: Setting time BFS_15

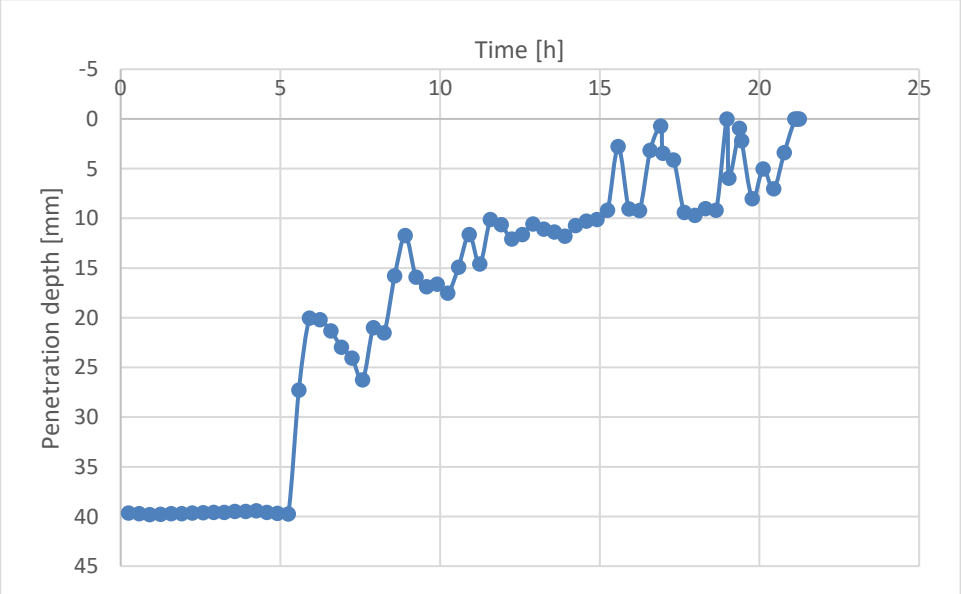

Figure 53: Setting time MK_10

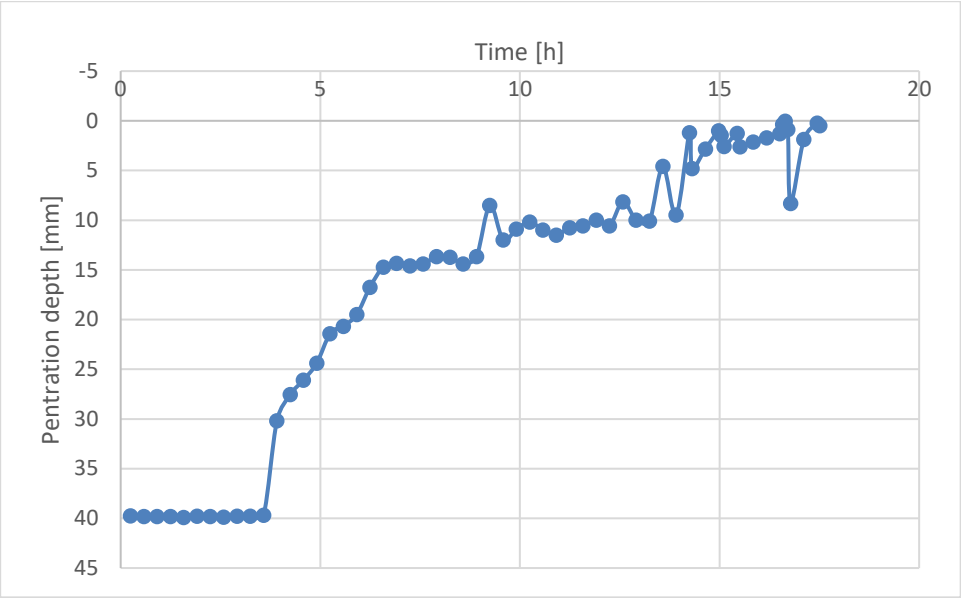

Figure 54: Setting time MK_15

Appendix D: Viscosity

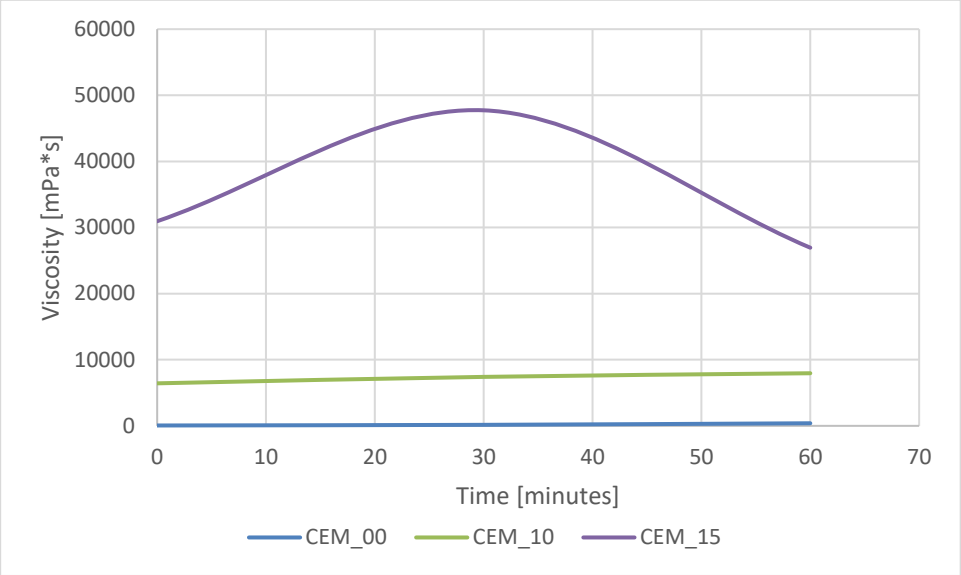

Figure 55: Viscosity CEM-based systems

Table 23: Temperature of viscosity CEM

Recipe	$T_{0\ min}$ [°C]	$T_{30\ min}$ [°C]	$T_{60\ min}$ [°C]
CEM_00	20,1	20,1	20,1
CEM_10	20,7	20,2	19,9
CEM_15	20,8	20,3	20,2

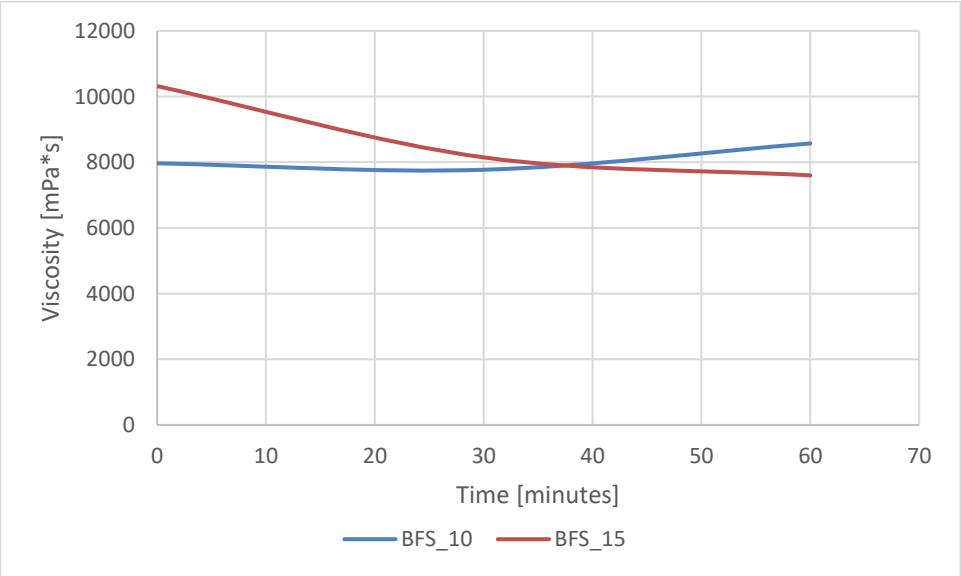

Figure 56: Viscosity BFS-based systems

Table 24: Temperature of viscosity BFS

Recipe	$T_{0\ min}$ [°C]	$T_{30\ min}$ [°C]	$T_{60\ min}$ [°C]
BFS_10	20,7	20,3	20,1
BFS_15	21,7	20,6	20,3

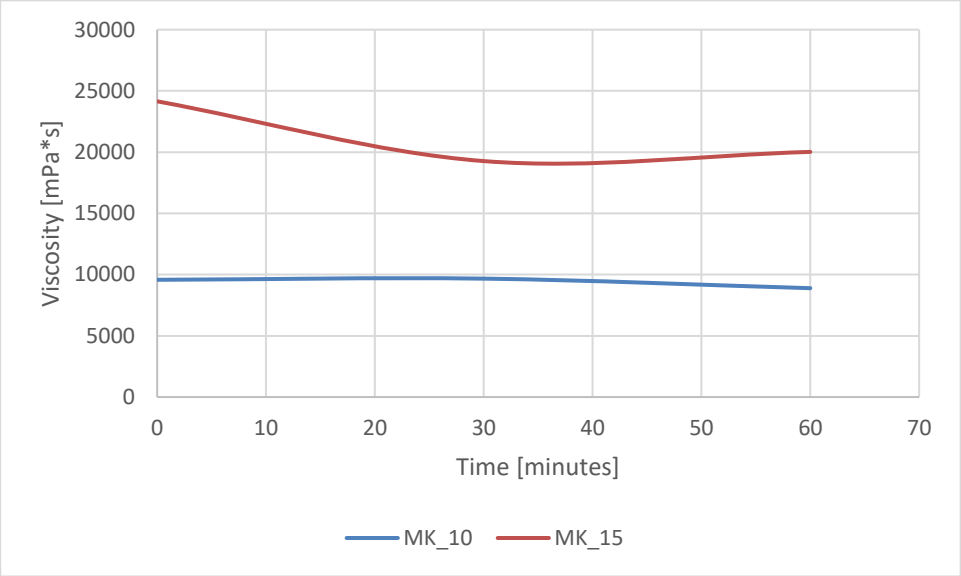

Figure 57: Viscosity MK-based systems

Table 25: Temperature of viscosity MK

Recipe	$T_{0\ min}$ [°C]	$T_{30\ min}$ [°C]	$T_{60\ min}$ [°C]
MK_10	20,4	20,2	20,2
MK_15	21,6	20,7	20,1

Appendix E: Hydration heat

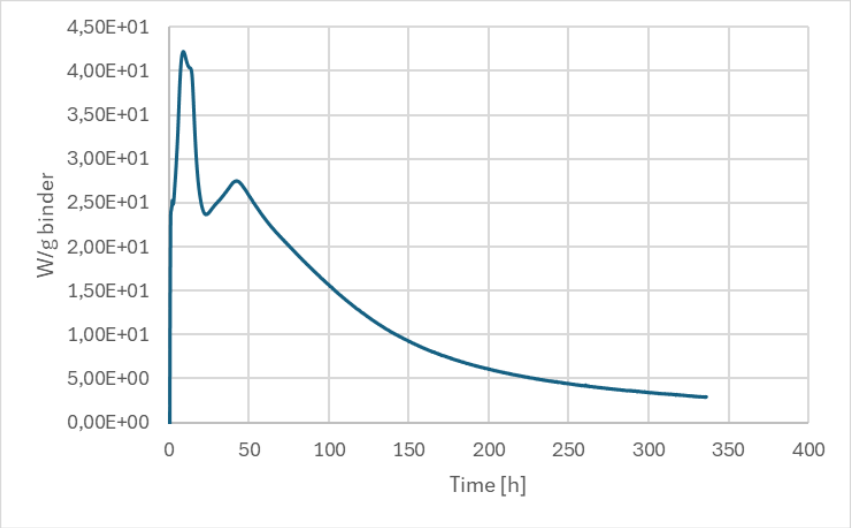

Figure 58: Heat flow CEM_00

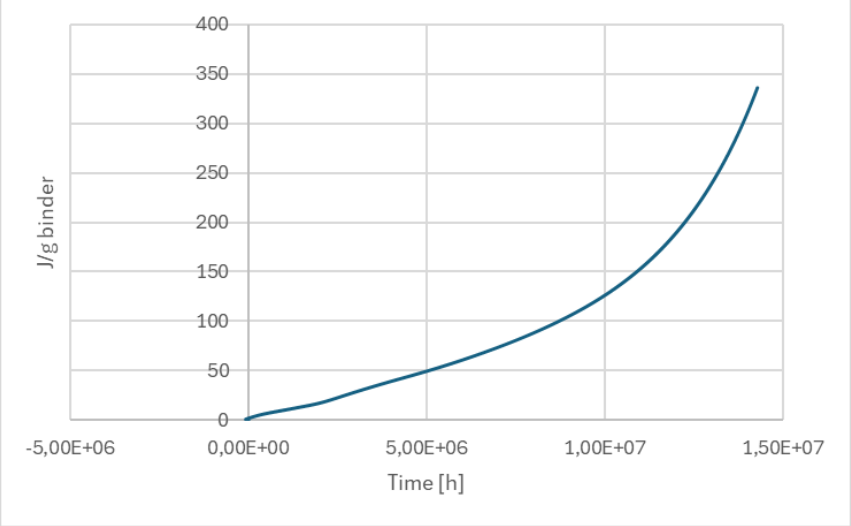

Figure 59: Cumulative heat CEM_00

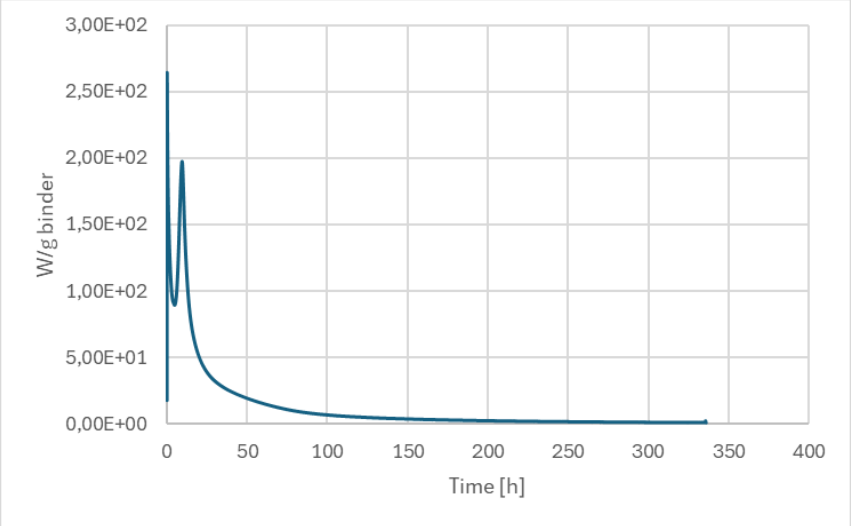

Figure 60: Heat flow CEM_10

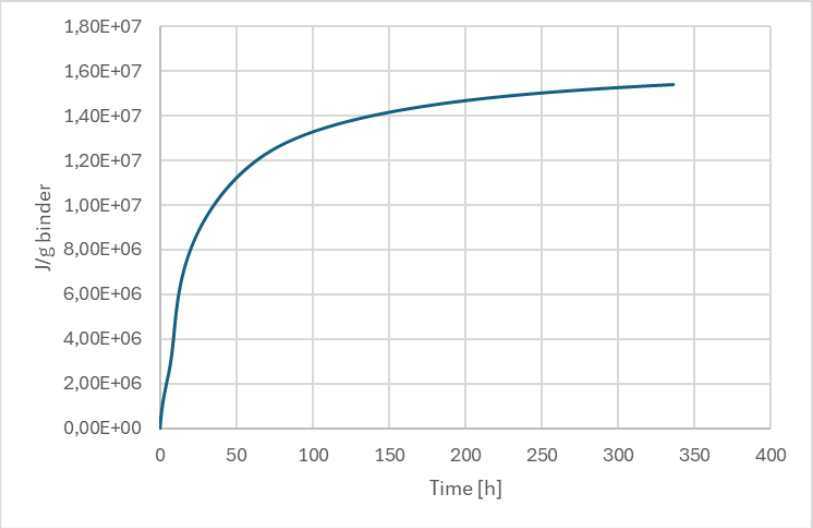

Figure 61: Cumulative heat CEM_10

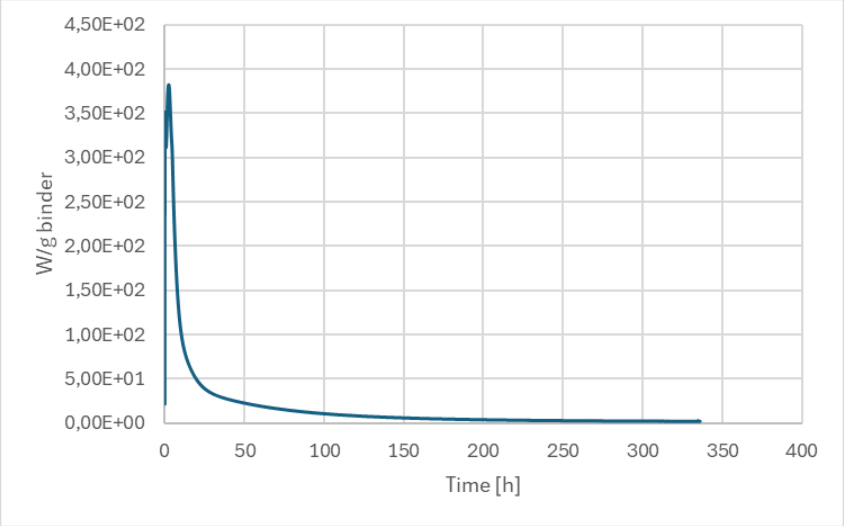

Figure 62: Heat flow CEM_15

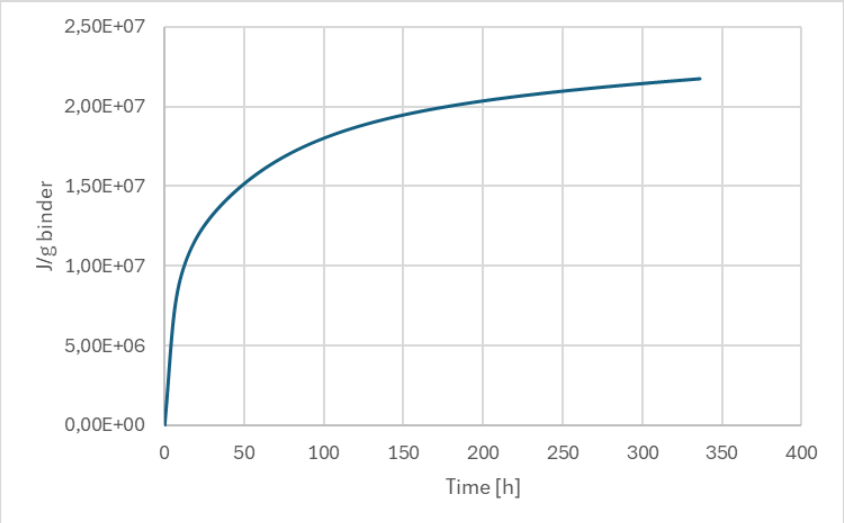

Figure 63: Cumulative heat CEM_15

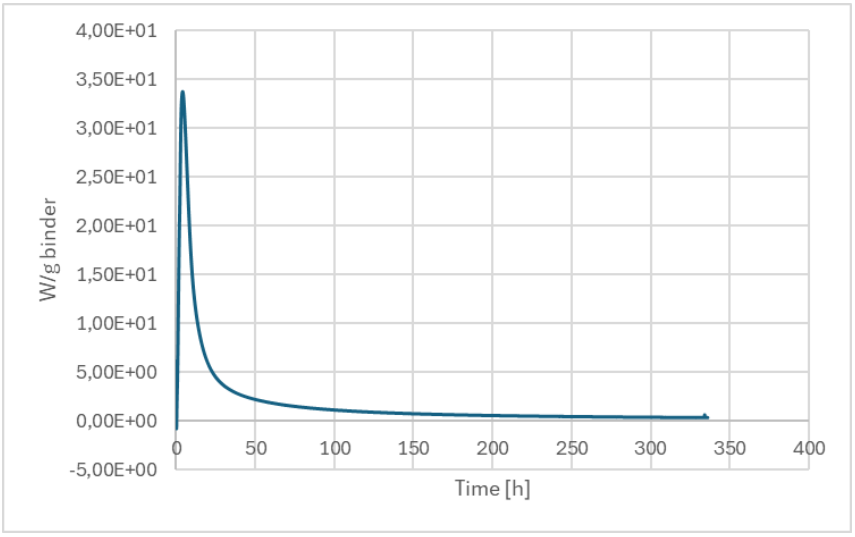

Figure 64: Heat flow BFS_10

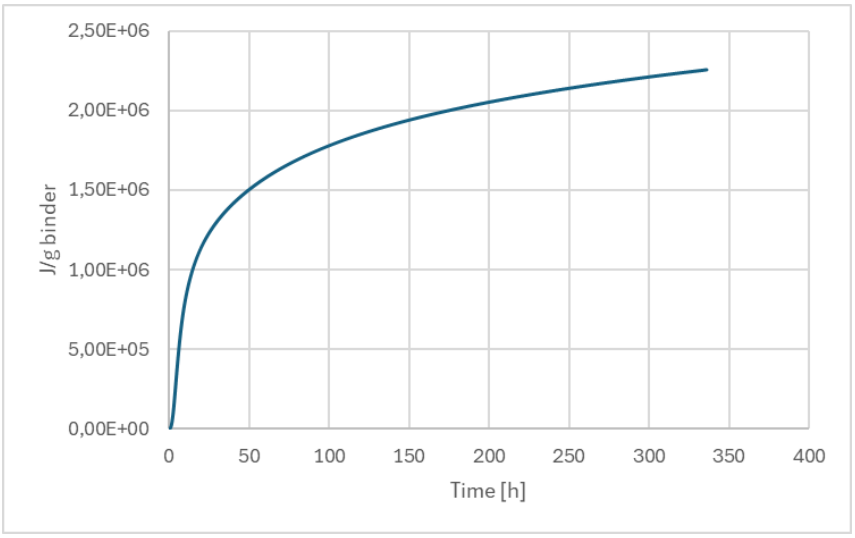

Figure 65: Cumulative heat BFS_10

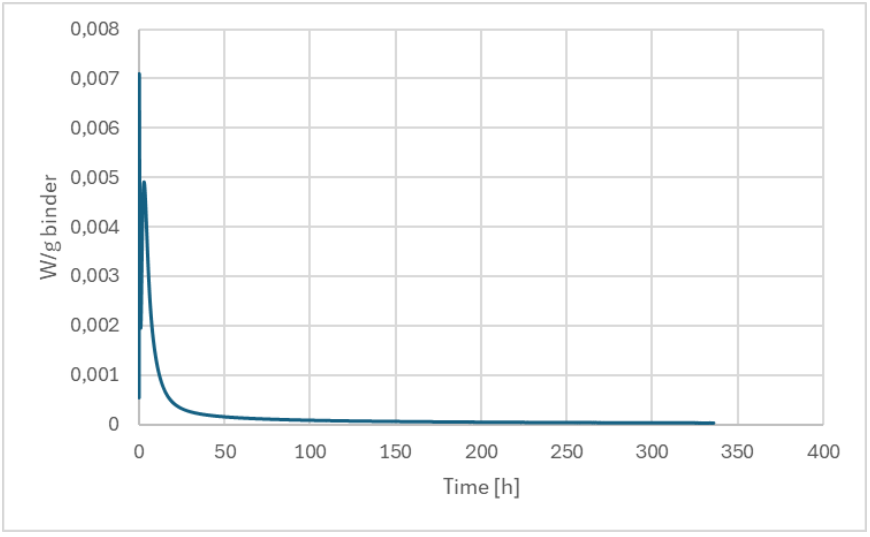

Figure 66: Heat flow BFS_15

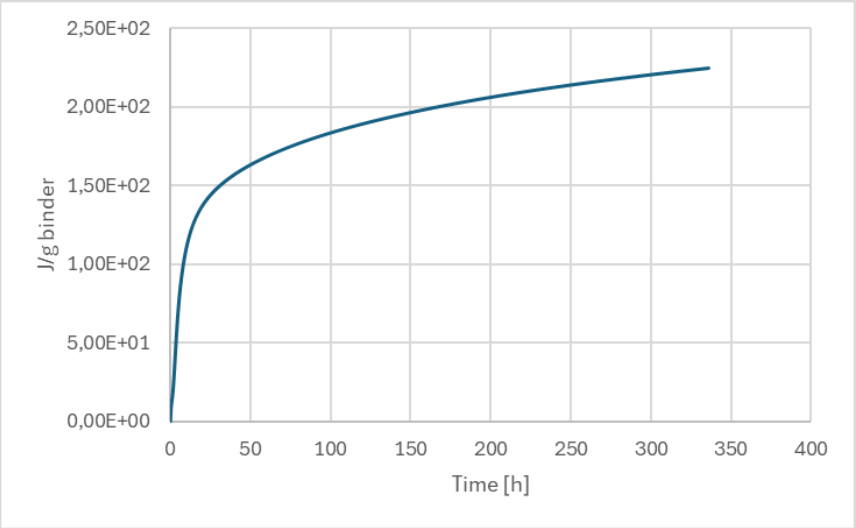

Figure 67: Cumulative heat BFS_15

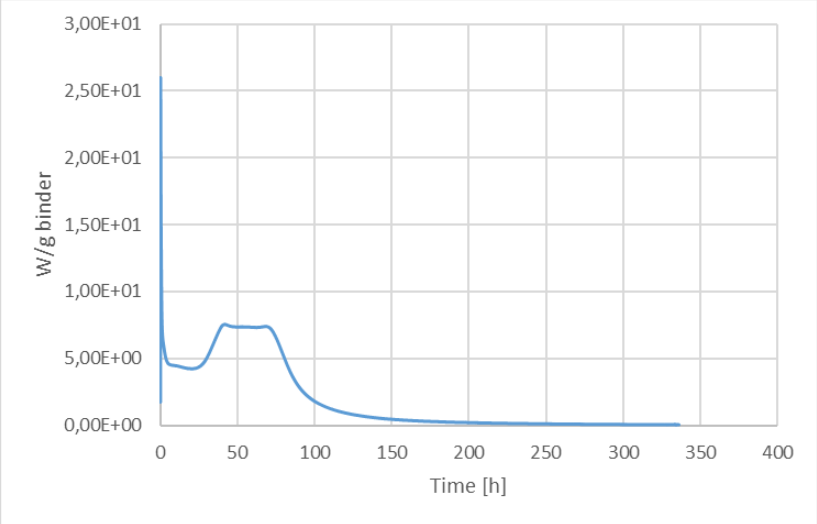

Figure 68: Heat flow MK_10

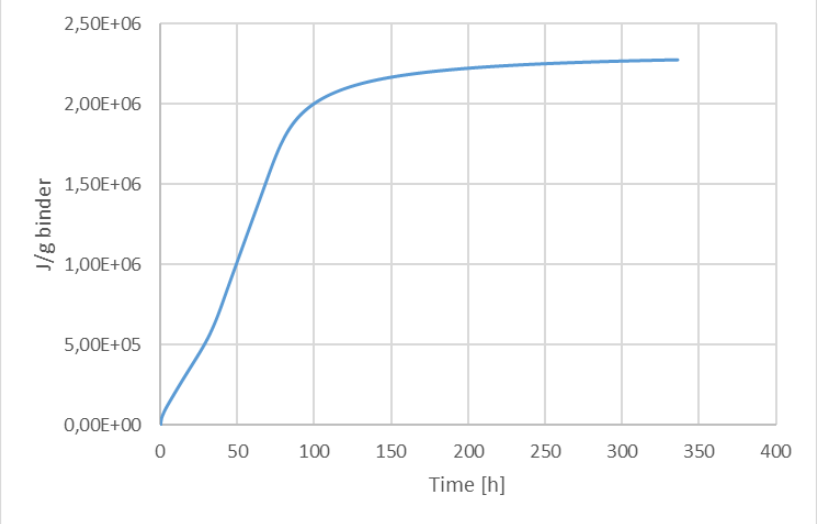

Figure 69: Cumulative heat MK_10

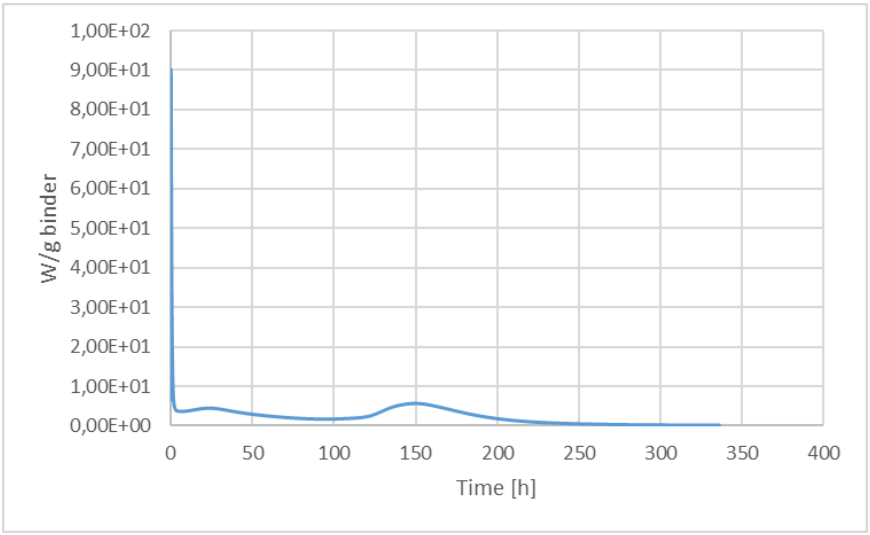

Figure 70: Heat flow MK_15

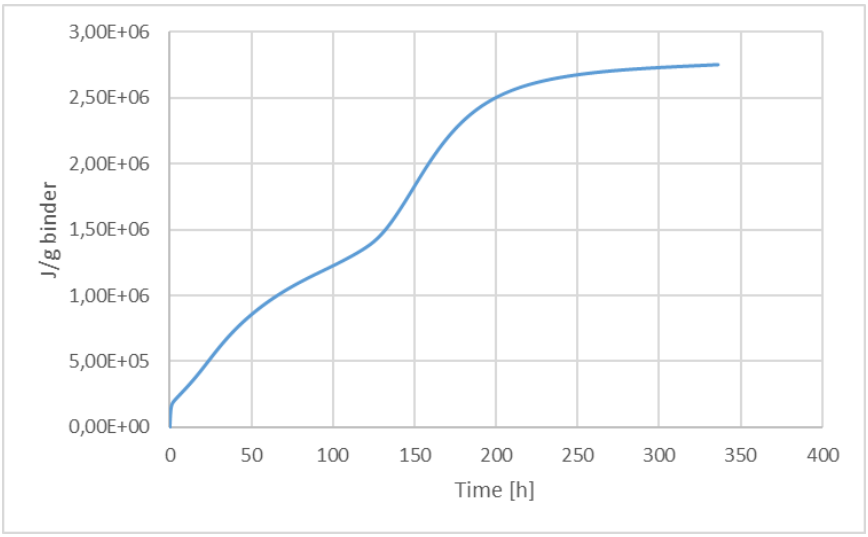

Figure 71: Cumulative heat MK_15

Appendix F: Carbonation resistance

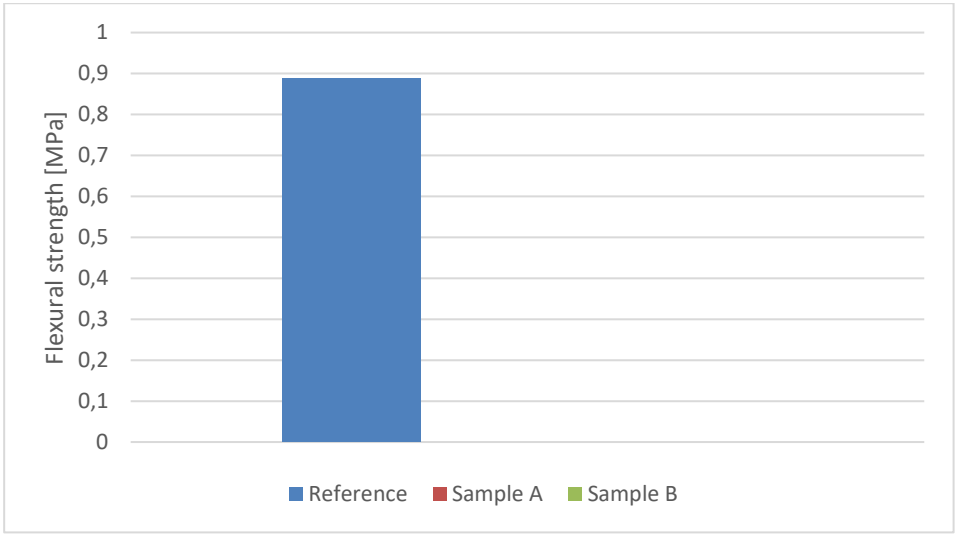

Figure 72: Carbonation flexural strength CEM_00

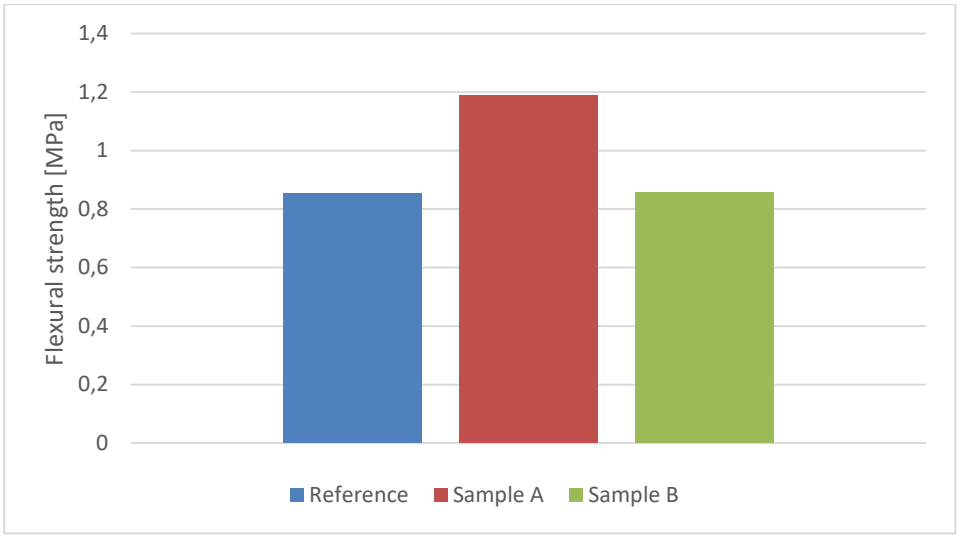

Figure 73: Carbonation flexural strength CEM_10

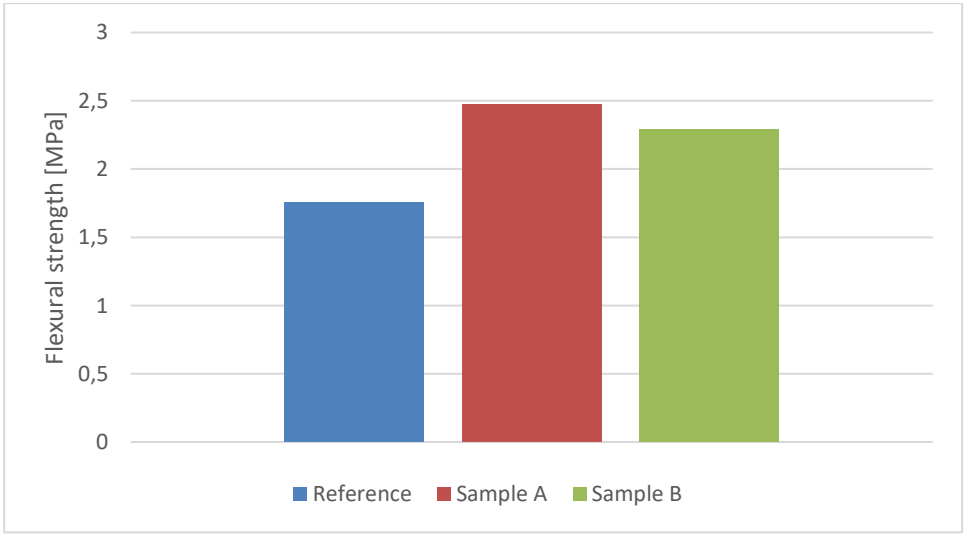

Figure 74: Carbonation flexural strength CEM_15

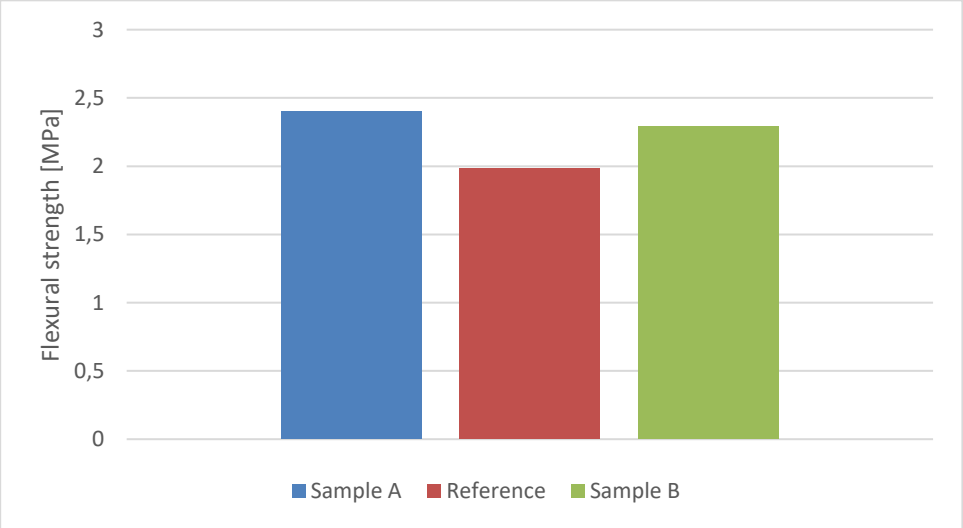

Figure 75: Carbonation flexural strength BFS_10

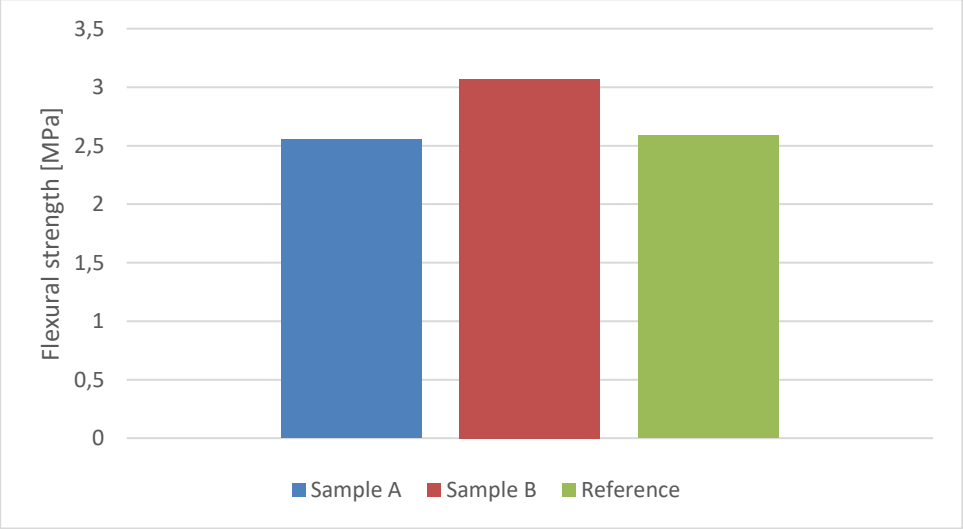

Figure 76: Carbonation flexural strength BFS_15

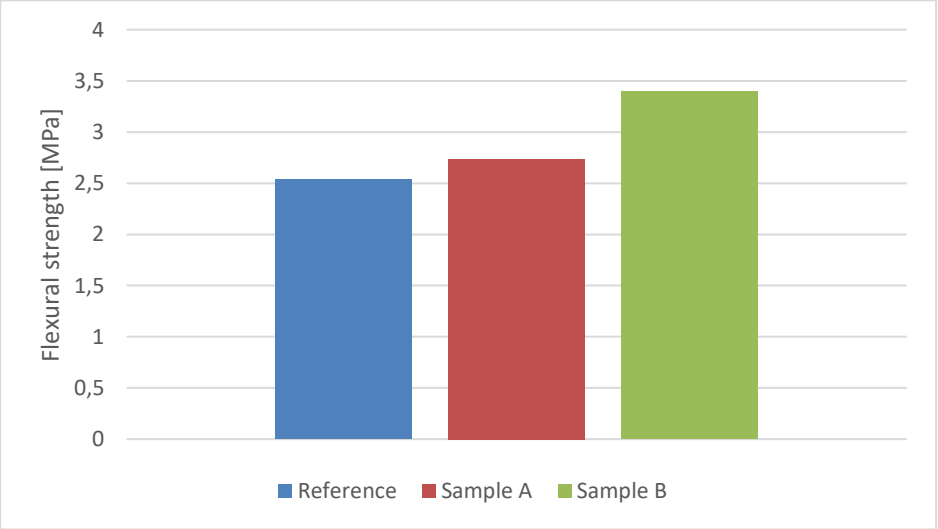

Figure 77: Carbonation flexural strength MK_10

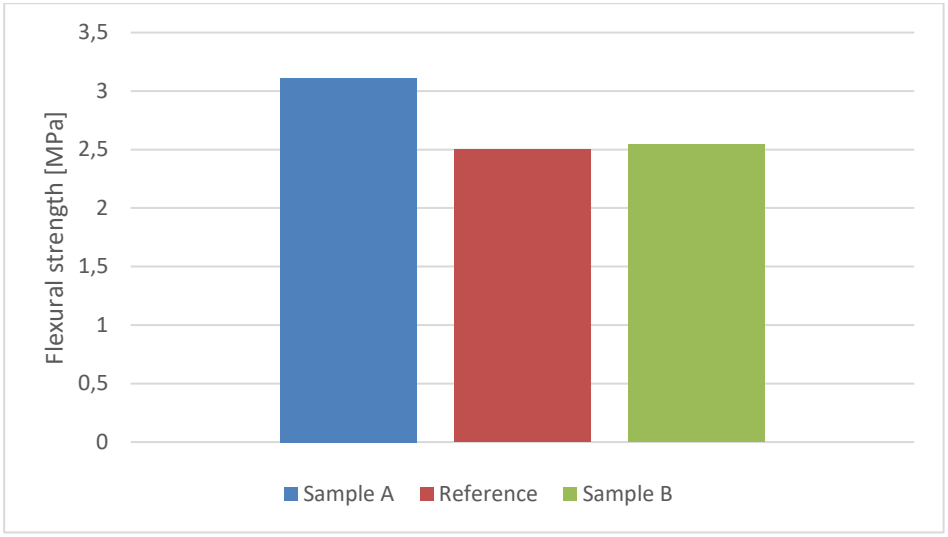

Figure 78: Carbonation flexural strength MK_15

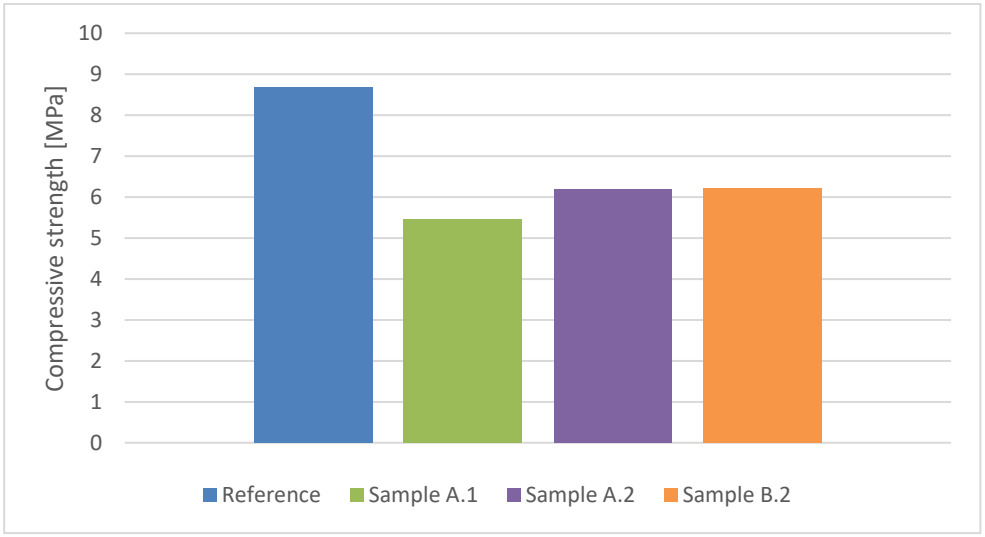

Figure 79: Carbonation compressive strength CEM_00

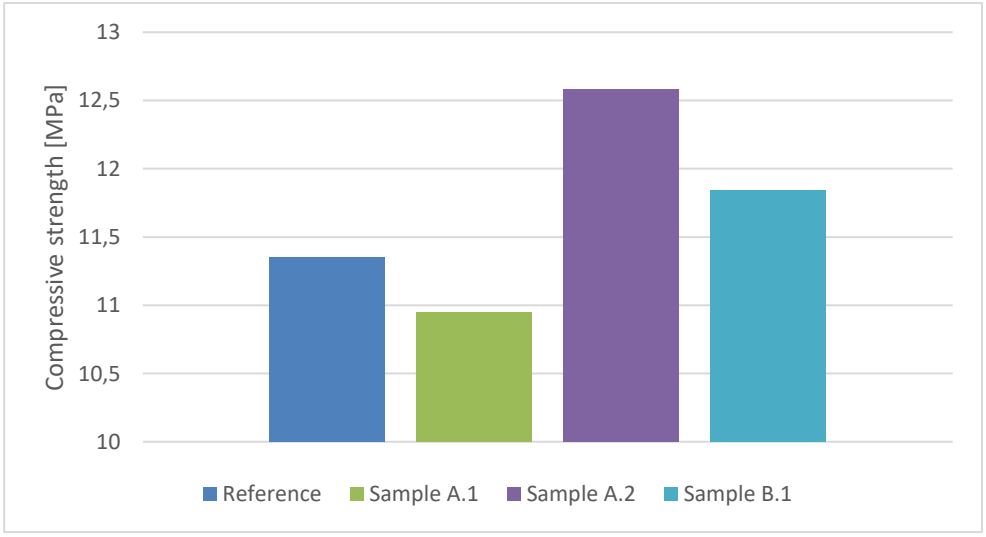

Figure 80: Carbonation compressive strength CEM_10

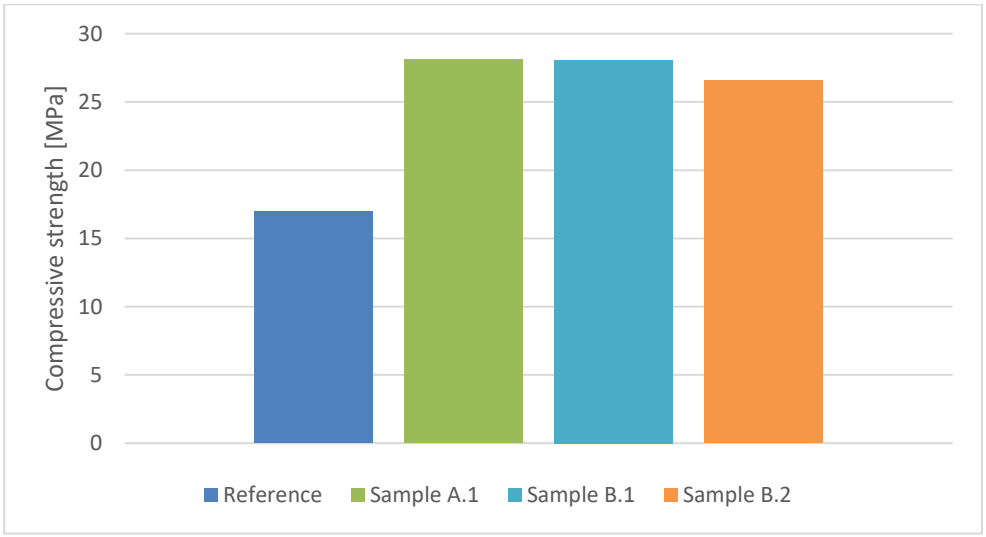

Figure 81: Carbonation compressive strength CEM_15

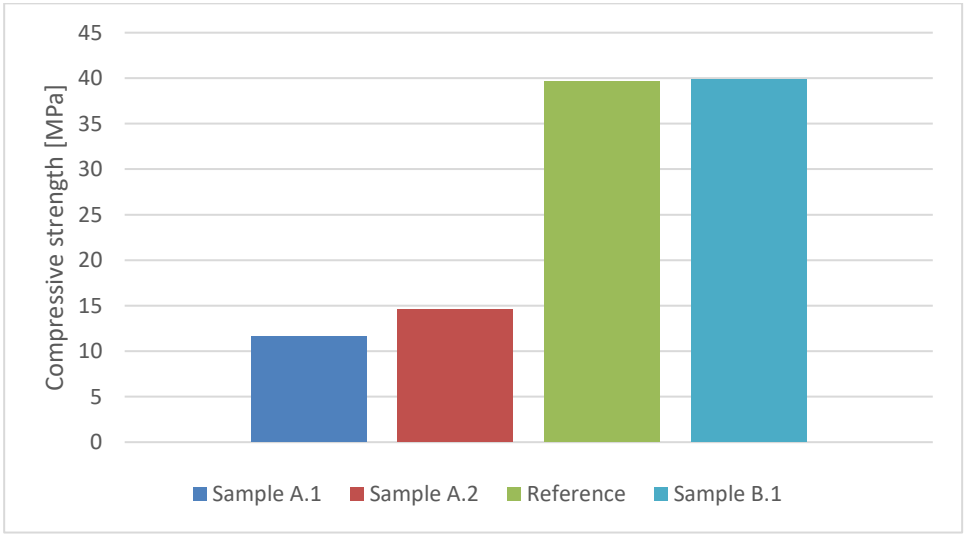

Figure 82: Carbonation compressive strength BFS_10

Figure 83: Carbonation compressive strength BFS_15

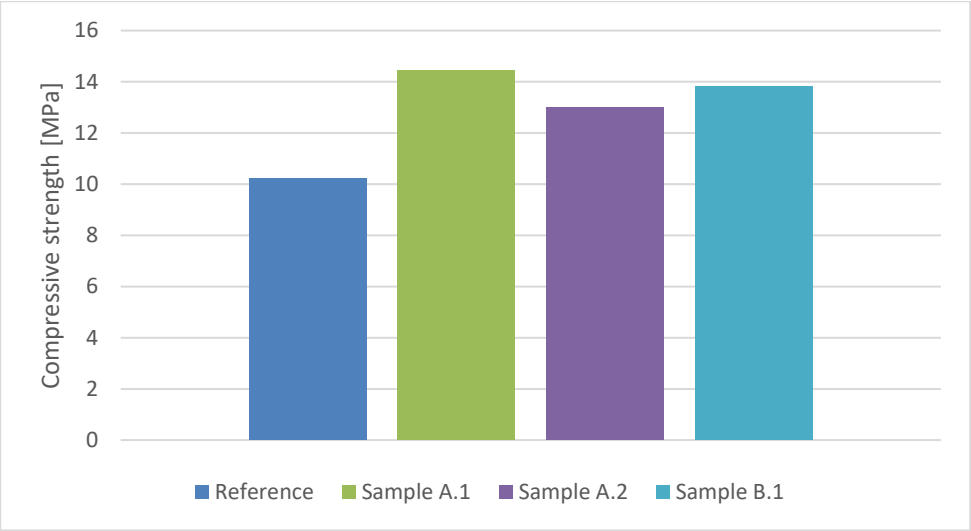

Figure 84: Carbonation compressive strength MK_10

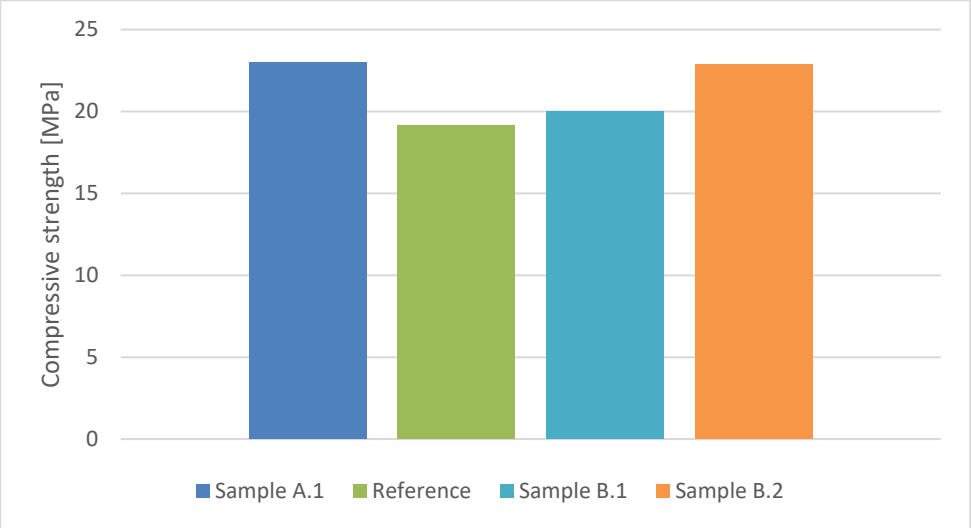

Figure 85: Carbonation compressive strength MK_15

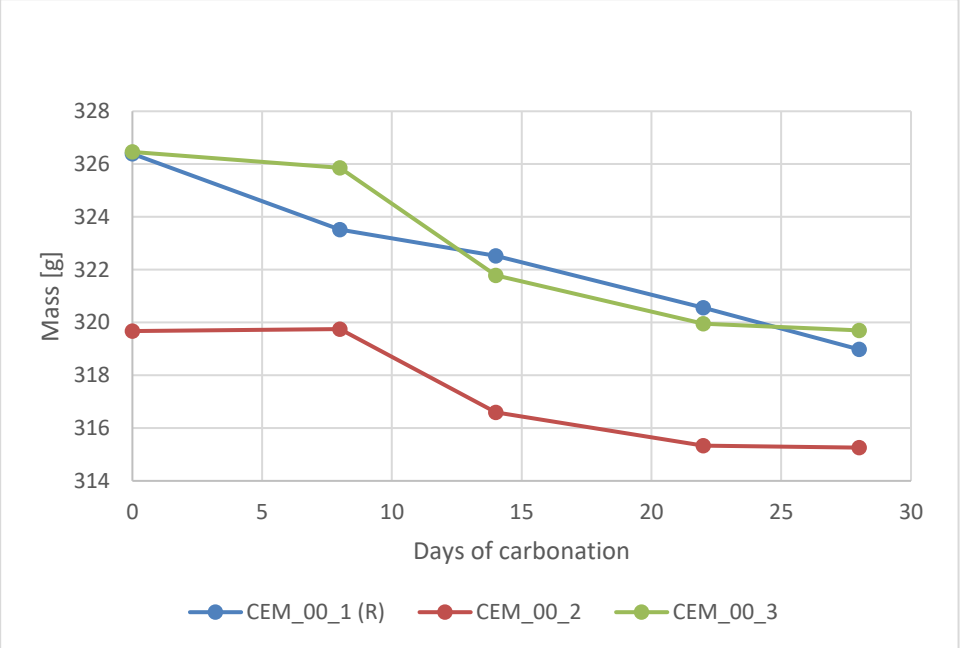

Figure 86: Mass evolution carbonation CEM_00

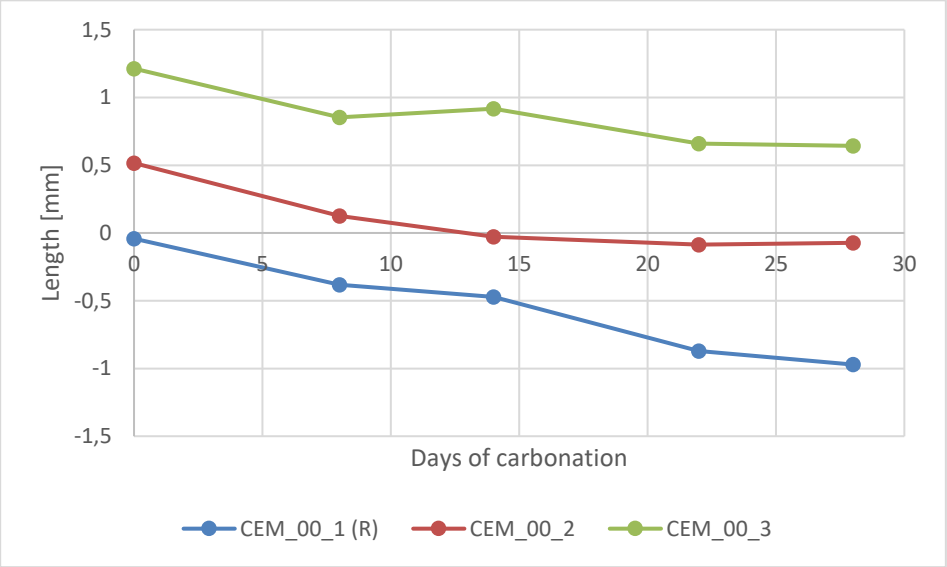

Figure 87: Length evolution carbonation CEM_00

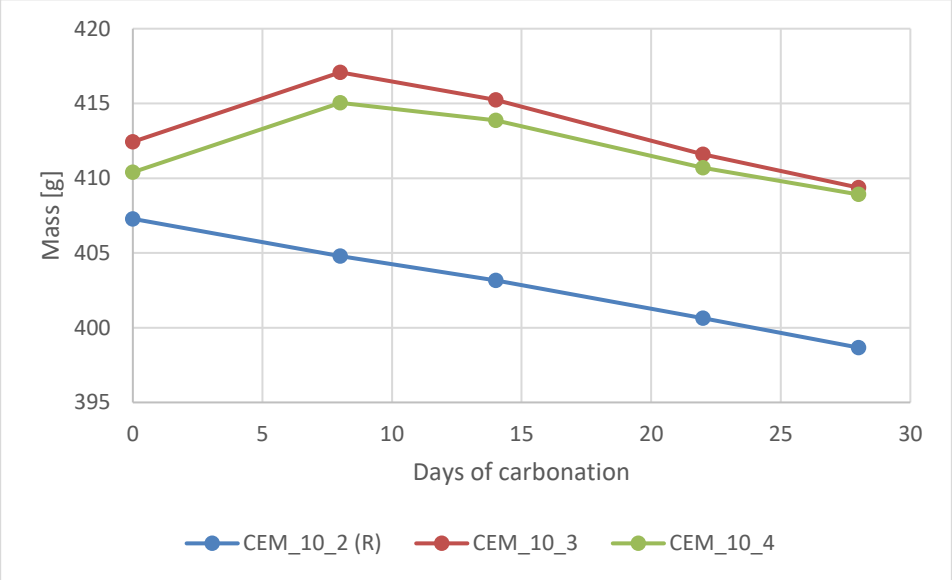

Figure 88: Mass evolution carbonation CEM_10

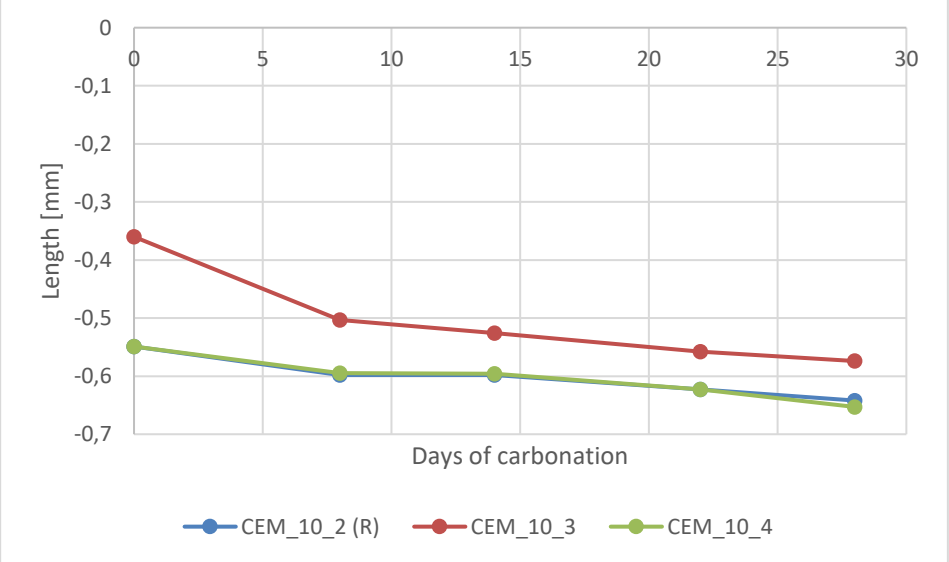

Figure 89: Length evolution carbonation CEM_10

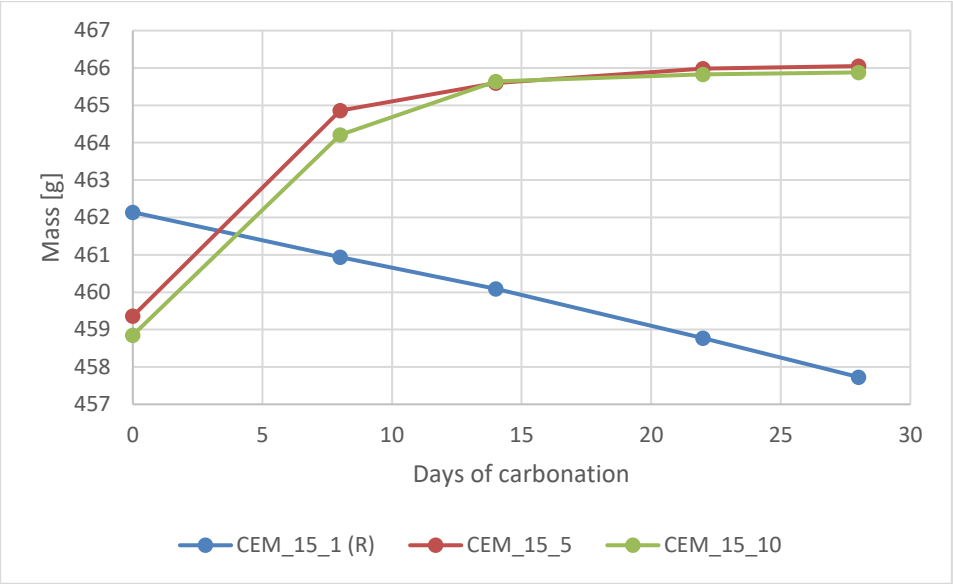

Figure 90: Mass evolution carbonation CEM_15

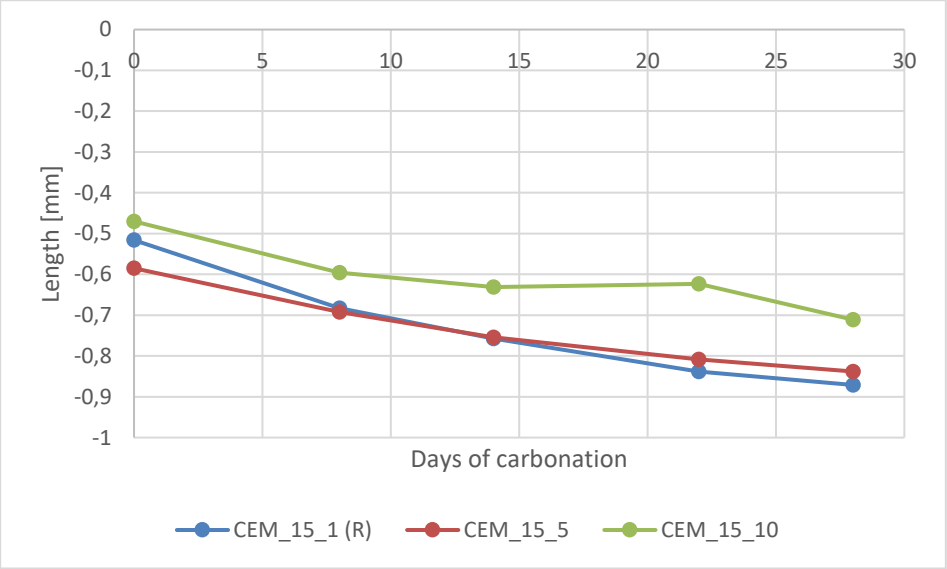

Figure 91: Length evolution carbonation CEM_15

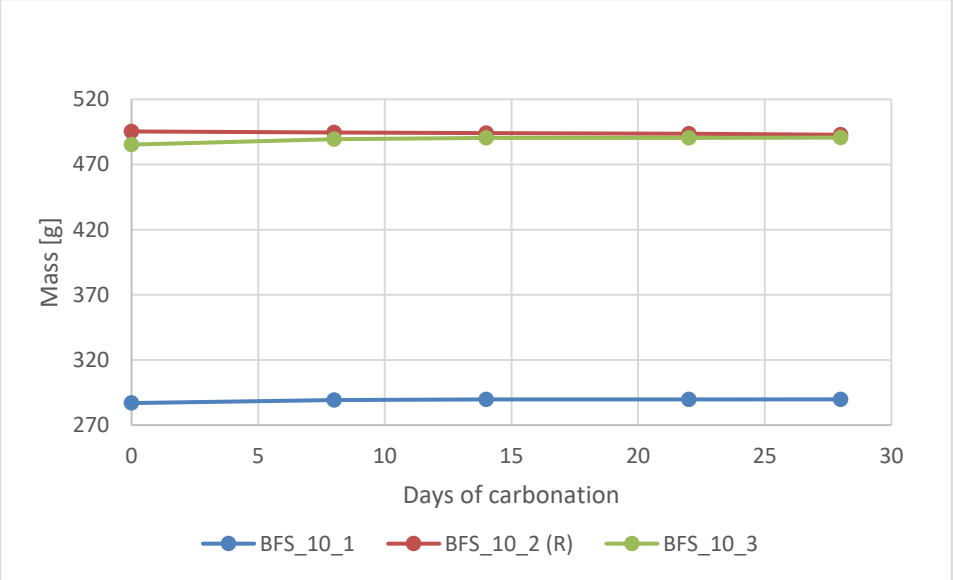

Figure 92: Mass evolution carbonation BFS_10

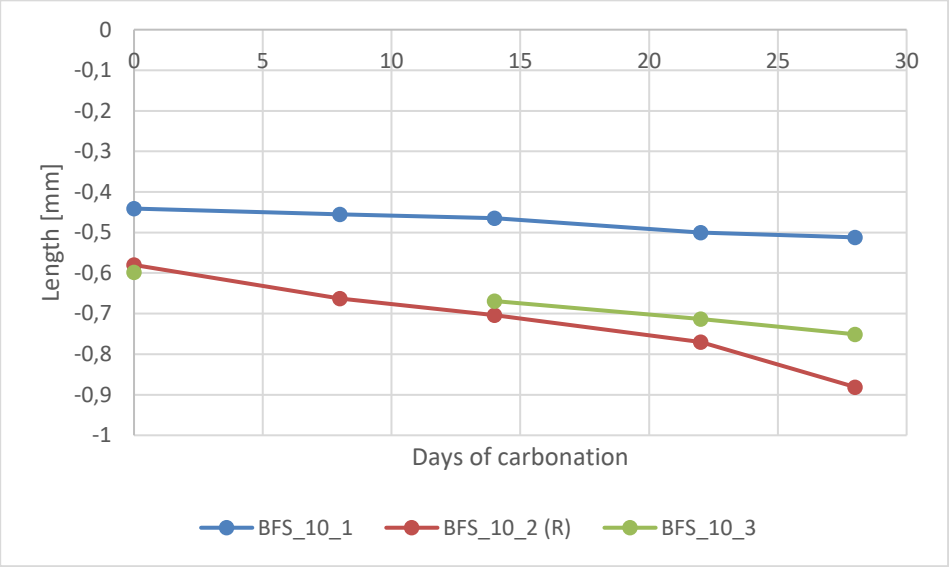

Figure 93: Length evolution carbonation BFS_10

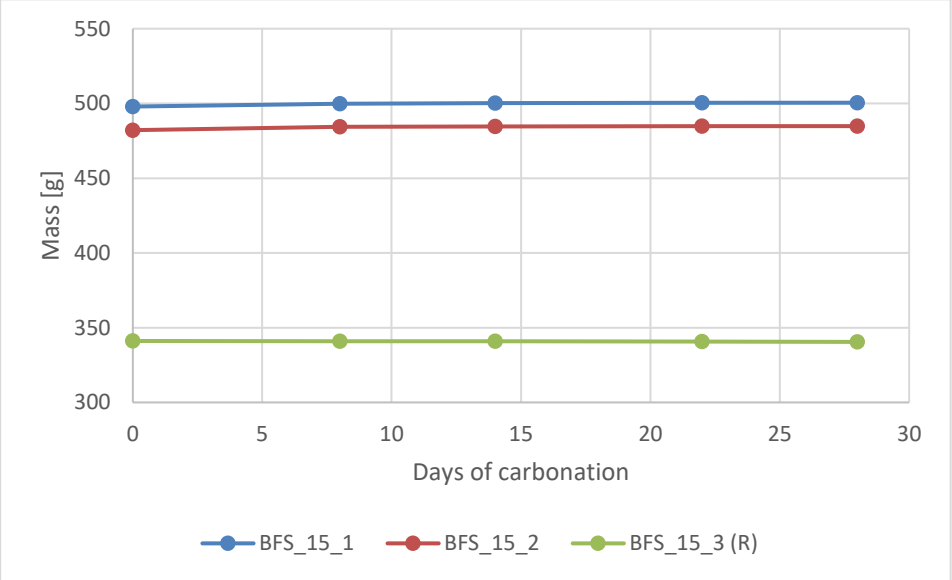

Figure 94: Mass evolution carbonation BFS_15

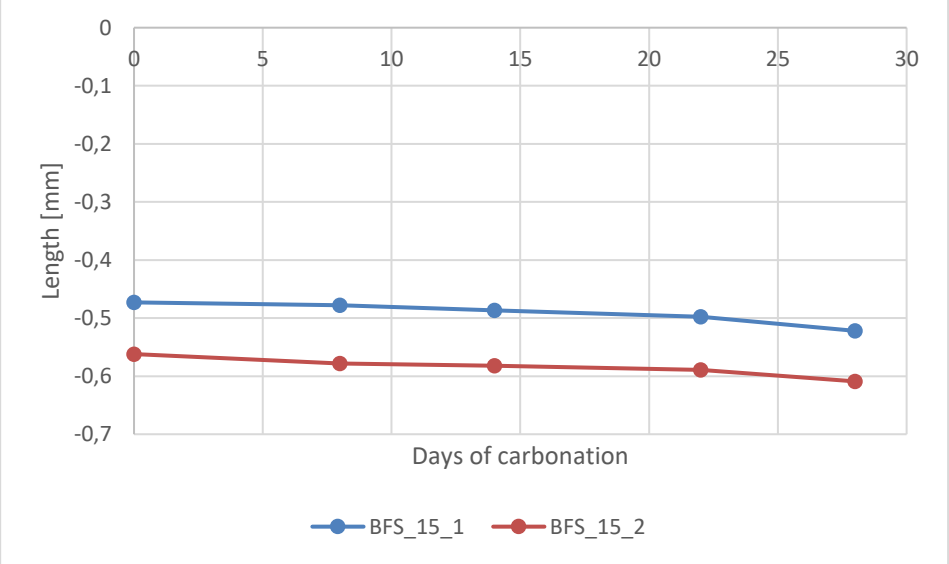

Figure 95: Length evolution carbonation BFS_15

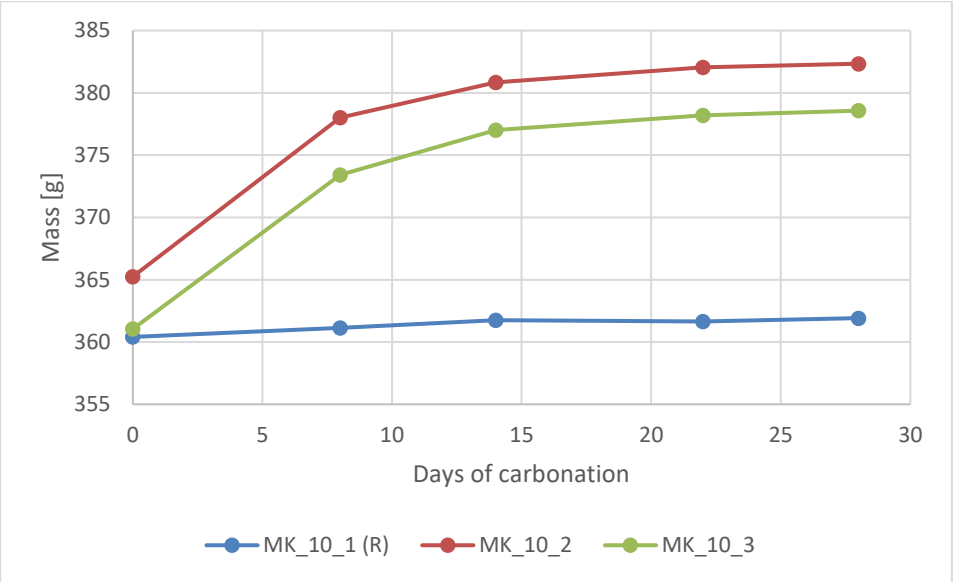

Figure 96: Mass evolution carbonation MK_10

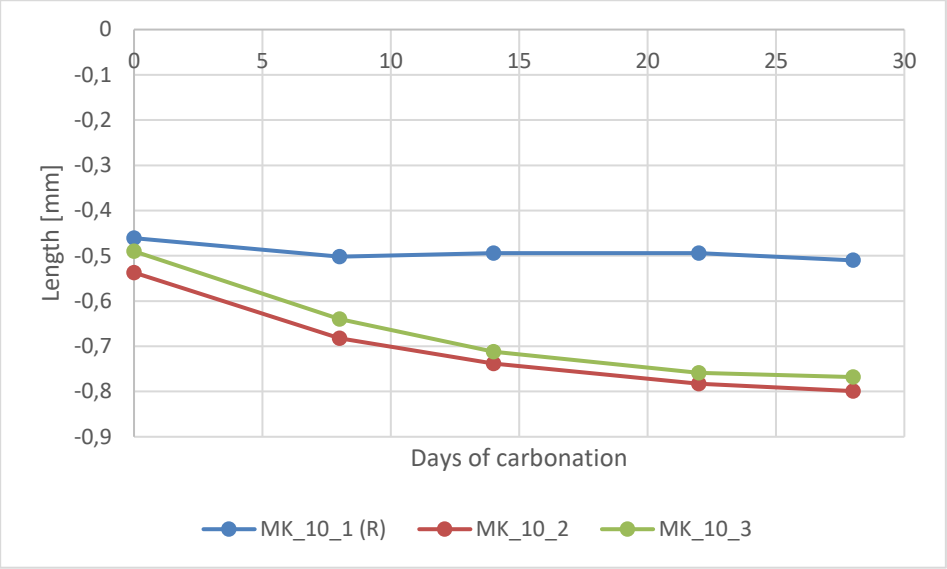

Figure 97: Length evolution carbonation MK_10

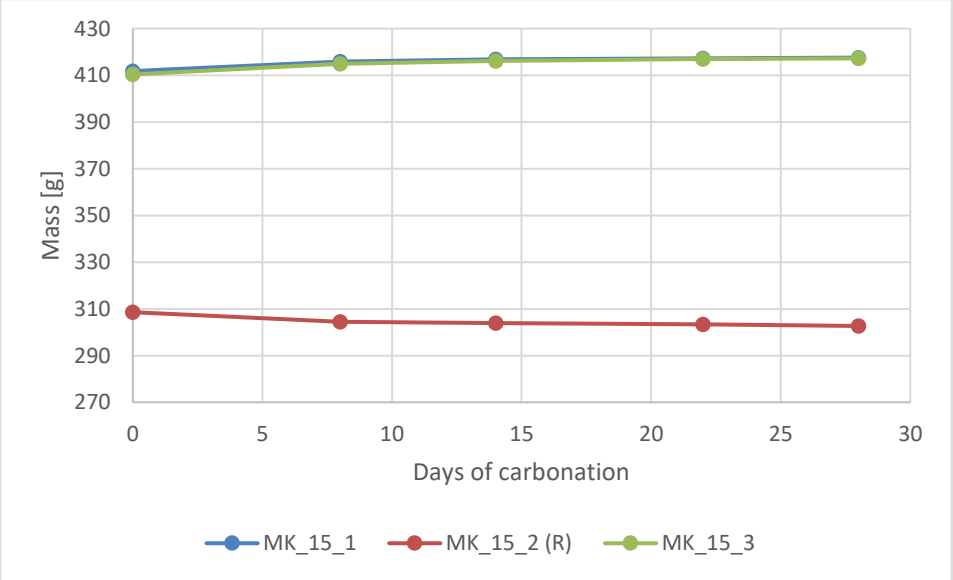

Figure 98: Mass evolution carbonation MK_15

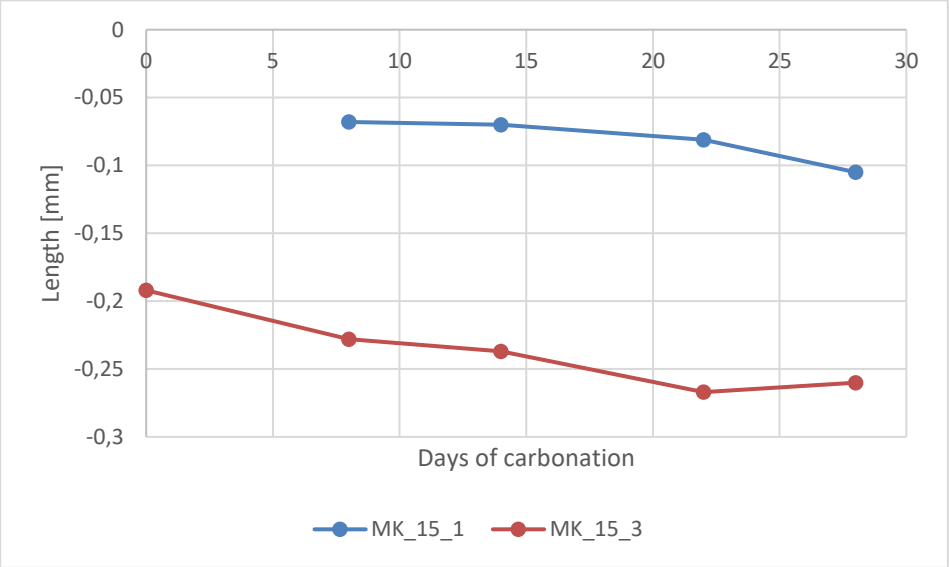

Figure 99: Length evolution carbonation MK_15

Appendix G: UT

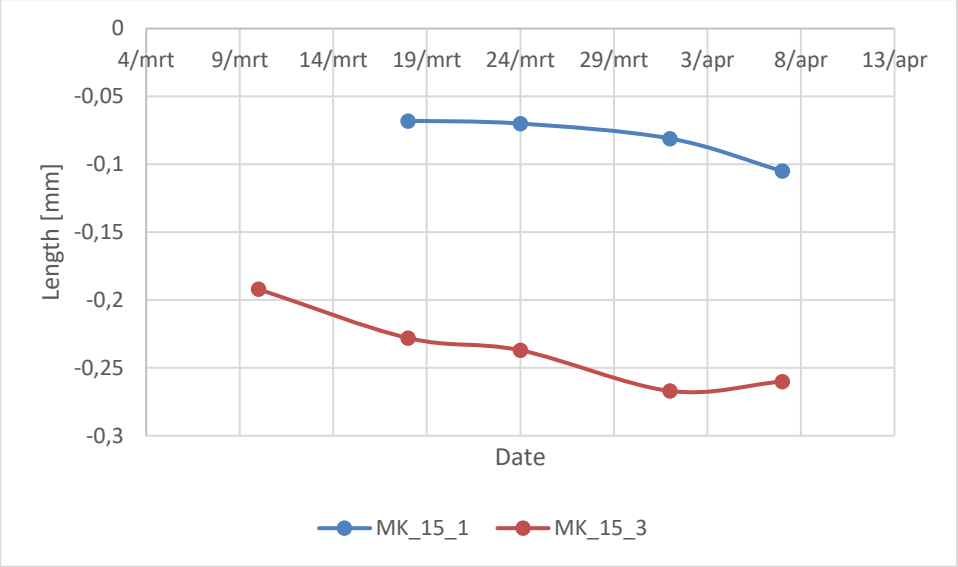

Figure 100: Length evolution carbonation MK_15

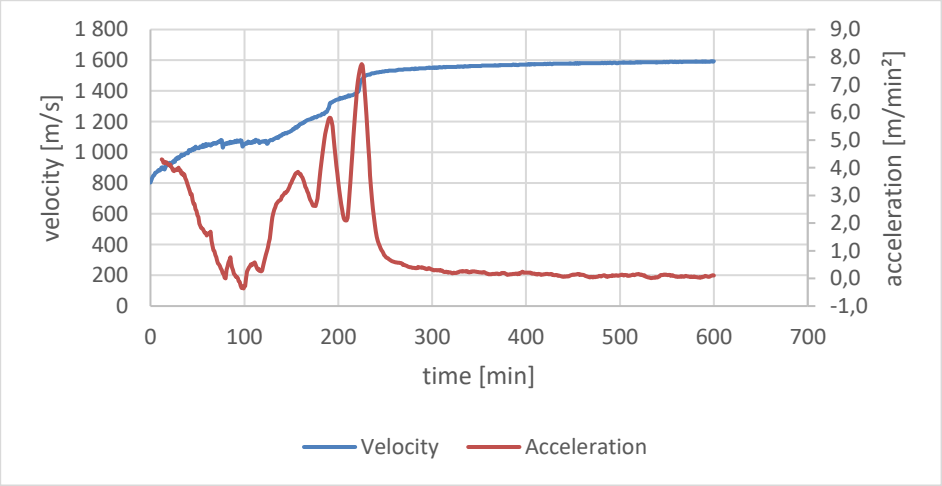

Figure 101: UT CEM_00

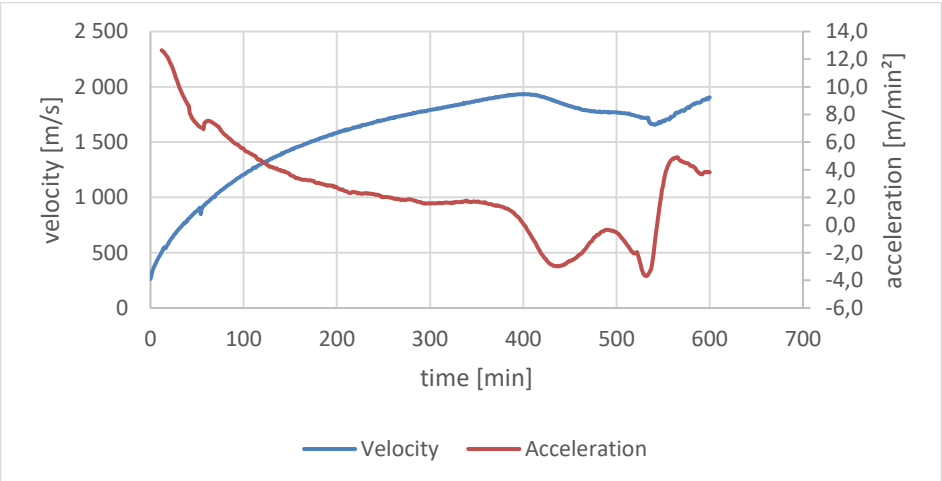

Figure 102: UT CEM_10

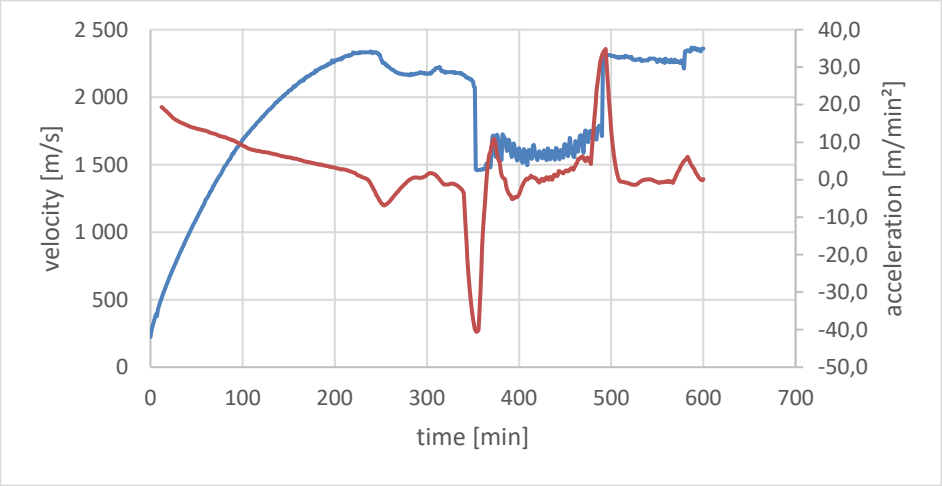

Figure 103: UT CEM_15

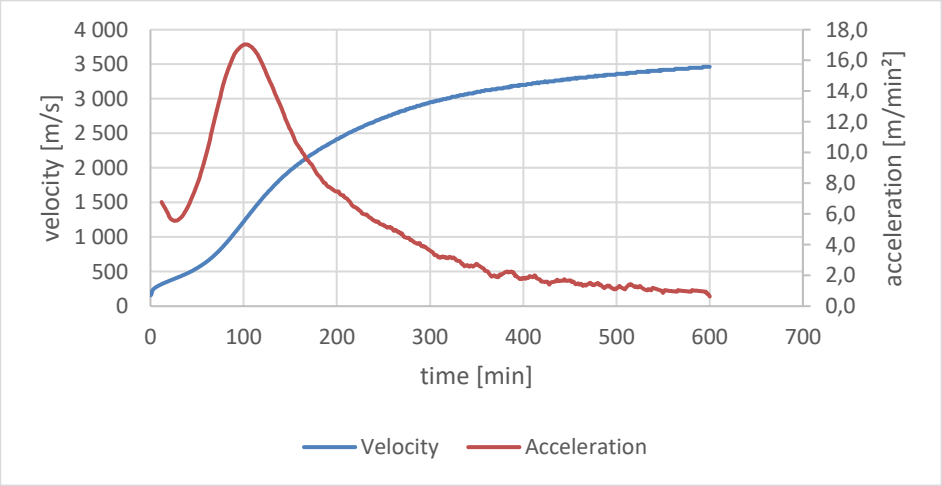

Figure 104: UT BFS_15

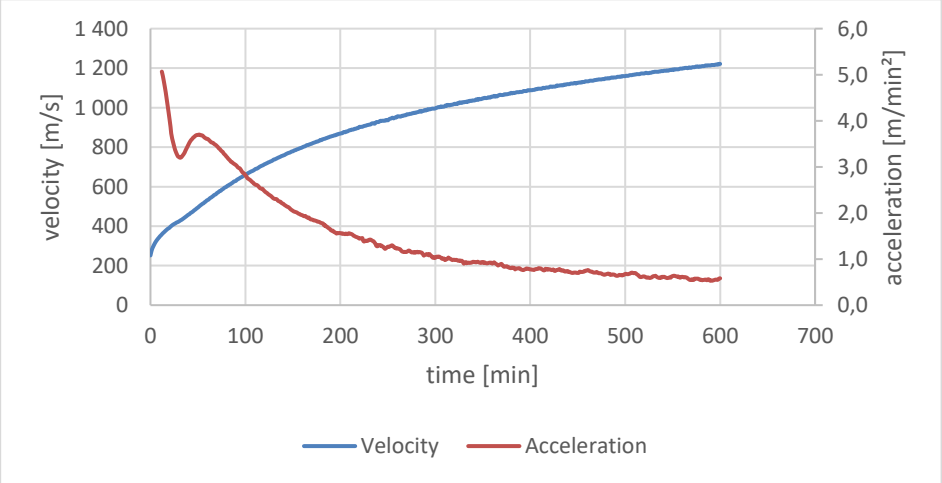

Figure 105: UT MK_10

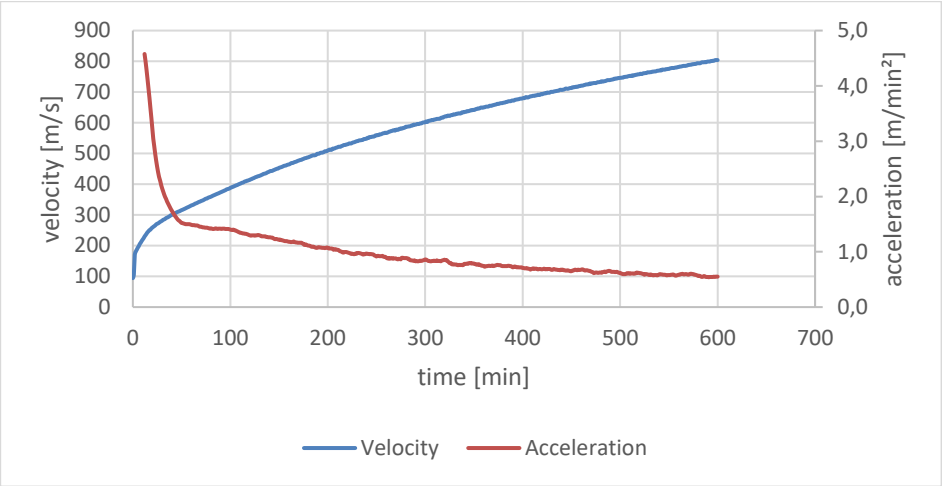

Figure 106: UT MK_15

Appendix I: NA

Table 26: NA surface area

Sample	BET Surface Area [m²/g]	t-Plot External Surface Area [m²/g]
CEM_00_A	14.14	17.01
CEM_00_B	14.38	16.86
CEM_10_A	10.15	9.06
CEM_10_B	8.94	7.65
CEM_15_A	4.61	3.28
CEM_15_B	5.54	4.69
BFS_10_A	2.93	2.26
BFS_10_B	2.80	1.59
BFS_15_A	2.86	1.99
BFS_15_B	1.83	0.71
MK_10_A	1.56	0.34
MK_10_B	1.54	0.25
MK_15_A	7.11	5.70
MK_15_B	7.88	7.09

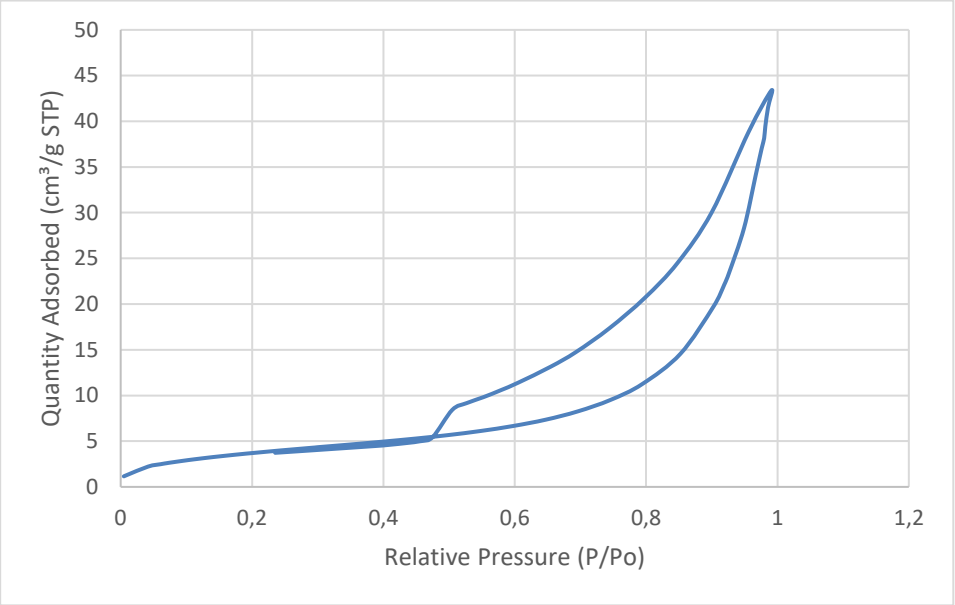

Figure 107: Quantity adsorbed CEM_00_A

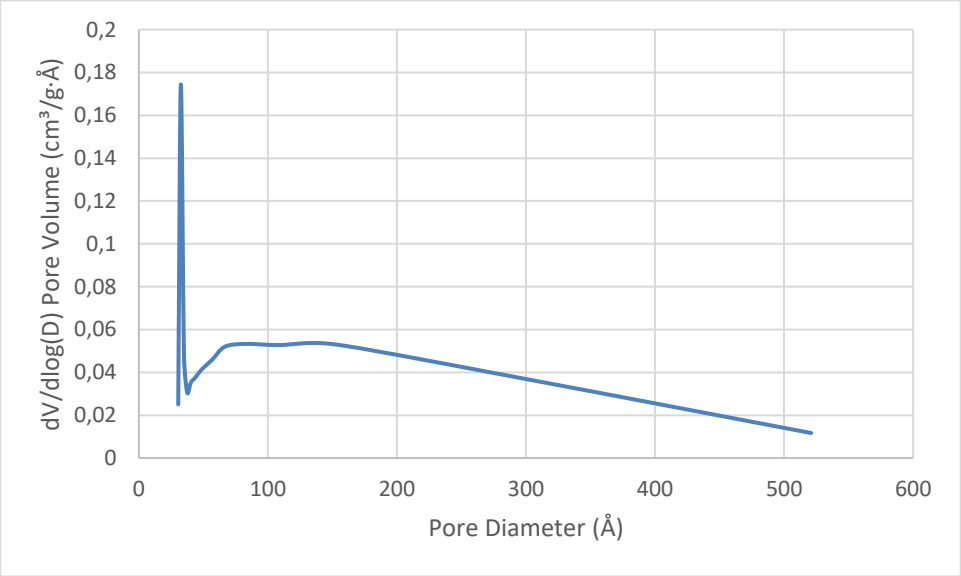

Figure 108: Pore distribution CEM_00_A

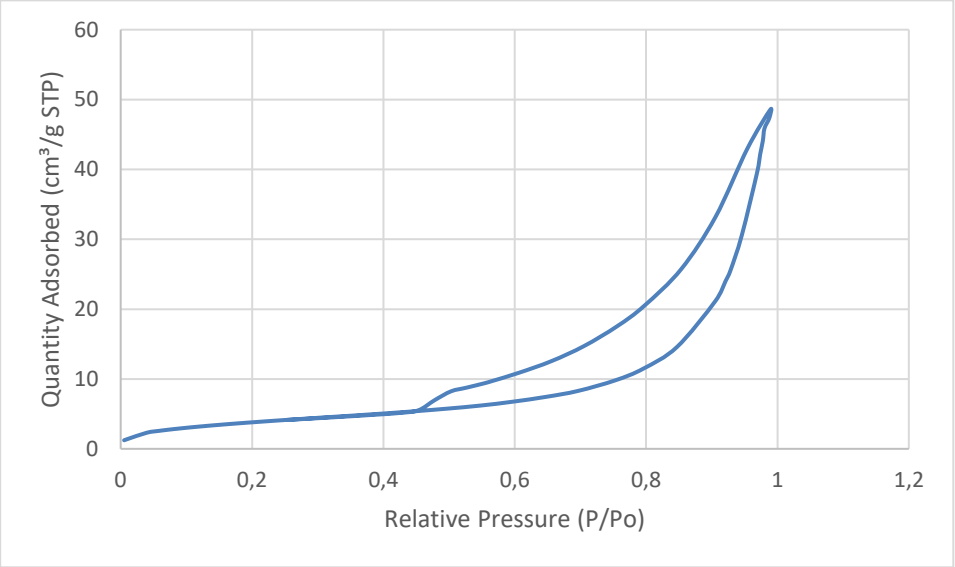

Figure 109: Quantity adsorbed CEM_00_B

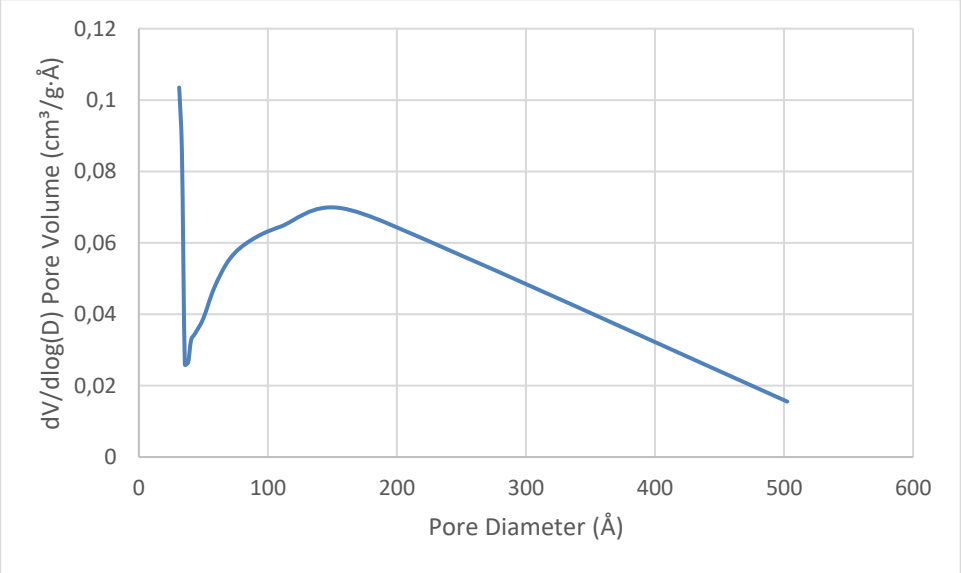

Figure 110: Pore distribution CEM_00_B

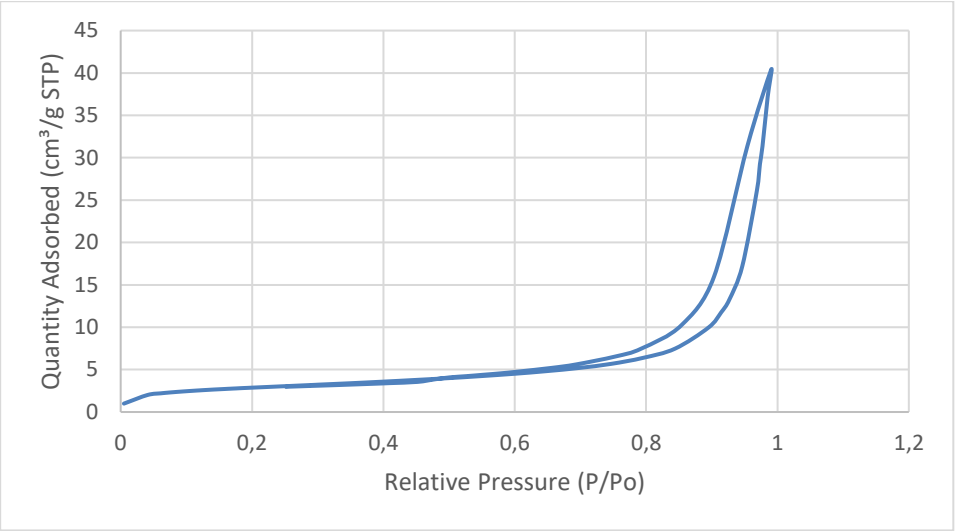

Figure 111: Quantity adsorbed CEM_10_A

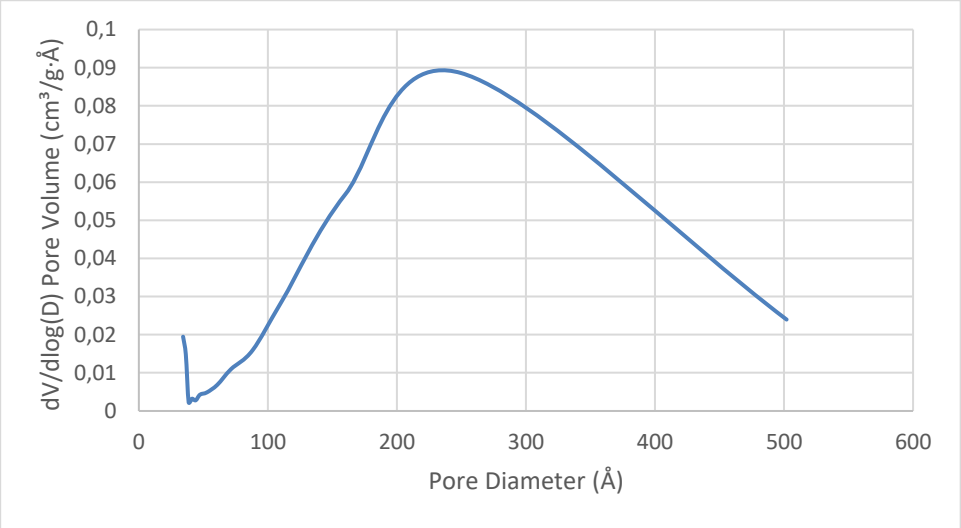

Figure 112: Pore distribution CEM_10_A

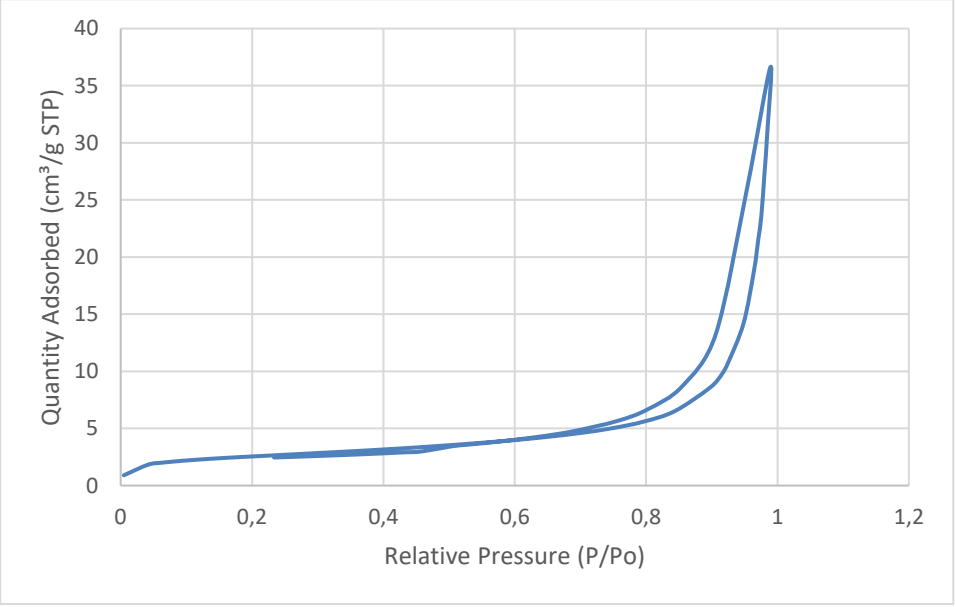

Figure 113: Quantity adsorbed CEM_10_B

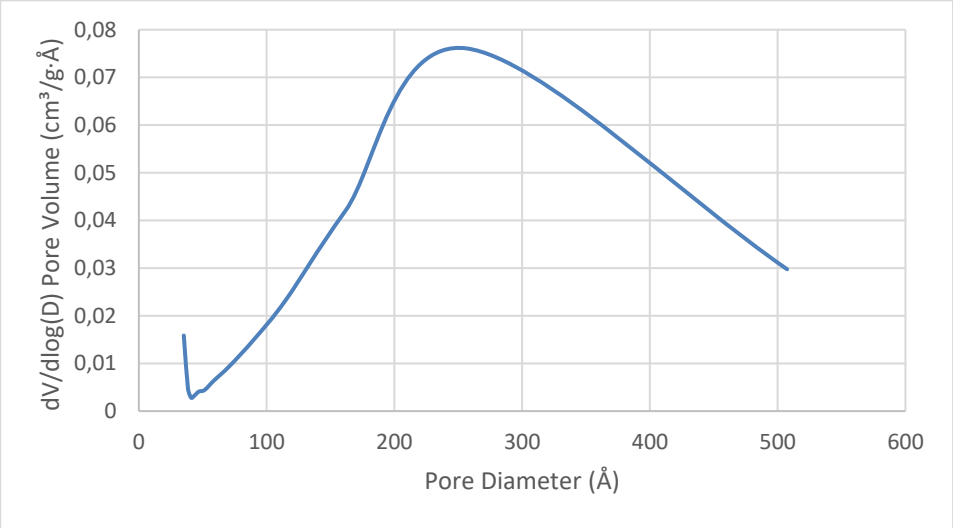

Figure 114: Pore distribution CEM_10_B

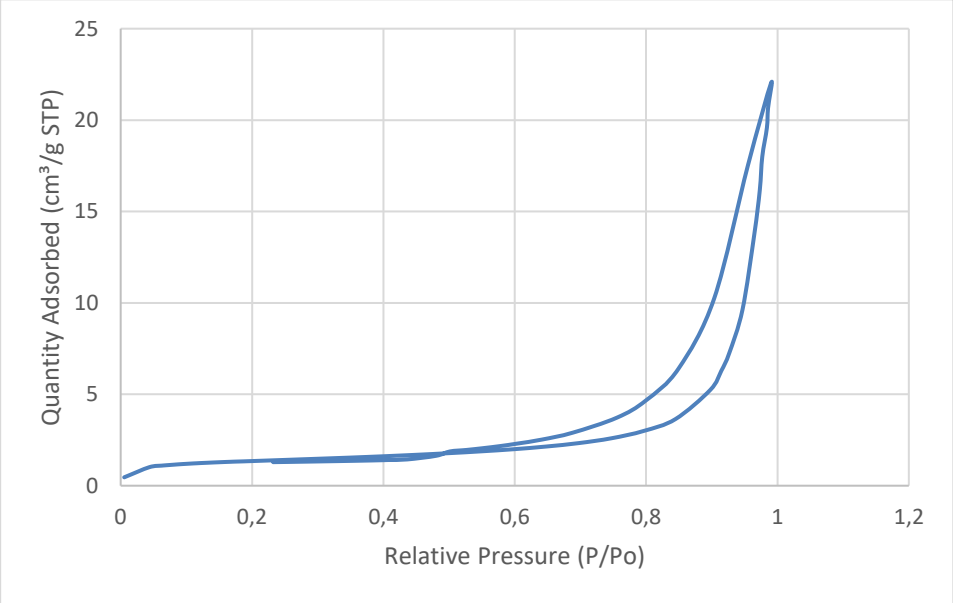

Figure 115: Quantity adsorbed CEM_15_A

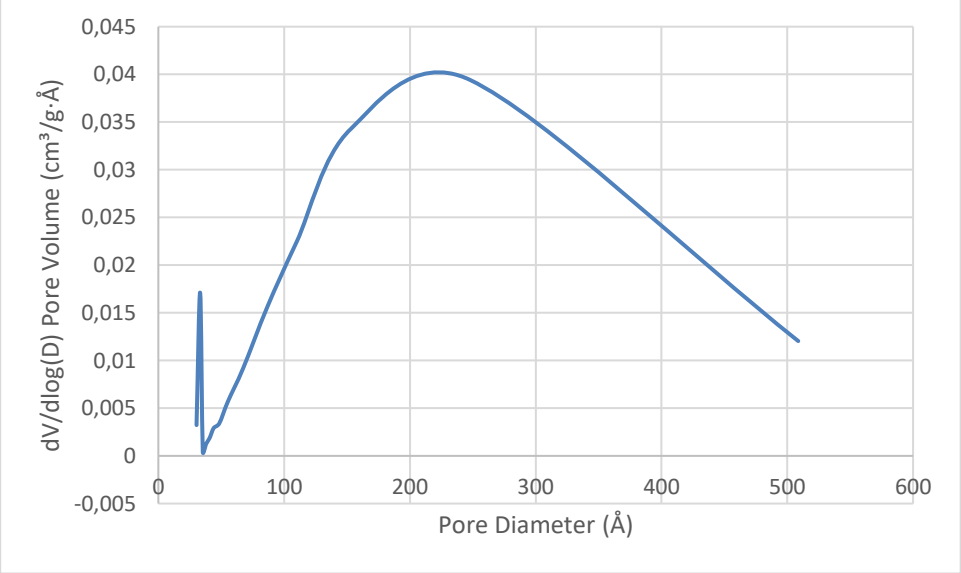

Figure 116: Pore distribution CEM_15_A

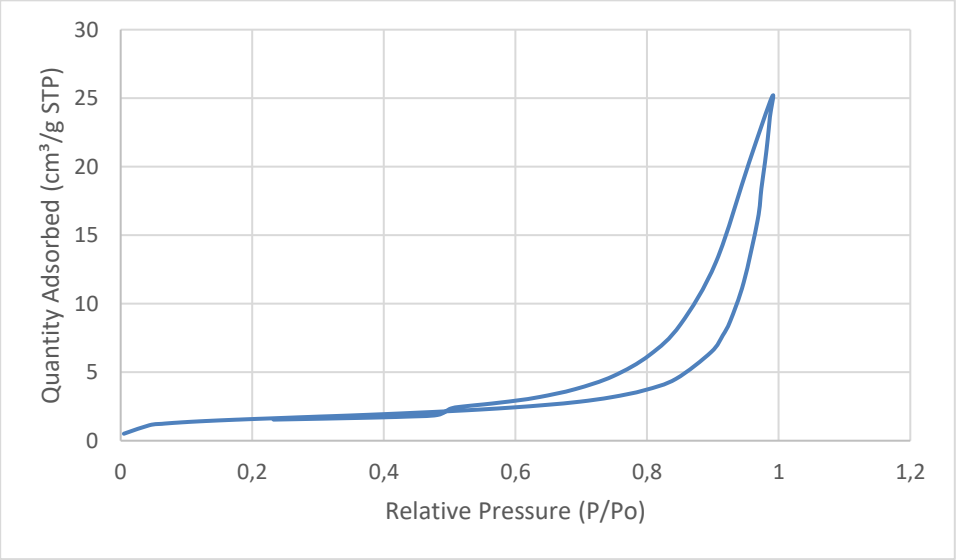

Figure 117: Quantity adsorbed CEM_15_B

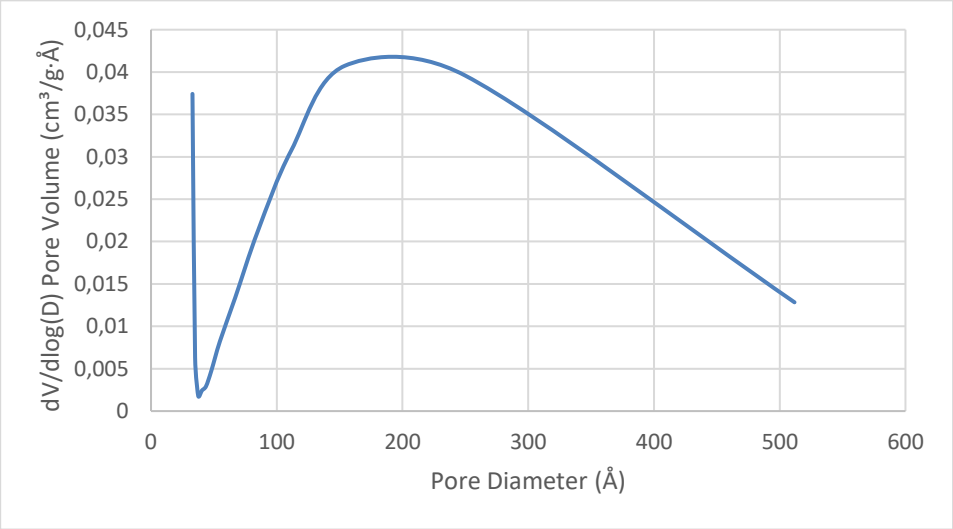

Figure 118: Pore distribution CEM_15_B

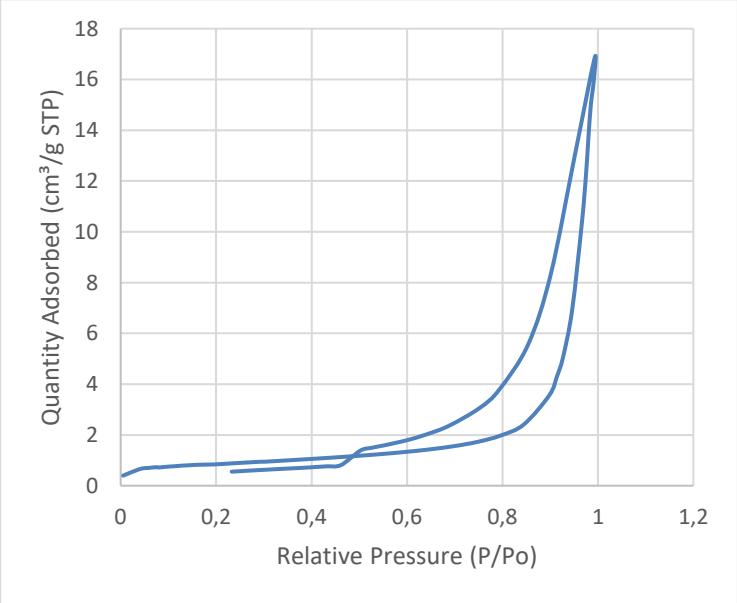

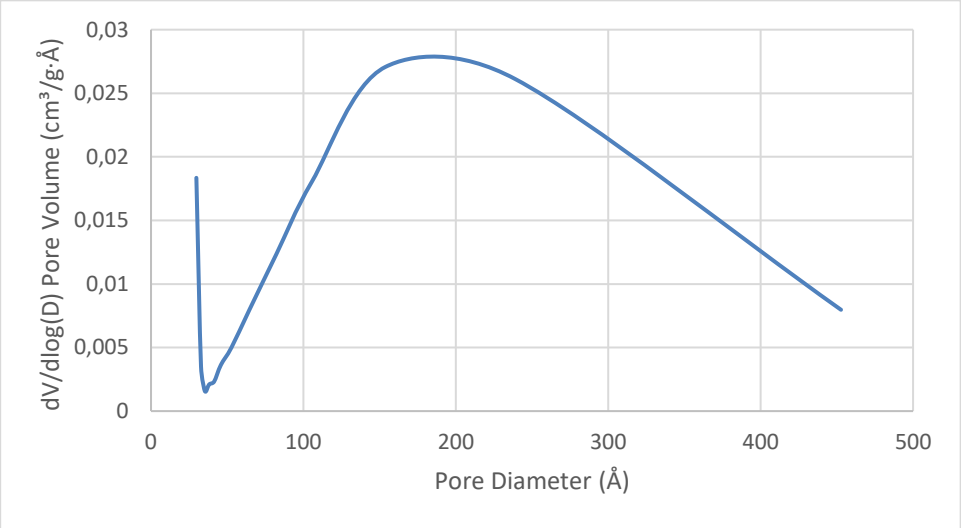

Figure 119: Pore distribution BFS_10_A

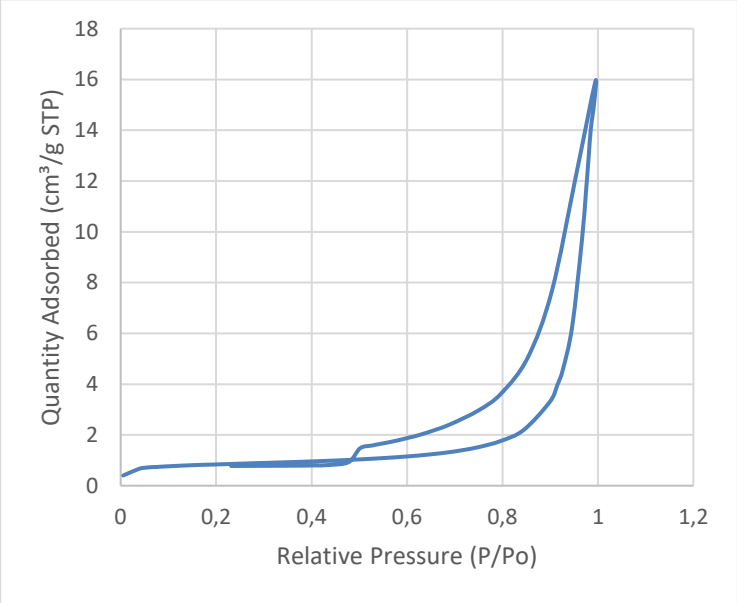

Figure 120: Quantity adsorbed BFS_10_B

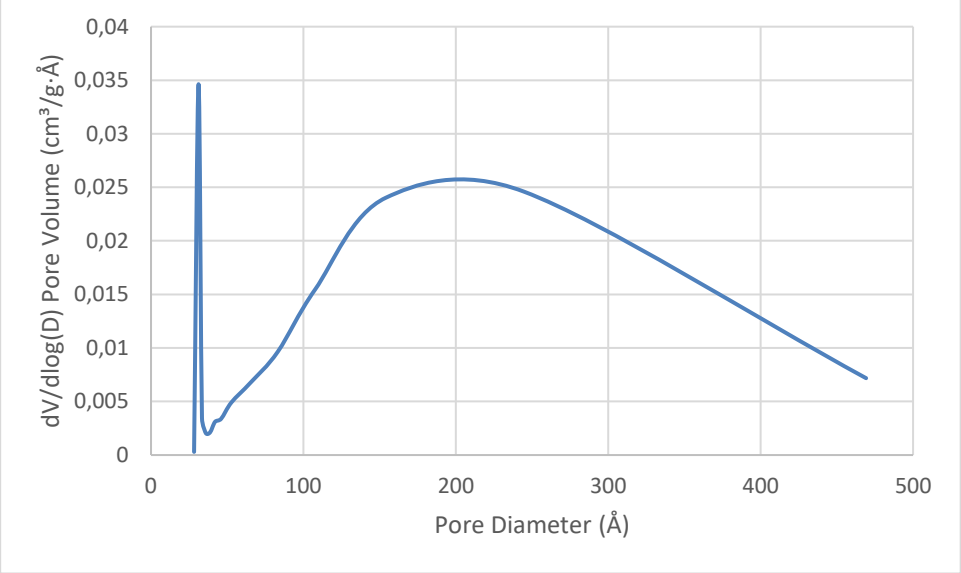

Figure 121: Pore distribution BFS_10_B

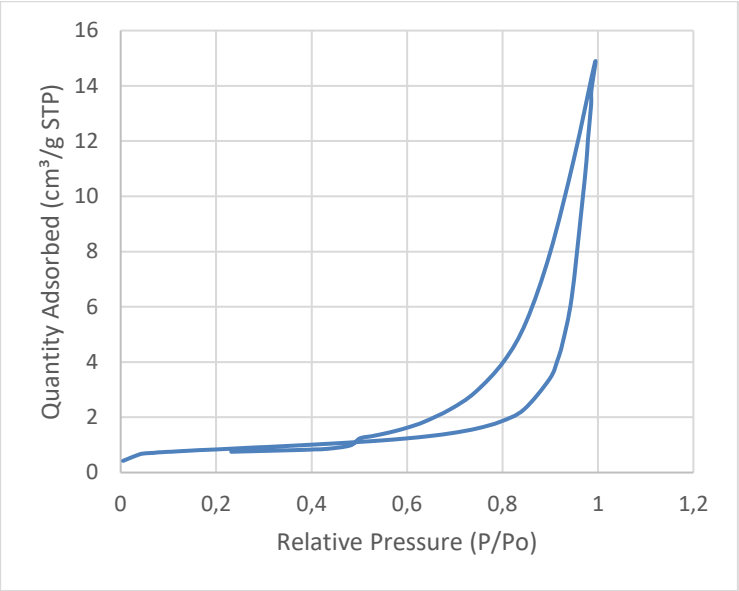

Figure 122: Quantity adsorbed BFS_15_A

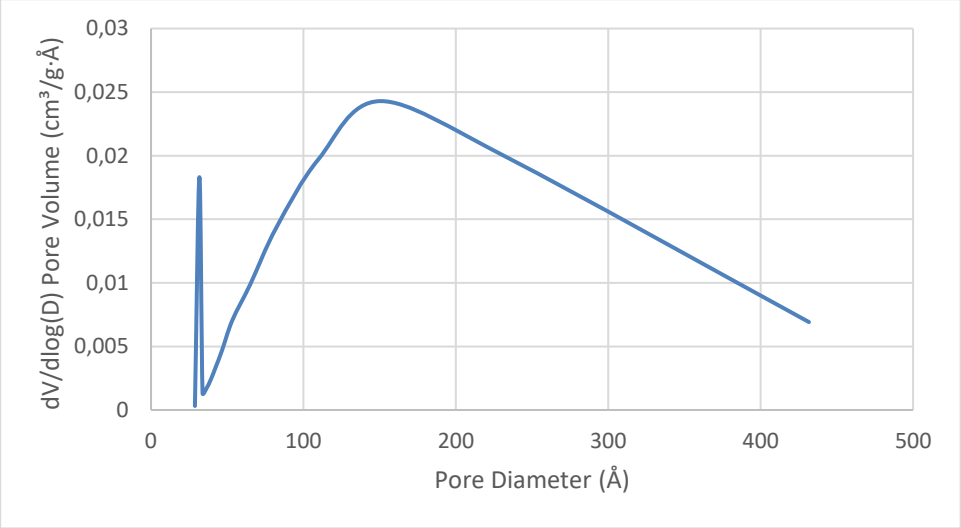

Figure 123: Pore distribution BFS_15_A

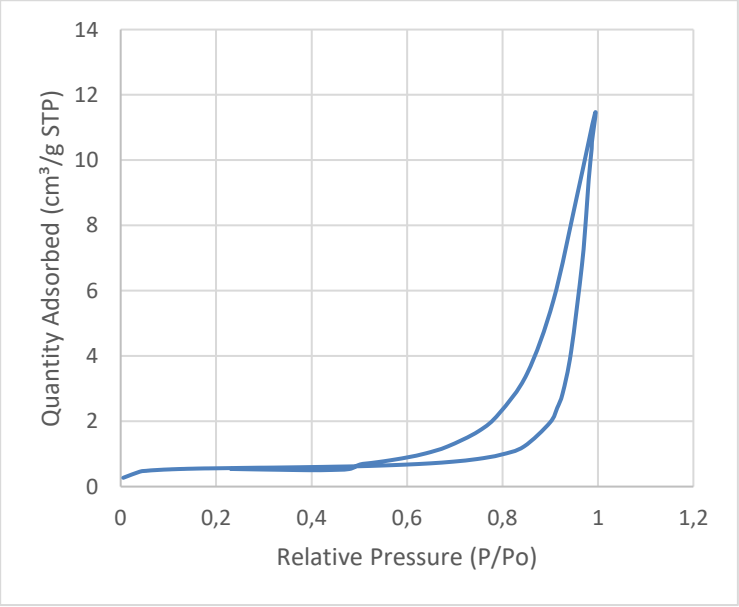

Figure 124: Quantity adsorbed BFS_15_B

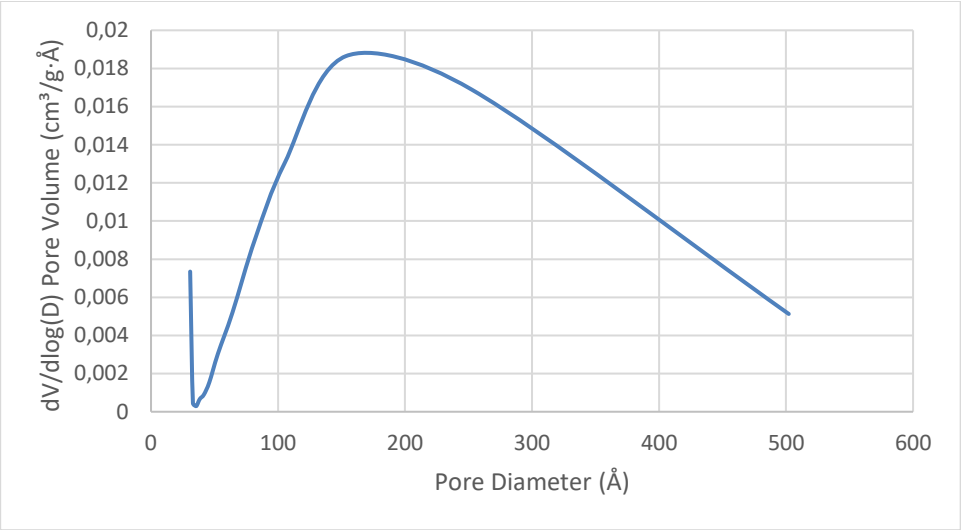

Figure 125: Pore distribution BFS_15_B

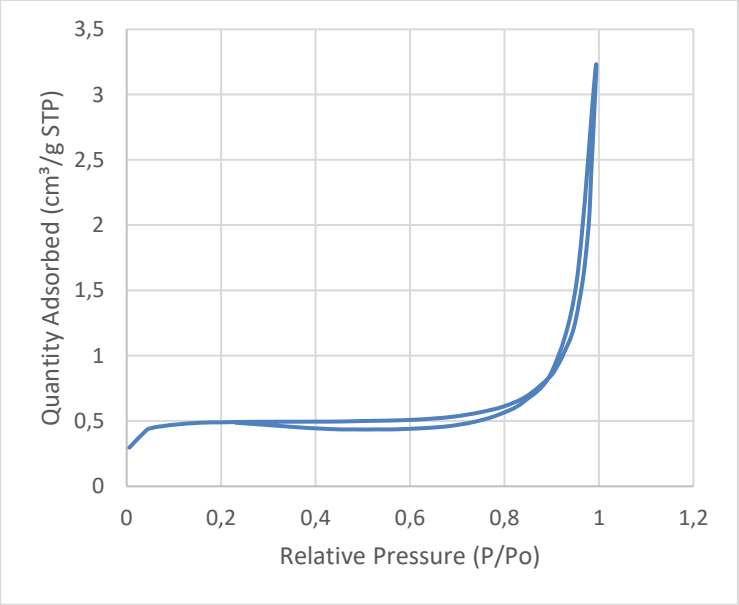

Figure 126: Quantity adsorbed MK_10_A

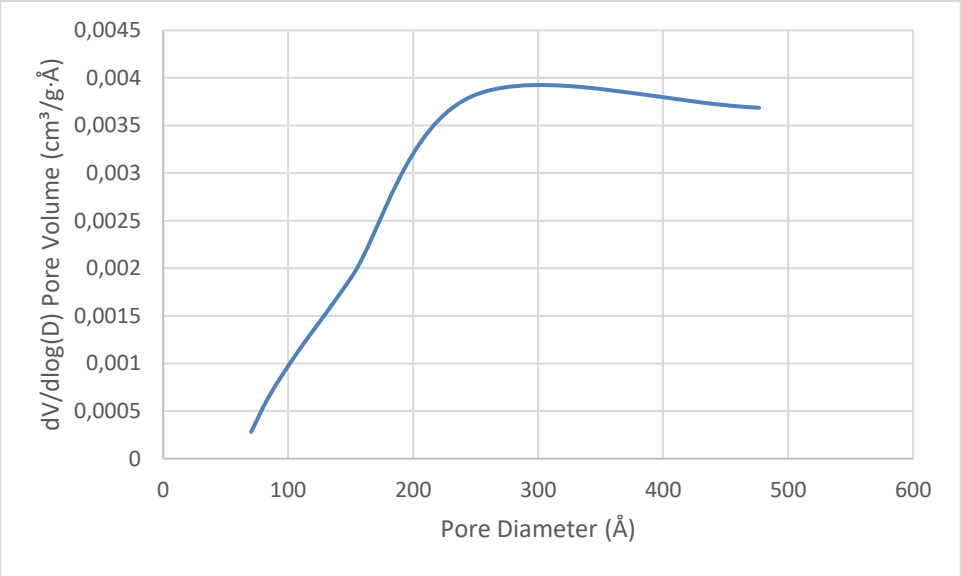

Figure 127: Pore distribution MK_10_A

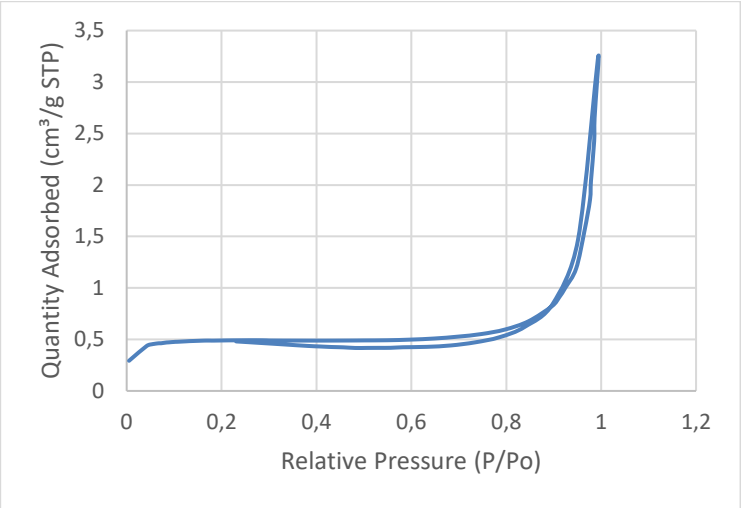

Figure 128: Quantity adsorbed MK_10_B

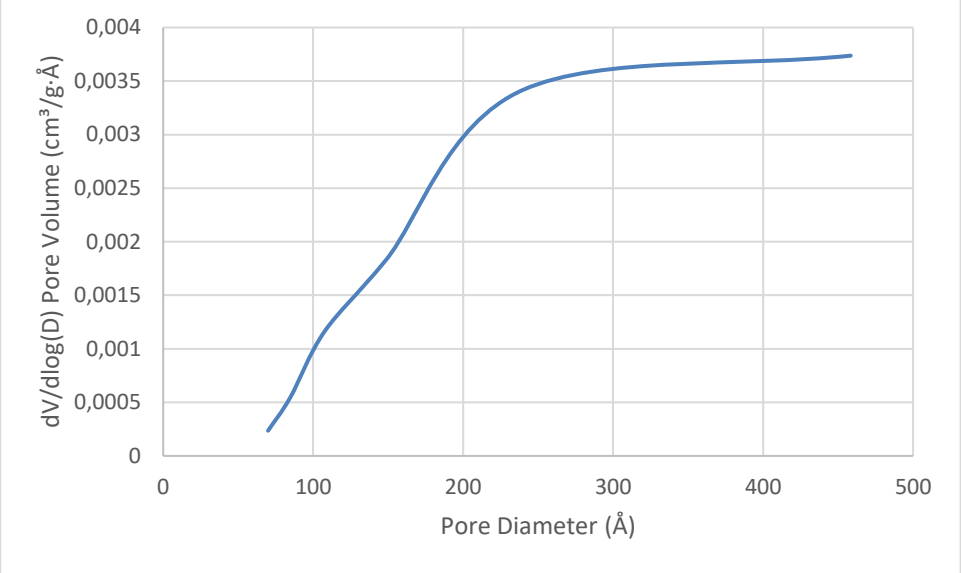

Figure 129: Pore distribution MK_10_B

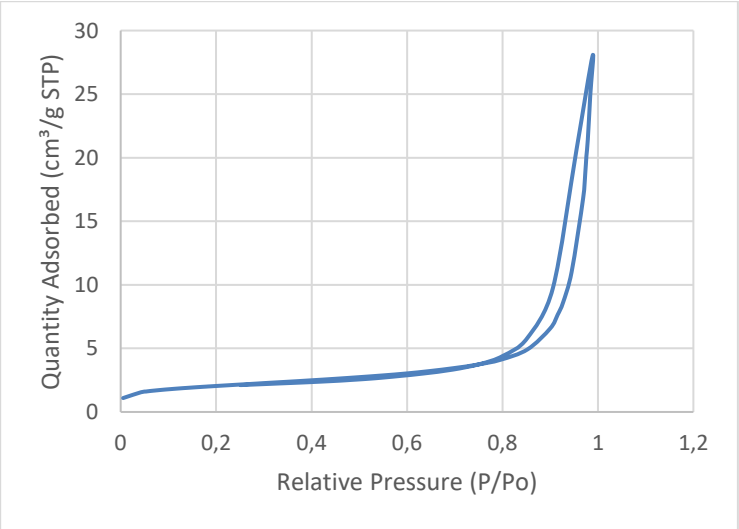

Figure 130: Quantity adsorbed MK_15_A

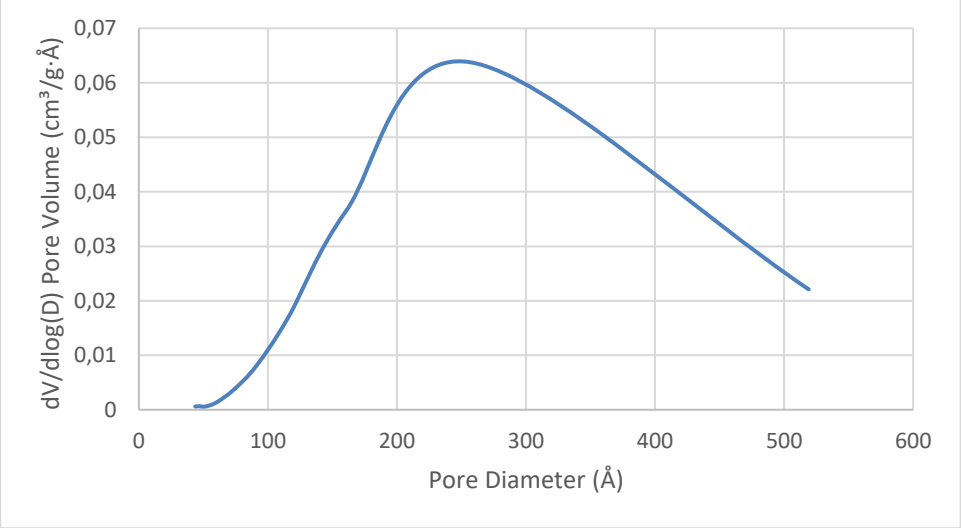

Figure 131: Pore distribution MK_15_A

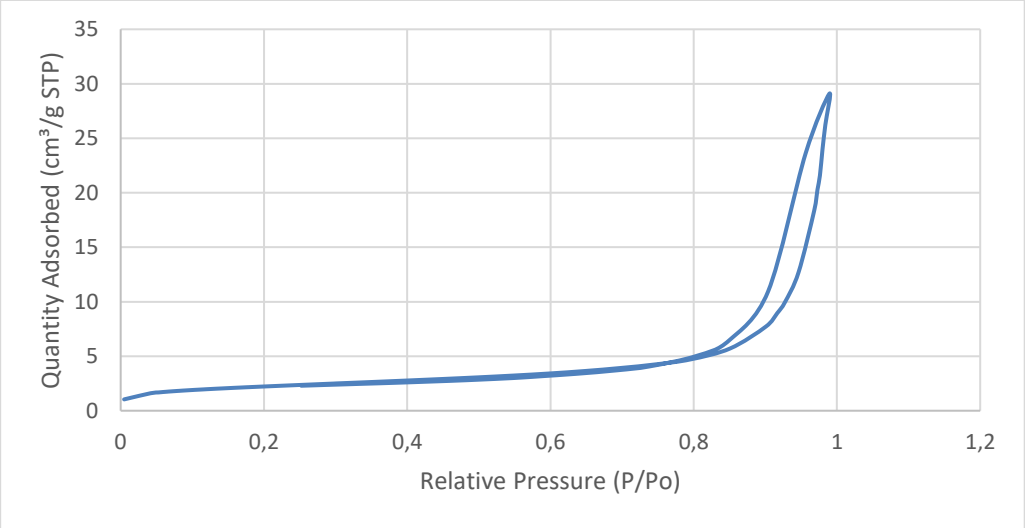

Figure 132: Quantity adsorbed MK_15_B

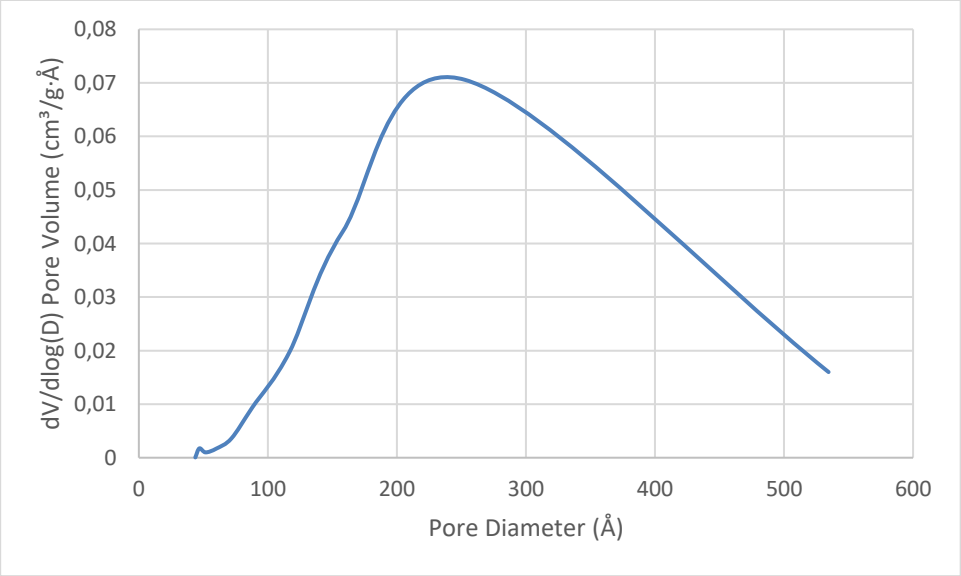

Figure 133: Pore distribution MK_15_B